Effect of Bacteria on Airway Submucosal Glands Liquid Secretion in Swine

A Thesis Submitted to the College of

Graduate and Postdoctoral Studies

In Partial Fulfillment of the Requirements

For the Degree of Doctor of Philosophy

In the Department of Physiology

University of Saskatchewan

Saskatoon

By

Xiaojie Luan

PERMISSION TO USE

In presenting this thesis/dissertation in partial fulfillment of the requirements for a Postgraduate degree from the University of Saskatchewan, I agree that the Libraries of this University may make it freely available for inspection. I further agree that permission for copying of this thesis/dissertation in any manner, in whole or in part, for scholarly purposes may be granted by the professor or professors who supervised my thesis/dissertation work or, in their absence, by the Head of the Department or the Dean of the College in which my thesis work was done. It is understood that any copying or publication or use of this thesis/dissertation or parts thereof for financial gain shall not be allowed without my written permission. It is also understood that due recognition shall be given to me and to the University of Saskatchewan in any scholarly use which may be made of any material in my thesis/dissertation.

Requests for permission to copy or to make other uses of materials in this thesis/dissertation in whole or part should be addressed to:

Head of the Physiology
2D01 Health Sciences Building
University of Saskatchewan
Saskatoon, Saskatchewan S7N 5E5
Canada

OR

Dean
College of Graduate and Postdoctoral Studies
University of Saskatchewan
116 Thorvaldson Building, 110 Science Place
Saskatoon, Saskatchewan S7N 5C9
Canada

Abstract

Cystic fibrosis (CF) is a genetic disorder caused by mutations in the gene encoding for the cystic fibrosis transmembrane conductance regulator (CFTR) anion channel. Currently, more than 4,100 Canadians have CF. The major cause of CF morbidity and mortality is airway disease, for which there is no cure.

The events leading from CFTR gene mutation to CF airway disease are not fully understood, and there is controversy regarding the primary defect responsible for CF airway disease pathogenesis. Newborn $CFTR^{\Delta F508/\Delta F508}$ and $CFTR^{-/-}$ swine show no sign of infection and inflammation in the lung but suffer from defective bacteria eradication caused by abnormal innate immune system. The cornerstone of the airway's innate immune defense is mucociliary clearance, which relies on the normal regulation of airway surface liquid (ASL), which covers the airway epithelium. It has been hypothesized that abnormal ASL is the primary defect that leads to the failure of the airway innate immune defense in CF. Evidence show that the airway submucosal gland functions abnormally in both CF patients and in animal models of CF. This is not surprising since airway submucosal glands normally express CFTR. However, the function of the gland in health and disease is not fully understood. The response of airway submucosal gland to inhaled bacteria has never been tested and its ion transport properties have not been fully described.

Our objective is to investigate the effect of inhaled bacteria on airway submucosal gland secretion, and to study and compare the function of different segments of airway submucosal gland in wild-type and CF airway. Knowledge generated by this thesis would help better understand CF airway pathophysiology and may contribute to improving treatment methods.

Acknowledgements

Firstly, I would like to thank my supervisor, Dr. Juan P. Ianowski. Dr. Ianowski supported me with tremendous amount of intellectual, logistic, and advisory resources, most importantly, his time, all of which helped me become the researcher I am today. I could walk into his office and discuss science with him anytime I wanted or needed. Aside from being an outstanding mentor, Juan has become one of my best friends, with whom I can have conversation regarding any aspect of my life.

Secondly, I would like to thank my co-supervisor, Dr. L. Dean Chapman, who guided me into the world of synchrotron imaging techniques.

I would also like to thank my committee members during my PhD, Dr. Veronica Campanucci, Dr. Nigel West, Dr. Michel Desautels, Dr. Thomas Fisher, Dr. Paul Lee, Dr. Baljit Singh and Dr. Gurpreet Aulakh for providing helpful criticisms and comments about my work.

And finally thank you to my family, especially my wife, Yanxue Liu, for making me the person I am today.

Table of Contents

Page

List of Tables

Page

List of Figures

Page

List of Abbreviations

ΔF508	delta-F508
Aδ fiber	A-delta fiber
ACh	acetylcholine
ANOVA	analysis of variance
ASL	airway surface liquid
ATP	adenosine triphosphate
Ba^{2+}	barium
BM	bending magnet
BMIT	biomedical imaging and therapy
BS	*Bacillus subtilis*
Bumet	bumetanide
CaCC	calcium-activated chloride channel
cAMP	cyclic adenosine monophosphate
CCD	charge-coupled device
CF	cystic fibrosis
CFTR	cystic fibrosis transmembrane conductance regulator
CFTRinh172	CFTR inhibitor 172
Cl^-	chloride
CLS	Canadian Light Source
COPD	chronic obstructive pulmonary disease
CT	computed tomography

Cu^{2+}	copper
DAPI	4',6-diamidino-2-phenylindole
DMSO	dimethyl sulfoxide
EC	*Escherichia coli*
ECG	electrocardiogram
ELISA	enzyme-linked immunosorbent assay
Eq	equation
ENaC	epithelial sodium channel
FITC	fluorescein isothiocyanate
FEF	forced expiratory flow
FEV_1	forced expiatory volume in 1 second
FLA	flagellin
HCO_3^-	bicarbonate
HR	heart rate
HTS	hypertonic saline
I^{2-}	iodide
IC	intestinal complications
ID	insertion device
IL-1β	interleukin 1 beta
IL-1R1	interleukin 1 receptor type 1
IL-6	interleukin 6
IL-8	interleukin 8

ITS	isotonic saline
K^+	potassium
LPS	lipopolysaccharides
Lyz	lysozyme
MRI	magnetic resonance imaging
MSD	membrane-spanning domain
N	newton
NA	nuflumic acid
Na^+	sodium
NBD	nucleotide-binding domain
NK-1	neurokinin 1 receptor
NMDG	N-methyl-D-glucamine
O_2-	% oxygen saturation
PBS	phosphate-buffered saline
PCI	phase contrast imaging
PRRs	pattern recognition receptors
qPCR	quantitative polymerase chain reaction
R domain	regulatory domain
RNA	ribonucleic acid
RS	respiratory symptoms
RT-PCR	reverse transcription polymerase chain reaction
RT-qPCR	quantitative reverse transcription polymerase chain reaction

SEM	standard error of the mean
SIET	scanning ion-selective electrode technique
SMG	submucosal gland
SO_4^{2-}	sulfate
SP	substance P
Temp	temperature in degree celsius
TLR	toll-like receptor
TNFα	tumor necrosis factor alpha
TTX	tetrodotoxin
Wt	weight
WT	wild type

Chapter 1

Introduction and Literature Review

1.1 Cystic fibrosis

Cystic fibrosis (CF) is the most common fatal genetic disease affecting young Canadians. CF is an autosomal recessive condition caused by mutations in the gene encoding the cystic fibrosis transmembrane conductance regulator (CFTR) anion channel. According to Cystic Fibrosis Canada, there are over 4,100 CF patients in Canada. One in every 3,600 newborn Canadian has CF, which means that about one baby every week is diagnosed with CF in Canada. And approximately one in every 25 Canadians carries a defective version of the gene responsible for CF (The Canadian Cystic Fibrosis Registry 2014 Report). Although the estimated median age of survival for CF patients in Canada is more than 50 years old, which is among the highest in the world, CF still remains a disease without a cure, and current treatments are inadequate.

CF was first recognized in the 1930s by Dorothy Hansine Andersen (Andersen, 1938), who described the medical condition 'cystic fibrosis of the pancreas', where the name of cystic fibrosis comes from. At that time, the estimated median age of survival was 6 months, and the poor growth resulting from digest system symptoms was the focus of CF treatments (Davis, 2005).

In 1989 researchers at The Hospital of Sick Children, in Toronto, discovered the mutated gene that causes CF, in the human chromosome 7 (Kerem et al., 1989; Riordan et al., 1989; Rommens et al., 1989). It was the CFTR gene, which encodes for an anion channel localized

on the membranes of epithelial cells and allows the movement of chloride and/or bicarbonate ions across the epithelial layer (Boucher, 1994).

The protein product of the CFTR gene has 1,480 amino acids and contains five different domains, as shown in Fig. 1.1. The CFTR protein consists of two transmembrane membrane-spanning domains (MSD1 and MSD2), which help form the central channel; two nucleotide-binding domains (NBD1 and NBD2) that can regulate the channel by ATP hydrolysis; and a regulatory domain (R), where phosphorylation of sites on R domain leads to the activation the CFTR channel (Sheppard and Welsh, 1999). As a member of the ATP-binding cassette transporter protein family, CFTR works as a cAMP-activated ATP-gated anion channel that transfers chloride and/or bicarbonate across the membrane along an electrochemical gradient (Wine, 2001). Both a phosphorylated R domain and ATP-hydrolyzed NBDs are required to open or close the CFTR channel that allows transmembrane flow of anions (Sheppard and Welsh, 1999).

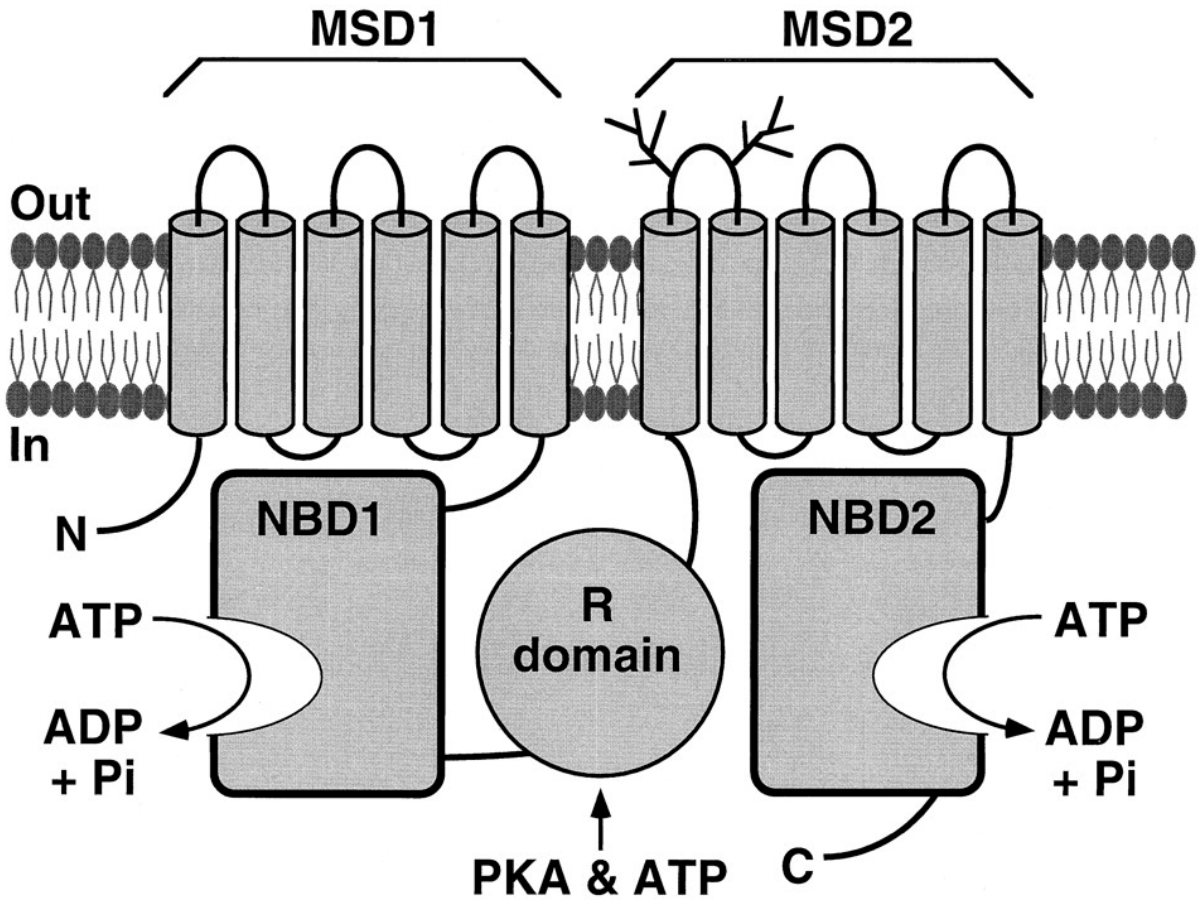

Fig. 1.1 Model showing proposed domain structure of cystic fibrosis transmembrane conductance regulator (CFTR). MSD, membrane-spanning domain; NBD, nucleotide-binding domain; R, regulatory domain; PKA, cAMP-dependent protein kinase (adapted from Sheppard and Welsh, 1999).

1.2 CFTR mutations

Over 2,000 mutations have been identified in the CFTR gene (Cutting, 2015; Castellani and Assael, 2017), which have been classified into 6 different classes based on the mechanism of dysfunction. Class 1 nonsense mutations cause no CFTR protein to be present due to premature stop codons. Class 2 mutations result in misfolded or improperly processed CFTR protein, and the unstable CFTR protein is degraded rapidly. Class 3 gating mutations lead to full-length CFTR protein to be present on the cell membrane, but the channel has difficulty to open. Class 4 mutations cause the CFTR channel on the membrane to have reduced conductivity. Class 5 mutations lead to a reduction in the amount of functional CFTR protein due to splicing defects or inefficient trafficking. Class 6 mutations result in functional CFTR protein to be unstable on the cell membrane (Egan, 2016; Castellani and Assael, 2017). The most common CFTR mutation is a class 2 mutation caused by the deletion of 3 base pairs, resulting in a loss of the amino acid phenylalanine at the 508^{th} position of the protein. This mutated protein is referred as ΔF508, and is found in about 70% of the patients. This mutation leads to abnormal folding of CFTR proteins and quick degradation of CFTR by the quality control mechanisms in the endoplasmic reticulum, thus there is low expression of CFTR on the cell membrane (Kerem et al., 1989; Cutting, 2016).

1.3 CF airway disease

CFTR is expressed in the epithelial cells of many organs, such as the lung, liver, pancreas, digestive tract, reproductive tract, and sweat glands (Sheppard and Welsh, 1999). Among these, the digestive and respiratory systems are most affected by CF disease. The gastrointestinal

symptoms cause problems digesting and absorbing nutrients, thus causing malnutrition and poor growth (O'Sullivan and Freedman, 2009). Digestive system abnormalities were the focus of CF treatment therapy in the early era of CF research. With the development of modern diets and pancreatic enzyme replacement therapies, the CF digestive symptoms have been significantly improved and most CF patients can manage gastrointestinal symptoms (Haack et al., 2013). Currently, most of the morbidity and mortality for CF patients arises from airway diseases (The Canadian Cystic Fibrosis Registry. 2009 Annual Report). Although the median age of CF patients in Canada has been significantly advanced in the last 25 years, from 13 to 22 years of age (The Canadian Cystic Fibrosis Registry. 2009 Annual Report), CF continues to be a lethal disease since CF patients suffer non-reversible lung damage.

The hallmarks of CF lung disease include chronic bacterial airway infection (frequently with *Pseudomonas aeruginosa*, *Staphylococcus aureus*, and *Haemophilus influenzae)*, prominent neutrophilic inflammation, and mucus accumulation in airways (Stoltz et al., 2010; Goetz and Singh, 2016). Chronic infection and inflammation results in airway remodeling and airway blockage in CF patients, which finally leads to chronic bronchoectasis. Bronchiectasis in CF patients leads to reduced lung function (reduced forced expiratory flow (FEF) and forced expiatory volume in 1 second (FEV_1)), pulmonary exacerbations, and in some cases respiratory failure (Castellani and Assael, 2017).

Many therapies have been used to treat CF, including antibiotics to prevent infection (Conway et al., 2014), anti-inflammatory drugs (O'Sullivan and Freedman, 2009; Castellani and Assael, 2017), airway hydrators (hypertonic saline) (Donaldson et al., 2006; Elkins et al., 2006; Tildy and Rogers, 2015; Reeves et al., 2015), mechanical airway clearance therapy (chest

percussion and drainage) (Flume et al., 2009), and lung transplantation (Flume and Van Devanter, 2012; Castellani and Assael, 2017). Most of the current treatments focus on improving the symptoms of CF airway disease. Thus, there is great interest in studying the relation between CFTR mutation and the pathogenic event that triggers the onset of CF lung disease.

1.4 CF airway disease pathogenesis

Although chronic infection and inflammation are hallmarks of CF lung disease, recent data show that lungs of newborn patients and CF animal models are mostly healthy (Stoltz et al., 2010; Ostedgaard et al., 2011). Thus, the central question is how a 'healthy' looking CF lung at birth, progresses to the heavily damaged respiratory system seen in later years. Several hypotheses have been generated to explain the onset of CF airway disease. These include abnormal adherence of bacteria to airway epithelia (Pier et al., 1997), pro-inflammatory tendency in the CF airway (Machen, 2006), and the failure of the innate immune defence system against bacteria due to reduced airway surface liquid (ASL) volume caused by increased liquid reabsorption (Boucher, 1994) and/or decreased liquid secretion (Joo et al., 2006), and changes in the composition of ASL (Guggino, 1999).

Over that last few years, especially since the development of swine CF models, research suggests that the pathogenic event that triggers the onset of CF airway disease is the failure of the innate immune defence system against bacteria in the airways (Stoltz et al., 2015).

1.4.1 Innate immune defence in the airway

A normal person inhales ~8,000 liters of air per day which may contain somewhere between 5,000 and 14,000 pathogens and irritants. Normal airways are protected from these inhaled particles by a complex immune defense system (Wine, 2007). The cornerstone of this airway defence consists of trapping particles in ASL and then clearing them out of the airway through ciliary flow, i.e. mucociliary clearance.

The ASL is an aqueous fluid containing ions, mucins, and antimicrobial factors including lactoferrin, lysozyme, and surfactant proteins. When inhaled pathogens land on the airway, they are trapped by the ASL layer. Antimicrobial factors in ASL kill and/or inactive inhaled microbes. Finally, pathogens are removed from the airway by efficient mucociliary clearance, which requires sufficient ASL height to maximize ciliary movement (Wine, 2007; Verkman et al., 2003).

This innate immune response seems to fail in the CF airway. There is increasing evidence showing that abnormal ASL in CF patients results in the loss of airway defence function (Verkman et al., 2003). In CF airways, the ASL composition and secretion is abnormal and thus fails to kill inhaled pathogens, leading to chronic infection and inflammation that may eventually cause respiratory failure (Stoltz et al., 2015; Williams and Davies, 2012).

Two hypotheses have been proposed to explain how CFTR mutation causes the abnormal airway ASL in CF patients: 1) increased liquid absorption causing ASL dehydration (Boucher, 2007) and/or 2) abnormal ASL secretion by airway submucosal glands (Wine and Joo, 2004).

The first hypothesis suggests that the loss of CFTR causes airway surface epithelia to hyper-absorb liquid from the lumen, i.e. drying the airway. Evidence indicates that CFTR normally inhibits the activity of the epithelial Na^+ channel (ENaC). In CF cells, the loss of

CFTR results in ENaC hyper-activity, which leads to excessive liquid absorption by airway epithelial cells (Boucher, 2007). This leads to dehydration of the CF airway ASL, and the collapse of mucociliary clearance. However, this hypothesis has been challenged recently by Welsh and colleagues who show that the loss of the CFTR channel in the CF pig and CF patients does not increase sodium absorption in the airway (Chen et al., 2010; Itano et al., 2011). In addition, accumulating evidence suggests that the second hypothesis may be correct, where the failure to eradicate bacteria effectively in CF airways may be the result of abnormal ASL secretion by submucosal glands.

1.5 Airway submucosal glands

The airway submucosal glands are located beneath the airway surface and seem to play an important role in CF pathobiology (Wine and Joo, 2004; Engelhardt et al., 1992). Submucosal glands secrete about 95% of the ASL in the upper airway (i.e. trachea and bronchi) (Joo et al., 2006; Wine and Joo, 2004). The glandular secretion consists 90-98% of water, different types of ions, gel-forming mucins, and antimicrobial factors that are essential for the airway defence against inhaled pathogen (Widdicombe and Wine, 2015).

However, the secretion, composition, and rheological properties of the ASL are abnormal in CF airway. Gland secretion collected from CF patients and CF swine was more viscous than that from healthy controls due to elevated mucin concentration in CF gland secretion and the lack of CFTR-dependent bicarbonate secretion (Widdicombe and Wine, 2015; Jayaraman et al., 2001; Hoegger et al., 2014). Moreover, abnormal pH and composition of the ASL have been proposed to result in reduced bacterial killing in CF airway, which facilitates infection of the

airways (Pezzulo et al., 2012; Verkman et al., 2003). And stimulation with secretagogues that normally trigger ASL secretion fails to stimulate ASL production in CF patients and in mice, rat, ferret, and swine CF models (Tarran et al., 2006; Joo et al., 2006; Engelhardt et al., 1992; Wine and Joo, 2004; Lee and Foskett, 2010; Ianowski et al., 2007; Joo et al., 2010; Choi et al., 2010). Thus, it has been proposed that failure to secrete ASL in response to inhalation of pathogens in CF may facilitate bacterial colonization by reducing the amounts of gland-derived antimicrobial factors in the airway (Joo et al., 2004).

1.6 Regulation of gland secretion

Since the liquid secretion from airway submucosal gland is very important for airway defence (Verkman et al., 2003; Haq et al., 2016), its secretion needs to be carefully regulated. The airways submucosal gland secretion is regulated by the central nervous system, and through airway local signals, which produce two separate responses: an emergency response and a 'housekeeping' response.

The emergency response of the gland is triggered by situations that are immediately deleterious to the individual, such as inhalation of water or toxic substances, and it is controlled by the central nervous system via the vagus nerve. When activated, the emergency response triggers large volumes of ASL secretion, and it is normally accompanied by airway constriction and cough. This pathway of stimulation of gland secretion is mediated by the release of acetylcholine (ACh), increases in intracellular Ca^{2+} concentration, and activation of calcium-activated chloride channels (CaCCs). This emergency response remains in CF patients, since it functions independently of CFTR (Choi et. al., 2009; Ianowski et. al., 2007; Joo et. al, 2010;

Joo et. al., 2002).

The ‘housekeeping’ function of airway submucosal glands has been proposed play a major role in protecting the airways from mundane, smaller insults, such as inhalation of small numbers of noxious particles during daily activities. It ensures sufficient ASL volume in the airway to allow for an efficient mucocilicary clearance process, which is required to keep the airways clean and uninfected (Wine, 2007; Widdicombe and Wine, 2015). However, little is known about the ‘housekeeping’ response of airway submucosal gland, specially about the response of submucosal gland secretion against inhaled pathogens. It remains unknown for example how airway submucosal glands respond to inhaled bacteria. Furthermore, it is also unclear why and how airway submucosal glands produce abnormal ASL in CF.

1.7 General hypothesis

The general hypothesis of this thesis is that inhalation of bacteria triggers airway submucosal glands to secrete ASL, which contains antimicrobial compounds and mucin required to help clear the insult. In CF airway this response fails and leads to the failure of pathogen eradication.

1.8 Thesis objectives

The objectives of my dissertation are:

1) to study the effect of inhaled bacteria, especially *P. aeruginosa*, on ASL secretion in the trachea of swine, and to test the role of CFTR in the process (Chapter 2),

2) to study the effect of inhaled bacteria on ASL secretion *in vivo* using $CFTR^{-/-}$ swine, and to study the possible mechanism of the proposed basal spontaneous ASL (Chapter 3),

3) to test the contribution of the nervous system and airway epithelia secretion to

hypertonic saline (HTS) nebulization-stimulated ASL production (Chapter 4),

4) to investigate the ion transport properties of different segments of airway submucosal gland in wild-type and $CFTR^{-/-}$ tissue (Chapter 5), and

5) to develop a new imaging strategy to study the pathogenesis of CF small airway disease (Appendix A).

1.9 Summary of manuscripts

Pseudomonas aeruginosa triggers CFTR-mediated airway surface liquid secretion in swine trachea

Significance: This study provides the first demonstration that inhalation of bacteria triggers CFTR-dependent ASL secretion. We suggest that this response to inhaled pathogens is an important but previously unknown part of the innate immune response that would be missing in CF patients, resulting in reduced bacterial killing and facilitating infection.

Contribution: I was the primary investigator of this study. I was involved in designing the research, performing the research, analyzing data, and writing the paper.

Cystic fibrosis swine fail to secrete airway surface liquid in response to inhalation of pathogens

Significance: The study represents the first study of ASL secretion mechanisms in a live animal. We show that a bacteria-triggered and a basal spontaneous ASL secretion in wild-type but not in pig models of CF, suggesting an impaired response to pathogens contribute to infection.

Contribution: I was the primary investigator of this study. I was involved in developing

the experimental techniques, conducting the experiments, analyzing data, interpreting data, and contributing to writing the manuscript.

Chapter 2

Pseudomonas aeruginosa triggers CFTR-mediated airway surface liquid secretion in swine trachea

Citation: Luan X, et al. (2014) *Pseudomonas aeruginosa* triggers CFTR-mediated airway surface liquid secretion in swine trachea. *Proc Natl Acad Sci U S A* 111(35):12930-12935.

Disclaimer: Manuscript has been reformatted for consistency with the dissertation, including some rearrangement. References have been moved to the end of the dissertation as per CGSR requirements. No other content has been changed.

2.1 Abstract

Cystic fibrosis (CF) is an autosomal recessive genetic disorder caused by mutations in the gene encoding for the anion channel CFTR. Several organs are affected in CF, but most of the morbidity and mortality comes from lung disease. Recent data show that the first consequence of CFTR mutation is the failure to eradicate bacteria prior to the development of inflammation and airway remodeling. Bacterial clearance depends on a layer of airway surface liquid (ASL) consisting of both a mucus layer that traps, kills and inactivates bacteria, and also a periciliary liquid layer that keeps the mucus at an optimum distance from the underlying epithelia to maximize ciliary motility and clearance of bacteria. The airways in CF patients and animal models of CF have abnormal ASL secretion and reduced antimicrobial properties. Thus, it has been proposed that abnormal ASL secretion in response to bacteria may facilitate the development of the infection and inflammation that characterize CF airway disease. However, whether the inhalation of bacteria triggers ASL secretion and the role of CFTR has never been tested. We developed a synchrotron-based imaging technique to visualize the ASL layer and

measure the effect of bacteria on ASL secretion. We show that the introduction of *Pseudomonas aeruginosa* and other bacteria into the lumen of intact isolated swine tracheas triggers CFTR-dependent ASL secretion by the submucosal glands. This response requires expression of the bacterial protein flagellin. In patients with CF, the inhalation of bacteria would fail to trigger ASL secretion, leading to infection and inflammation.

2.2 Introduction

The human airway is normally protected from injury caused by microbial colonization and viral infection by a complex immune defence system. The cornerstone of airway defence is mucociliary clearance. Particles, including bacteria, are captured in mucus and removed by an efficient mucociliary clearance mechanism. Airway host defence is compromised in people with cystic fibrosis (CF). As a result, their lungs suffer from chronic bacterial infections, frequently with *Pseudomonas aeruginosa,* and inflammation that may eventually cause lung tissue damage and respiratory failure (Pilewski and Frizzell, 1999; Sheppard and Welsh, 1999). The events leading from Cystic Fibrosis Transmembrane conductance Regulator (CFTR) gene mutation to airway disease are not fully understood**,** but accumulating evidence suggests that CF airway disease results from abnormal microbial clearance (Pezzulo et al., 2012; Stoltz et al., 2010).

Although chronic inflammation is a major part of CF lung disease, recent data show that the first consequence of CFTR mutation is an impaired ability to eradicate bacteria. Lungs from animal models of CF (F508del and $CFTR^{-/-}$ pigs) (Rogers et al., 2008; Sun et al., 2010) fail to eradicate bacteria as effectively as wild-type littermates before the development of

inflammation (Pezzulo et al., 2012; Stoltz et al., 2010). These results suggest that impaired bacterial elimination is the pathogenic event that initiates a cascade of inflammation and pathology in CF lungs (Stoltz et al., 2010).

The failure to clear bacteria likely results from abnormal airway surface liquid (ASL) secretion and properties (Sun et al., 2010; Ianowski et al., 2007; Joo et al., 2010; Joo et al., 2002; Wine, 2007). The ASL consists of a layer of mucus that traps inhaled particles, and a periciliary liquid layer that keeps the mucus at an optimum distance from the underlying epithelia to maximize ciliary mobility (Wine, 2007; Knowles and Boucher, 2002). The mucus layer is a sophisticated mixture of water, salts, gel-forming mucins and antimicrobial compounds that helps inactivate, kill, and trap pathogens and facilitates mucociliary clearance (Wine, 2007; Knowles and Boucher, 2002). In CF airways, both the bacteria-killing properties and the secretion of the ASL are abnormal (Pezzulo et al., 2012, Joo et al., 2002). The airway liquid produced by $CFTR^{-/-}$ swine has lower bactericidal properties compared to wild type littermates due to abnormal pH (Pezzulo et al., 2012; Stoltz et al., 2010). In addition, human CF airways, 1-day old CF piglets, newborn $CFTR^{-/-}$ ferrets and $CFTR^{-/-}$ mice fail to respond to stimulatory signals that normally elicit strong ASL secretion (Sun et al., 2010; Ianowski et al., 2007; Joo et al., 2010; Joo et al., 2002). Thus, it has been proposed that abnormal secretion of fluid and mucin in response to bacterial infection may contribute to CF lung disease pathogenesis (Ianowski et al., 2007; Joo et al., 2010; Joo et al., 2002; Wine, 2007; Martens et al., 2011; Baniak et al., 2012; Reid, 1960; Ianowski et al., 2008). However, the central question of whether bacteria trigger ASL secretion in the airways and the role of CFTR in such a process has never been tested due to the lack of a suitable experimental technique.

We developed a novel synchrotron-based method to measure the height of the airway surface liquid (ASL) layer covering the epithelium of intact, isolated swine trachea. We show that the introduction of *P. aeruginosa* into the lumen of intact isolated swine tracheas triggers CFTR-dependent ASL secretion by the submucosal glands. This is a local response that only affects the glands in close proximity to the bacteria and requires expression of the bacterial protein flagellin. We also show that *Staphylococcus aureus* and *Haemophilus influenzae* also trigger CFTR-dependent ASL secretion, indicating that this response is not unique to *P. aeruginosa*. In patients with CF, the inhalation of bacteria would fail to trigger ASL secretion by submucosal glands facilitating infection and inflammation.

2.3 Materials and Methods

Animals

Tracheas were obtained from juvenile female and male pigs weighing 15-25 kg from the Prairie Swine Centre, University of Saskatchewan. The tracheas were dissected within 15-30 minutes of euthanasia, clamped at both ends in order to prevent fluid from entering the trachea and placed in ice-cold Krebs-Ringer solution (mM): 115 NaCl, 2.4 K_2HPO_4, 0.4 KH_2PO_4, 1.2 $CaCl_2$, 1.2 $MgCl_2$, 25 $NaHCO_3$, 10 glucose (pH=7.4) equilibrated with 95% O_2, 5% CO_2 until used.

X-ray imaging

Experiments were performed on the BioMedical Imaging and Therapy-Bend Magnet (BMIT-BM) beamline 05B1-1 at the Canadian Light Source (CLS). All the experiments were

approved by the CLS and the Animal Ethics Committee at the University of Saskatchewan.

The experimental hutch was located 25.5 meters away from the storage ring. Phase contrast imaging (PCI) was performed using monochromatic 20 keV (λ=0.062 nm) x-rays, selected using a standard double-crystal monochromator. Iodine K-edge subtraction imaging was performed using monochromatic 33.20 keV and 33.35 keV. Barium K-edge subtraction imaging was performed using monochromatic 37.50 keV and 37.65 keV. The beam size was 100.0 mm (wide) x 8.0 mm (vertical). The distance between sample and detector was 65 cm. Images were captured using a high resolution x-ray converter (AA-60, Hamamatsu Photonics) with a charge-coupled device (CCD) detector (C9300-124, Hamamatsu Photonics). The converter used a 10 μm-thick scintillator (Gd2O2S:Tb) to convert x-rays to visible light, which was then directed to the CCD. The pixel size of the image was 8.75 x 8.75 μm. The exposure time ranged from 600 to 900 ms.

The trachea preparation was placed in a custom-built chamber. The tissue was immersed in Krebs solution plus 1 μM indomethacin at 35ºC and equilibrated with 95% O_2 and 5% CO_2. The lumen of the trachea preparation remained free of solution and sealed, but was accessible to the researchers to introduce the agarose beads. Agarose beads, ~200 to 800 μm diameter, were blotted dry and placed in the lumen of the preparation using a cotton swab. Before measuring ASL height each bead was placed at the point where the air-ASL interface is parallel to the x-rays reaching the sample, i.e. the top or bottom of the preparation (Fig. 2.1a), using a computerized experimental stage. We made two ASL height measurements, one 5 min after instillation of the beads and another after 35 min after instillation. For our experiments, the measurements made at 5 min should be interpreted as the initial state of the airway, i.e. before

exposure to bacteria. We labeled the first time point as 5 min because there was a 5 min delay between instillation of the beads and acquisition of the first image.

Preparation of agarose beads

We used agarose beads as devices to measure the height of the ASL (Fig. 2.S1). The height of the ASL layer was measured as the distance between the air-liquid interface and the edge of the agarose bead touching the surface epithelia (Fig. 2.S1).

Agarose beads were made in sterile conditions with 4% agarose in PBS as described elsewhere (Cash et al., 1979; Chmiel et al., 2002). In order to make the beads visible by x-ray we added $BaSO_4$ or CuI (1 M) as contrast agents. These salts were chosen because they are not soluble in water and, thus, did not contribute to the osmotic pressure of the bead. The osmolarity was 278 ± 0.1, 276 ± 0 and 279 ± 0 mOsm for PBS, 1M $BaSO_4$ and 1M CuI, respectively (n=6 per group).

In addition, the beads were used as a delivery system for bacteria to the airway. Bacteria-laden agarose beads were made by adding 10% of bacteria stock solution to sterile PBS. *P. aeruginosa* stock solution was made with a clinical isolate *P. aeruginosa* generously provided by Dr. Gordon at the University of Saskatchewan (NH57388) (Hoffmann et al., 2005). An aliquot of *P. aeruginosa* NH57388 was inoculated in 80 ml of TSB in a 2 l Erlenmeyer flask and incubated for 28 h at 37ºC shaking at 170 rpm. The culture was then heat killed (incubated at 80ºC for 30 min) and stored at -20ºC until use. Clinical isolates of *Hemophilus influenzae* and *Staphylococcus aureus* (generously provided by Dr. Blondeau at the Royal

University Hospital, Saskatoon, Saskatchewan, Canada) and *P. aeruginosa* strains PAK and PAKΔfliC strains were prepared in an identical manner.

Secretion assay

A small piece of trachea was cut along the trachealis muscle and the airway submucosa, containing the glands, was dissected from the cartilage as described previously (Joo et al., 2001). This submucosa preparation was placed in a custom built chamber with the serosal side bathed in Krebs solution containing 1 μM indomethacin. The mucosal side was cleaned, dried with a stream of air and coated with ~5 μl mineral oil. Mucus secreted by the submucosal glands formed a spherical droplet under the mineral oil. The preparation was maintained at 37ºC and equilibrated with warm and humidified 95% O_2 5% CO_2 gas (TC-102, Medical Systems Corp., Greenvale, NY, US). Flagellin (10 ng/ml) was added to the serosal side, and the droplets of ASL secreted by the glands were imaged every 120s and stored for offline analysis using ImageJ 1.43u (NIH). The volumes of the secreted droplets were calculated assuming a spherical shape ($V = 4/3\pi r^3$) (Joo et al., 2001). The secretion rate was calculated by fitting the volume versus time plots with straight lines using linear regression, and the slopes were taken as the secretion rates using at least four points (Joo et al., 2002).

We used a modified secretion assay to test whether bacteria stimulate the release of paracrine signals that may trigger ASL secretion. A piece of trachea was prepared as described above except that the mucosal side was not cleaned or dried. Instead, we incubated the mucosal side of the preparation with ~5 μl of PBS or *P. aeruginosa* stock solution. After 35 min we collected the Krebs solution bathing the serosal side of the preparation and tested it using the

secretion assay as described above.

Surgical removal of the submucosal glands

The trachea preparation was clamped at both ends so that the lumen was filled with air. The cartilage was removed with the aid of a scalpel and a blunt-ended elevator. Once the cartilage was removed the submucosal glands and other tissue in the submucosa was dissected out by "shaving" with a breakable scalpel blade (Fine Science Tools, Vancouver, Canada). The procedure took ~30 min. We tested the effectiveness of our procedure by performing it in a set of tracheas and then counting the number of viable glands in a secretion assays. We compared the number of viable glands in tracheas with glands removed with control tracheas that were subjected to the same procedure but without removing the glands. The data showed that our procedure allowed us to remove 90% of glands from the trachea.

The surface epithelium was not affected by the dissection procedure. During gland dissection the trachea remains filled with air and clamped on both ends. The dissection tools never touched the surface epithelia. We tested the condition of the surface epithelium after dissection of submucosal glands by measuring short circuit currents in an Ussing chamber. The experiments showed that preparations subjected to the dissection procedure (removal of the cartilage) but with submucosal glands intact had a short circuit current (I_{sc}) of 24 μA/cm^2. Similarly, preparations where we dissected the glands out had a I_{sc} of 20 μA/cm^2. Addition of amiloride (10^{-4} M apical side) reduced the I_{sc} to 12 and 9 μA/cm^2 for preparations with and without glands, respectively. Stimulation with forskolin (10^{-5} M apical side) stimulated I_{sc} to 20 and 17 μA/cm^2 for preparations with and without glands, respectively. These results showed

that the surface epithelium was not affected by the dissection procedure.

RT-PCR

Total RNA was extracted from 10-20 mg of tissue (surface epithelia, submucosal glands, heart and lung) using RNAqueous kit (Ambion). Airway surface epithelium was dissected from swine trachea and was free of submucosal glands. Submucosal glands were individually dissected and cleaned of connective tissue. RNA was reverse transcribed using Platinum II *Taq* DNA Polymerase (Invitrogen) using the following gene specific primers: TLR5 (AB208697) 5'-GGCCATAGTCAGATCGCATTCTTGC-3'and 5'-GATCAATGGCCTTCAAGGAATTCAG-3', amplicon size 223 bp (Shinkai et al., 2006), IL-1R1 (XM005662366) 5'- ACGGGTCCACCTCTAACTCA-3' and 5'-CAGCAATGCTTTCCCCAACG-3', amplicon size 123 bp and glyceraldehyde-3-phosphate dehydrogenase (GAPDH; AF017079) 5'- GATGGTGAAGGTCGGAGTGAACGG-3'and 5'-CCTGGAAGATGGTGATGGGATTTCC-3', amplicon size 231 bp (Ostedgaard et al., 2011). Annealing temperature was 58°C. Negative controls were performed by omitting the MMLV reverse transcriptase enzyme (Ambion) in the RT reaction or omitting the input cDNA in the PCR reaction. The positive control was lung parenchyma for TLR5 (Ostedgaard et al, 2011) and heart muscle for IL-1R1 (Zitta et al., 2010). PCR was held at 94°C for 2 min and cycled 40 times. Each cycle consisted of 94°C for 30 s (denaturation), 58°C for 30 s (annealing), and 72°C for 1 min (extension). This was followed by a 10 min final extension at 72°C. PCR products were visualized on an ethidium bromide-stained 2% agarose gel under ultraviolet illumination. The product of the PCR was extracted from the gel and sequenced (Pure Link gel

extraction kit, Invitrogen). The amplified product matched the DNA sequence for TLR5 and IL-1R1 from *Sus scrofa* Blast database.

Confocal Immunofluorescence

Freshly-dissected submucosal glands from pig trachea were fixed in 4% paraformaldehyde overnight at 4° C. After washing in PBS (3 × 5 min) submucosal glands were incubated with antibodies for confocal immunofluorescence. The following antibodies were applied sequentially: 1) polyclonal rabbit antibody anti-human (pig reactive) lysozyme, (Lyz; 12 mg/L; Abcam, Cambridge, MA, USA) applied overnight at 4 °C; 2) FITC-conjugated secondary antibody against rabbit (1:100; Abcam) applied for 1 hr at RT; 3) polyclonal rabbit anti-human (pig reactive) interleukin 1 receptor type 1 (IL-1R1; 1:100; Santa Cruz Biotechnology Inc., Dallas, TX, USA) applied for 1hr at 37 °C; 4) Texas Red-conjugated secondary antibody against rabbit (1:100; Abcam) applied for 1hr at RT. Antibodies were diluted in PBS containing 1 % BSA (Sigma) and 0.5 % Triton X-100 (Sigma). After each incubation, the samples were washed in PBS (3 × 5 min). Samples were covered with the anti-photobleaching mounting medium Vectashield with DAPI (Vector Laboratories, Burlingame, CA, USA) and viewed with a confocal microscope (LSM 510 Confor 2, Carl Zeiss, Oberkochen, Germany) equipped with diode (405nm), argon (488nm), and helium/neon (543 nm) lasers. Tissue was scanned in optical sections using LSM510/ConfoCor2 (Version 3.2 SP2) software (Zeiss). In control experiments pre-incubation with either blocking peptide or omission of the primary antibody resulted in complete abolition of staining. In control experiments blocking peptide for IL-1R1 (Santa Cruz Inc.) was pre-incubated with primary

antibody (5 μg peptide/1 μg antibody) overnight at 4° C before application. Image processing was performed using Adobe Photoshop CS5 software.

Reagents

CFTRinh172, IL-1β, and flagellin from *Salmonella typhimurium* were obtained from Cedarlane Labs (Burlington, ON, CA). A stock solution of CFTRinh172 was dissolved in DMSO. The final concentration of DMSO was less than 0.1%. The solution of IL-1β and flagellin were dissolved directly in Krebs solution.

Statistics

Data sets displaying normal distribution are presented as means ± SEM while other data sets are presented as median and scatter plot. The data were tested for normality using Kolmogorov-Smirnov test and the variances were tested using F test for unequal variances. Those data sets that showed normal distribution and variances were not different were analyzed using Student's t-test or ANOVA as appropriate. Other data sets were analyzed using the non-parametric paired test, Wilcoxon signed-rank test. Analysis was performed using GraphPad Prism 5 (GraphPad Software Inc., San Diego, CA, US). All statistical analysis were two-tailed and differences were considered significant when $p < 0.05$.

2.4 Results and Discussion

Our novel synchrotron-based method to measure the height of the airway surface liquid layer covering the epithelium lining the lumen of intact, isolated swine trachea takes advantage

of the large difference in refractive index between the air and the airway liquid layer, which produces a strong signal at the air-liquid interface using phase contrast imaging (PCI, Fig. 2.1a) (Lewis et al., 2005; Morgan et al., 2013; Parsons et al., 2008; Siu et al., 2008). The position of the tissue was determined using agarose beads (Cash et al., 1979; Chmiel et al., 2002) that come into direct contact with the surface epithelium (Fig. 2.S1). The height of the ASL layer was measured as the distance between the air-liquid interface and the edge of the agarose bead touching the surface epithelium (Fig. 2.1b and Fig. 2.S1) by a researcher blinded from the experimental conditions. Preliminary experiments showed that beads larger than 100 μm do not migrate during experimentation due to mucociliary clearance. In our experiments we use beads larger than 200 μm.

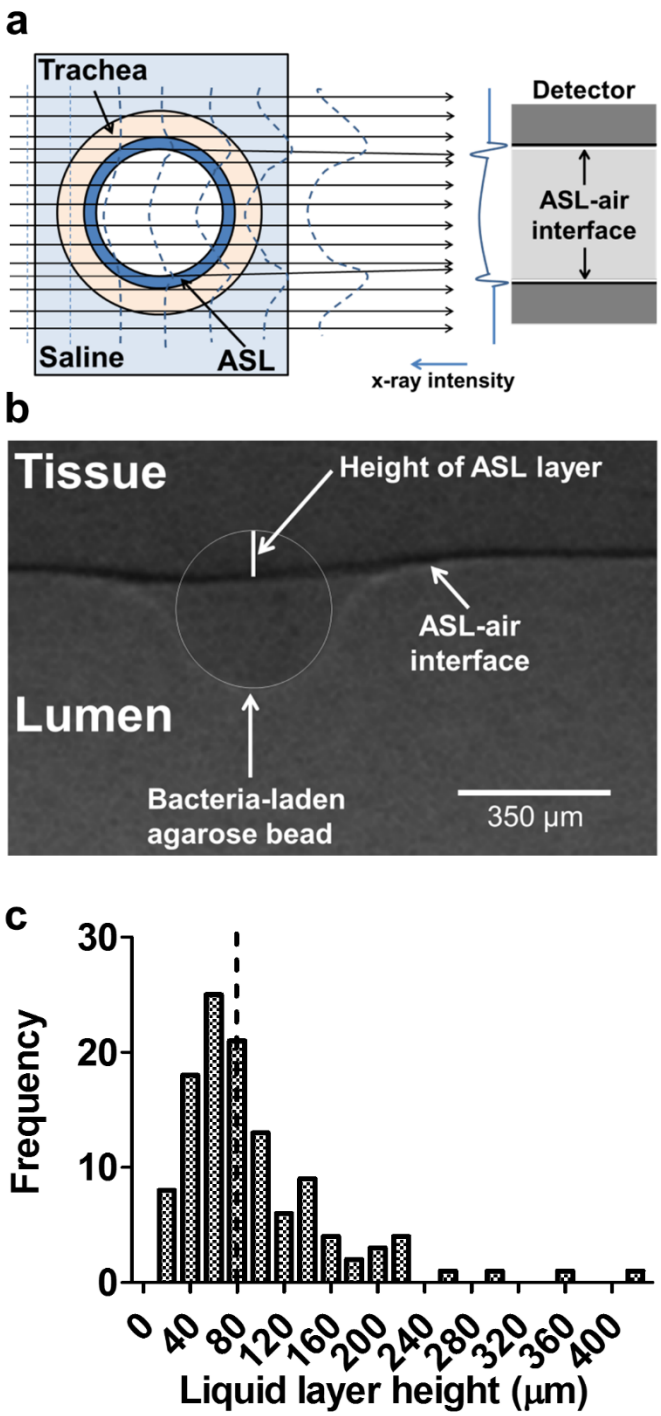

Fig. 2.1. Synchrotron-based phase contrast imaging. (a) Schematic showing the detection of ASL–air interface in the lumen of an intact trachea using PCI. The synchrotron provides a sufficient amount of parallel spatial coherence X-ray to enhance the contrast between air and ASL using PCI. When X-rays pass through the preparation, the difference in refractive index between ASL and air results in a phase shift of X-rays that causes an interference pattern shown on the detector as variations in X-ray intensity. Since the ASL refractive index is

very similar to that of the tissue, PCI cannot resolve the ASL–tissue interface. Thus, we use agarose beads to detect the position of the tissue with respect to the ASL–air interface. (b) Measurement of ASL height in an intact trachea as the distance between the ASL–air interface (arrow) and the edge of the agarose bead touching the surface epithelium by a researcher blinded to the experimental conditions. The agarose bead sits in the ASL layer, and the border of the agarose bead is highlighted. The distance from the bottom of the agarose bead to ASL–air interface is used to measure the height of the ASL layer. The measured height of the ASL layer in this experiment is 115 μm. (c) Frequency distribution and median (dotted line) of ASL height in control tracheas exposed to agar beads containing no bacteria for 5 min; n = 117 agarose beads obtained from tracheal preparations from 39 pigs.

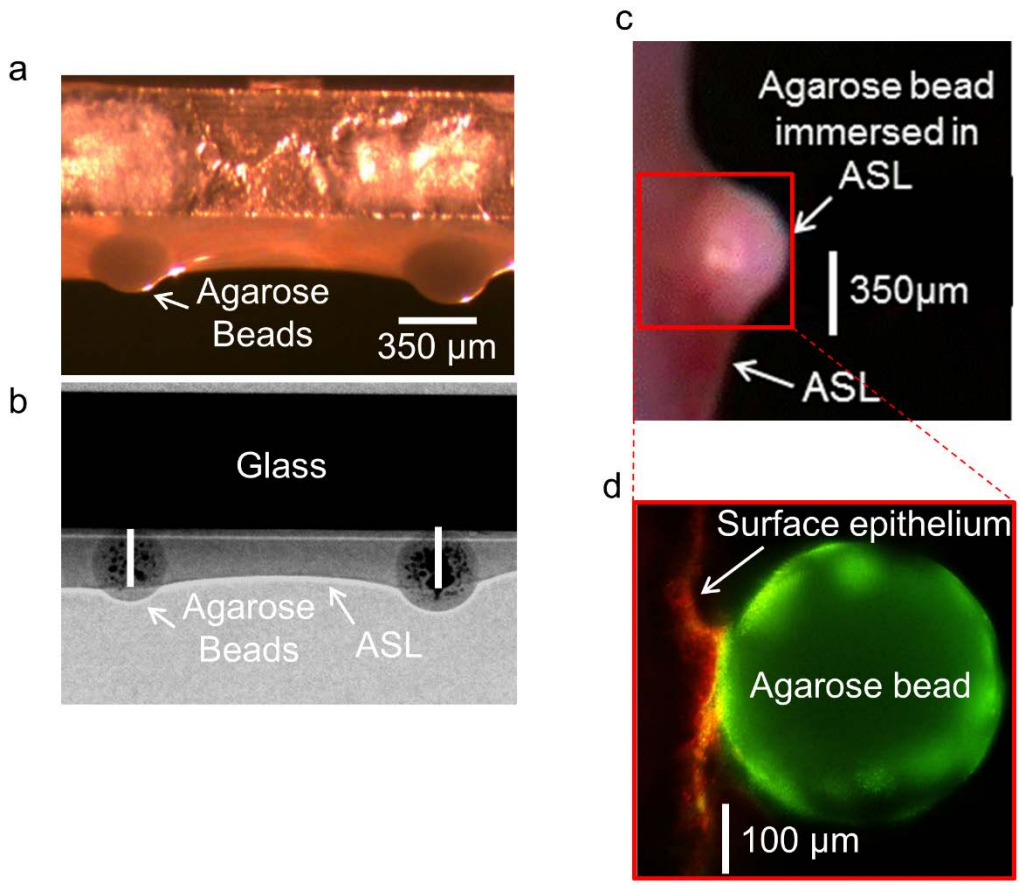

Fig. 2.S1. Agarose beads come into direct contact with the surface epithelium. The agarose beads that we use for measuring airway surface liquid (ASL) layer height must be positioned at either the top or the bottom of the preparation, where the ASL–air interface is parallel to the X-rays reaching the sample. The position of the beads in the ASL depends on the forces acting on them (i.e., gravity, surface tension, and buoyancy); however, buoyancy is a minor force acting on the beads, because the beads are loaded with X-ray–absorbing salts with high molecular weight, and the density of the beads exceeds that of the ASL (1.3 g cm^{-3} vs.1 g cm^{-3}) (Lee et al., 2011). As a result, the position of the beads is determined largely by gravity and surface tension. Beads located at the bottom of the preparation are subject to both gravity and surface tension pushing them against the tissue. For beads located at the top of the preparation, gravity and surface tension will have opposing effects, with surface tension pushing the beads against the tissue and gravity pulling away from the tissue. (a and b) Mathematically calculating whether surface tension will be sufficient to push the beads against the tissue is difficult; thus, we directly tested whether the surface tension of the ASL is sufficient to force the beads located at the top of the preparation up against the tissue. To this end,

we placed ASL collected from swine trachea on the underside of a cover glass and immersed agarose beads in it, then imaged the preparation with light microscopy (a) and synchrotron-based phase-contrast imaging (b). In this preparation, gravity is pushing the beads away from the cover glass, and surface tension of the ASL is pulling them toward the glass. The images show that the beads are touching the glass cover, indicating that surface tension is greater than gravity. To further test whether the force of gravity affects the position of the beads in the ASL, and thus the ASL height measured, we compared the ASL height measurements obtained from beads placed at the top of the preparation and those placed at the bottom. If the force of gravity was pushing the beads away from the epithelium, we would expect to see smaller ASL height measurements obtained from beads located at the top of the preparation compared with those obtained from beads at the bottom of the preparation. Our analysis found no significant differences in ASL measurements from beads at the top and beads at the bottom. (c) Scatterplot and median ASL height measured with beads placed at the top and bottom of the preparation ($n = 132$ for top and $n = 51$ for bottom; $P = 0.19$, Mann–Whitney test). Thus, the results suggest that the force of gravity does not influence our measurements (i.e., ASL surface tension is greater than gravity) and that the measured height of the ASL is not dependent on the position of the beads. We performed a final test of whether the beads are in direct contact with the surface epithelium by labeling the beads with FITC and labeling the surface epithelium with Rhod-2-AM. A piece of trachea was dissected, as described for secretion assays. The mucosal side was incubated in PBS containing Rhod-2-AM (50 μM) and pluronic F-127 (0.1%) for 30 min, then washed with PBS and dried with a stream of air while the serosal side was incubated in Krebs solution. The preparation was then stimulated with carbachol (1 μM on the serosal side) for 20 min, to stimulate ASL secretion by the submucosal glands. The FITC-labeled agarose beads were then placed in the ASL, and the preparation was viewed under a two-photon excitation microscope. (d) With the aid of a dissecting microscope, we verified that the beads were immersed in the ASL. (E) The two photon microscope images showed that the beads (green) and surface epithelium (red) were in direct contact (yellow, $n = 47$ repetitions).

The ASL height on the surface of untreated epithelia showed heterogeneity, as previously described using electron microscopy (Sims and Horne, 1977). The ASL layer height ranged from 16 to 400 µm with a median height of 77 µm, consistent with previous reports of average ASL heights ranging from 3 to 100 µm depending on species and state of the airway (Fig. 2.1e; Worthington and Tarran, 2011).

To test the effect of *P. aeruginosa*, agarose beads were loaded with bacteria and instilled in the trachea preparation for 35 min. Exposure of the trachea to bacteria-free agarose beads for 35 minutes produced a small but significant increase in the height of the ASL (Fig. 2.2a). However, when tracheas were exposed to *P. aeruginosa*-laden agarose beads, ASL secretion was much greater (Figs. 2.2b, c). In contrast, tracheal preparations that had been pre-incubated for 30 min with the CFTR blocker, CFTRinh172 (100µM), failed to respond to *P. aeruginosa* (Figs. 2.2d, e, f), indicating that *P. aeruginosa* triggered CFTR-dependent ASL secretion in the airways.

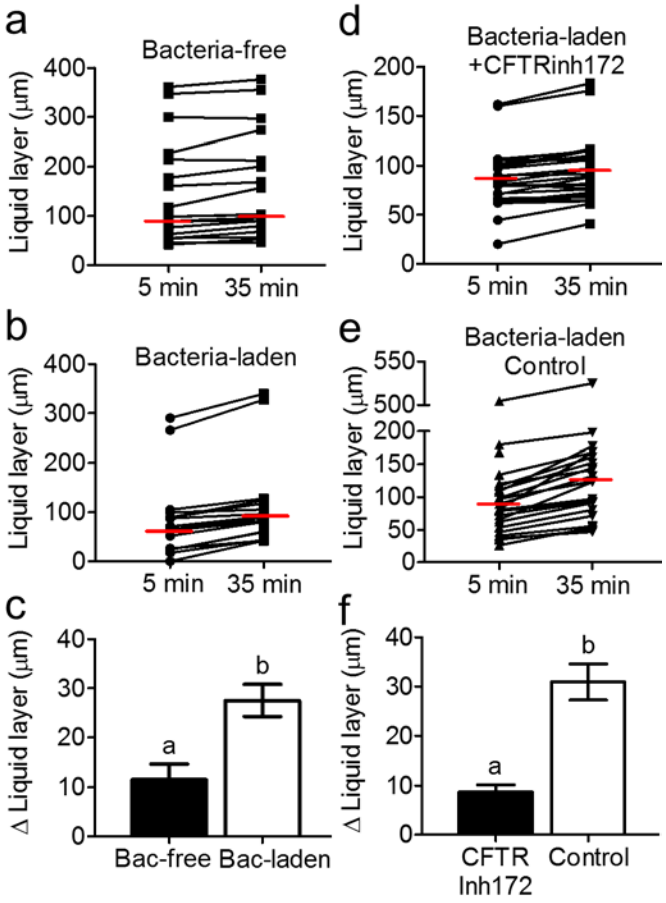

Fig. 2.2. Bacteria stimulate ASL secretion (a–c), which is inhibited by CFTRinh172 (d–f). (a and b) Scatterplot and median of ASL height in tracheas exposed to bacteria-free (a) and *P. aeruginosa*-laden (b) agarose beads. The median ASL height increased from 99 µm to 103 µm after a 35-min incubation with bacteria-free agarose beads (n = 18) and from 66 µm to 89 µm after a 35-min incubation with bacteria-laden agarose beads (n = 19) ($P < 0.05$, Wilcoxon signed-rank test). (c) Average increase in ASL height triggered by bacteria-laden (n = 19) and bacteria-free (n = 18) agarose beads ($P < 0.05$, Student t test). Columns labeled with different letters differ significantly). (d) Scatterplot and median values of ASL heights of tracheal preparations incubated for 30 min with CFTRinh172 (100 µM) before exposure to *P. aeruginosa*-laden agarose beads. The median ASL height did not change after a 35-min incubation with bacteria-laden agarose beads in CFTRinh172-treated preparations (n = 26; $P > 0.05$, Wilcoxon signed-rank test). The cartilage surrounding the trachea was dissected out to ensure access of the blocker. (e) Scatterplot and median values of ASL heights of tracheas that underwent the same surgical

procedure as tracheas in D and before exposure to *P. aeruginosa*-laden agarose beads. The median ASL height increased from 86 μm to 143 μm after a 35-min incubation with bacteria-laden beads ($n = 26$; $P < 0.05$, Wilcoxon signed-rank test). (f) Average increase in ASL height triggered by bacteria-laden beads in CFTRinh172-treated and untreated controls ($n = 26$ for both CFTRinh172 and controls; $P < 0.05$, Student t test). Columns labeled with different letters differ significantly.

Most of the ASL secreted in the upper airways is produced by the submucosal glands, with a smaller contribution from surface epithelium cells (Reid, 1960). To test whether the ASL produced in response to bacteria comes from submucosal glands, we surgically removed the glands from halves of tracheas and compared the ASL secretion with the halves containing glands. The segments of the tracheas containing submucosal glands secreted more fluid in response to *P. aeruginosa* (Fig. 2.3a), thus indicating that most of the ASL produced in response to bacteria comes from the submucosal glands. Thus, the composition of the ASL secreted in response to *P. aeruginosa* may be similar to the fluid secreted by the submucosal glands, i.e. containing 94 mM Na^+, 92 mM Cl^-, pH 6.97 and many proteins including mucins, lysozyme, siderocalin, HSC-71, α-1-antitrypsin and α-1-antichymotrypsin (Jayaraman et al., 2001; Joo et al., 2004).

To test whether the response to the bacteria involved all glands in the preparation or just those in close proximity to the bacteria, we developed a method, based on K-edge subtraction (Rubenstein et al., 1986), that allowed us to distinguish bacteria-laden and bacteria-free beads in the same preparation (Fig. 2.3b). When we instilled both *P. aeruginosa*-laden and bacteria-free agarose beads in a trachea, the bacteria-laden beads showed a much larger increase in ASL height after 35 min incubation (Fig. 2.3c). These results indicated that the response to *P. aeruginosa* was not a general response affecting all glands, but rather a local response by submucosal glands adjacent to the bacteria (Wine, 2007; Ianowski et al., 2008).

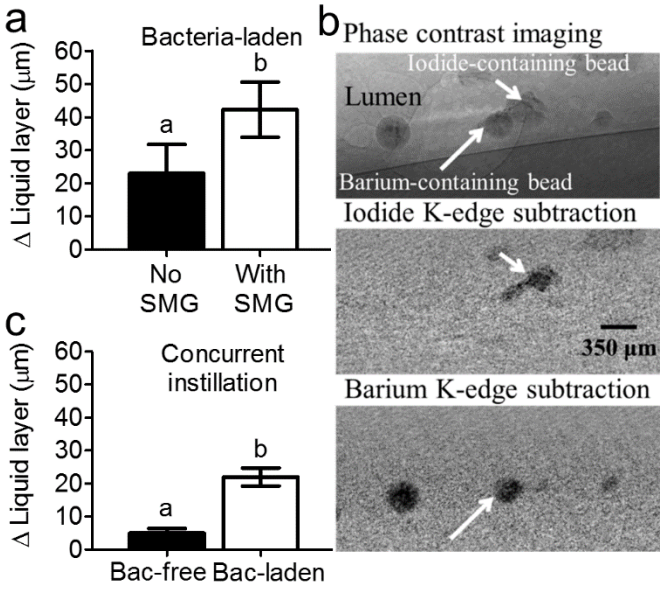

Fig. 2.3. Submucosal glands are major contributors to bacteria-stimulated ASL secretion. (a) Tracheas with submucosal glands (SMG) surgically removed produced less fluid than tracheas with intact SMG (n = 13 with SMG and n = 11 without SMG; $P < 0.05$, Student t test). Columns labeled with different letters differ significantly). (b) Bacteria-free and *P. aeruginosa*-laden agarose beads were differentially labeled with barium or iodine and detected using K-edge subtraction. ASL height was measured at each individual bead by a researcher blinded to the experimental conditions. Only bacteria-laden beads showed increases in ASL after a 35-min incubation. On average, there were eight agarose beads per trachea, and the average distance between beads was 1.6 mm. (c) Increase in ASL height after a 35-min concurrent instillation of bacteria-free and *P. aeruginosa*-laden agarose beads (n = 23 for both groups; $P < 0.05$, Student t test). Columns labeled with different letters differ significantly.

The detection of *P. aeruginosa* by the nasal epithelial cell line CF15 requires the expression of flagellin, an abundant bacterial structural protein (Hybiske et al., 2004). We therefore tested the effect of *P. aeruginosa* mutant strain PAKΔfliC, which lacks flagellin. PAKΔfliC failed to stimulate ASL secretion in swine trachea, compared to the wild-type PAK strain (Fig. 2.4a). In addition, agarose beads loaded with flagellin produced similar ASL secretion as PAK (Fig. 2.4a). These results suggest that *P. aeruginosa* must express flagellin in order to stimulate ASL secretion.

Direct addition of flagellin (10 ng/ml) to the serosal side, i.e. in direct contact with the submucosal glands, did not stimulate secretion, while addition of the proinflammatory cytokines IL-1β did (50 ng/ml, Fig. 2.4b, Baniak et al., 2012). These results suggest that flagellin does not directly stimulate submucosal glands to trigger ASL secretion but that it may bind to toll-like receptor-5 (TLR5) in the surface epithelia lining the lumen of the airways and trigger one or more paracrine signals such as IL-1β, which, in turn, stimulate submucosal gland ASL secretion (Illek et al., 2008). Consistent with this hypothesis, TLR5 expression was detected in surface epithelia but not in the submucosal glands using RT-PCR (Fig. 2.4c). In addition, RT-PCR shows that submucosal glands express IL-1β receptor, IL-1R1 (Fig. 2.4f). IL-1R1 immunostaining colocalizes with lysozyme, a marker for serous cells that are the driving force for submucosal gland secretion (Fig. 2.4e). If flagellin does trigger the release of paracrine signals to the submucosa, these signals should accumulate in the solution bathing the submucosa. To test this hypothesis, we used a modified airway submucosal gland secretion assay preparation with intact surface epithelia. We incubated the surface epithelia with *P. aeruginosa* (PAK or PAKΔfliC) or PBS for 35 minutes and then collected the Krebs solution

bathing the serosal side of the preparation. We tested the effect of the collected fluid on submucosal gland secretion using a secretion assay. The liquid collected from preparations incubated with PAK stimulated significantly greater submucosal gland secretion than the liquid collected from those incubated with PAKΔfliC or PBS (Fig. 2.4d). Thus, the results suggest that flagellin shed by inhaled *P. aeruginosa* bind TLR5 expressed by the surface epithelium cells (Lambrecht and Hammad, 2012) triggering the release of proinflammatory cytokines into the submucosa within few minutes (Reiniger et al., 2007). The cytokines diffuse from the surface epithelium to the glands located ~150 µm away (Kreda et al., 2005; Ostedgaard et al., 2011) stimulating CFTR-dependent ASL secretion (Baniak et al., 2012). Flagellin will also induce mucin expression within 18-24 h and further contribute to bacteria clearance (Ben Mohamed, 2012; Li et al., 1998).

Pseudomonas aeruginosa is not the only bacteria encountered by CF patients. Other pathogens such as *Staphylococcus aureus* and *Haemophilus influenzae* may appear in the airways before *P. aeruginosa*. Thus, we tested whether the airways responded to instillation of *S. aureus*- and *H. influenzae*-laden agarose beads. The results show that both of these pathogens triggered CFTR-dependent ASL secretion (Fig. 2.4g and h). Interestingly, these bacteria do not express flagellin, suggesting that there may be other pattern recognition receptor pathways involved in triggering CFTR-dependent ASL secretion.

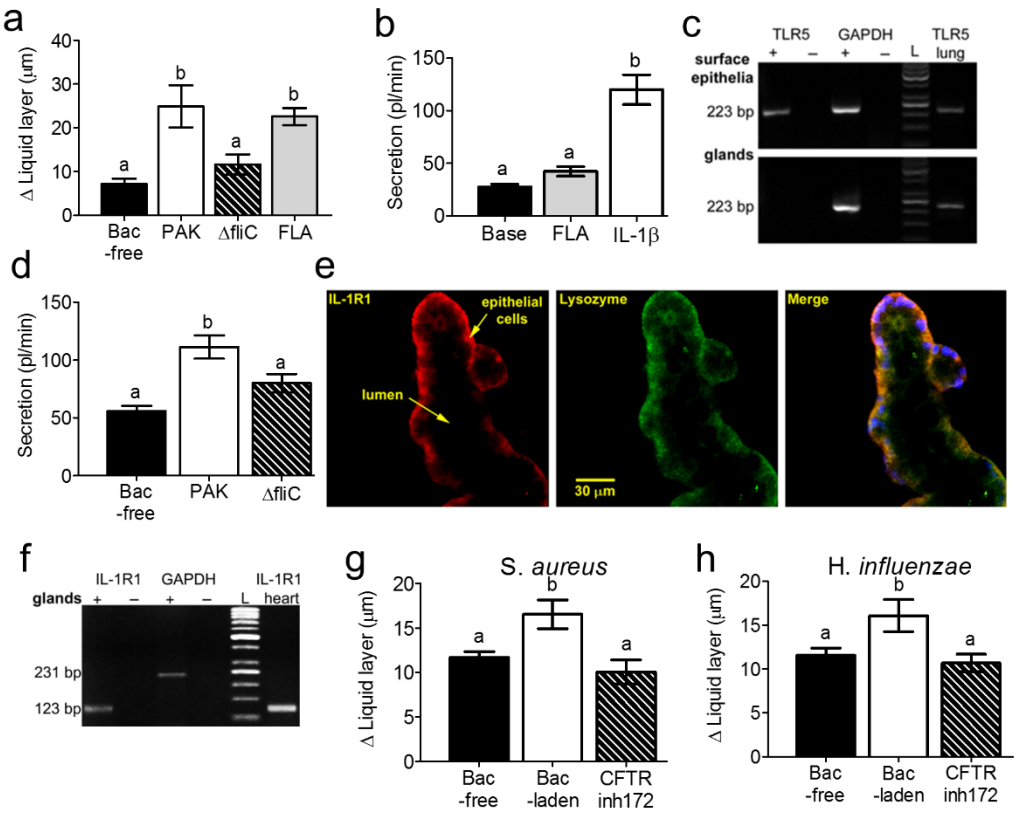

Fig. 2.4. *P. aeruginosa*-triggered ASL secretion requires expression of flagellin. (a) PAKΔfliC-laden agarose beads produced less ASL than PAK-laden agarose beads, and flagellin-laden (10 ng/mL) agarose beads (FLA) triggered a similar response as PAK-laden beads (n = 12 bacteria-free, n = 7 PAK, n = 10 PAKΔfliC, and n = 15 FLA; $P < 0.05$, ANOVA and Bonferroni's multiple comparison test). Columns labeled with different letters differ significantly. (b) Secretion assay data shows that the addition of flagellin (10 ng/mL) to the Krebs solution bathing the submucosal glands did not stimulate ASL secretion, whereas the addition of IL-1β (50 ng/mL) did (n = 10 for flagellin and n = 9 for IL-1β; $P < 0.05$, ANOVA and Bonferroni's multiple comparison test). Columns labeled with different letters differ significantly. (c) Airway surface epithelia (Upper) express the flagellin receptor TLR5, whereas submucosal glands do not (Lower). The lung is a positive control for TLR5, and + and – indicate RT positive and negative, respectively. (d) The Krebs solution bathing the submucosa of trachea preparations incubated with *P. aeruginosa* strain PAK on the mucosal side stimulated ASL secretion in a secretion assay, whereas PAKΔfliC and PBS did not (n = 9 for all groups; $P < 0.05$, ANOVA and Bonferroni'smultiple comparison

test). Columns labeled with different letters differ significantly. (e) Confocal immunofluorescence of IL-1β receptor IL-1R1 (Left), lysozyme (Middle), and both merged (Right) in submucosal glands. The images show that IL-1R1 is colocalized with lysozyme, a marker for serous cells. (f) Airway submucosal glands express IL-1R1. The heart is a positive control for IL-1R1, and + and − indicate RT positive and negative, respectively. (g and h) Bacteria-triggered ASL secretion is not limited to *P. aeruginosa*. Both *S. aureus* (g) (n = 8 bacteria-free, n = 10 *S. aureus*, and n = 12 *S. aureus* + CFTRinh172; $P < 0.05$, ANOVA and Bonferroni's multiple comparison test) and *H. influenzae* (h) stimulate ASL secretion that is inhibited by CFTRinh172 (n = 19 bacteria-free, n = 11 *H. influenzae*, and n = 10 *H. influenzae* + CFTRinh172; $P < 0.05$, ANOVA and Bonferroni's multiple comparison test). Columns labeled with different letters differ significantly.

Our results are the first demonstration that bacteria-triggered, CFTR-dependent ASL secretion is part of the normal innate immune response to inhaled bacteria. CFTR is required for normal fluid secretion, which washes mucins and antimicrobial compounds from the submucosal glands into the airway lumen (Ianowski et al., 2007; Joo et al., 2010; Joo et al., 2002; Wine, 2007; Martens et al., 2011; Baniak et al., 2012; Reid, 1960; Ianowski et al., 2008). The loss of CFTR-mediated fluid secretion reduces ASL secretion, supporting the hypothesis that CFTR mutations lead to reduced secretion of antimicrobial compounds and mucins into the lumen of the airway which facilitate chronic infection and inflammation (Pezzulo et al., 2012; Sun et al., 2010; Cho et al., 2011; Meyerholz et al., 2010). Eventually the airway undergoes remodeling, including goblet cell hyperplasia, and more severe pathologies such as mucus hypersecretion (Stoltz et al., 2010). These results suggest that the progression of cystic fibrosis airway disease may be ameliorated by treatments that improve the response of the airways to inhaled bacteria, such as prophylactic antibiotic treatment. In addition, abnormal ASL secretion in response to microbes may contribute to other pathological conditions such as COPD and asthma where airway remodeling occurs and responses to microbes could be blunted (Matkovic and Miravitlles, 2013).

Finally, the synchrotron-based technique we have developed is applicable to living animals (Luan et al., 2013), thereby making it possible to study the response to bacteria in animal models of CF *in vivo* and the effect of treatments such as CFTR trafficking correctors.

Chapter 3

Cystic fibrosis swine fail to secrete airway surface liquid in response to inhalation of pathogens

Citation: Luan X, et al. (2017) Cystic fibrosis swine fail to secrete airway surface liquid in response to inhalation of pathogens. *Nat Commun* 8(1):786.

Disclaimer: Manuscript has been reformatted for consistency with the dissertation, including some rearrangement. References have been moved to the end of the dissertation as per CGSR requirements. No other content has been changed.

3.1 Abstract

Cystic fibrosis is caused by mutations in the gene encoding the cystic fibrosis transmembrane conductance regulator channel, which can result in chronic lung disease. The sequence of events leading to lung disease is not fully understood but recent data show that the critical pathogenic event is the loss of the ability to clear bacteria due to abnormal airway surface liquid secretion. However, whether the inhalation of bacteria triggers airway surface liquid secretion and whether this is abnormal in cystic fibrosis has never been tested. Here we show, using a novel synchrotron-based *in vivo* imaging technique, that wild-type pigs display both a basal and a toll-like receptor-mediated airway surface liquid secretory response to the inhalation of cystic fibrosis relevant bacteria. Both mechanisms fail in $CFTR^{-/-}$ swine, suggesting cystic fibrosis airway do not respond to inhaled pathogens, thus favoring infection and inflammation that may eventually lead to tissue remodeling and respiratory disease°

3.2 Introduction

Cystic fibrosis (CF) is an autosomal recessive genetic disorder caused by mutations in *CFTR* gene. Although CF is a multisystemic disease, much of the morbidity and mortality arises from lung disease (Stoltz et al., 2015). CF patients can develop chronic bacterial pulmonary infections and inflammation that may eventually cause end-stage lung disease. However, the sequence of events that result in lung disease from cystic fibrosis transmembrane conductance regulator (CFTR) mutations is not fully understood. Recent data show that the first outcome of CFTR mutation is an impaired ability to eliminate bacteria. Lungs from CF animal models (F508del and $CFTR^{-/-}$ pigs) (Ostedgaard et al., 2011; Stoltz et al., 2010) fail to purge bacteria as effectively as wild-type littermates before the development of inflammation (Stoltz et al., 2010; Pezzulo et al., 2012). These results suggest that impaired bacterial elimination is the pathogenic event initiating a cascade of inflammation and pathology in CF lungs (Stoltz et al., 2010).

The failure to clear bacteria seems to result from abnormal airway surface liquid (ASL) layer in the CF lung (Sun et al., 2010; Joo et al., 2010; Joo et al., 2002; Ianowski et al., 2007). The ASL is a complex mixture of water, salts, gel-forming mucins, and antimicrobial compounds that contribute to trapping, inactivating, killing, and clearing pathogens through mucociliary clearance (Knowles and Boucher, 2009; Smith et al., 1996; Roy et al., 2014). Airway samples from CF patients (Joo et al., 2002), 1-day old $CFTR^{-/-}$ piglets (Joo et al., 2010), newborn $CFTR^{-/-}$ ferrets (Sun et al., 2010), and $CFTR^{-/-}$ mice (Ianowski et al., 2007) fail to respond to stimulatory signals that normally elicit strong ASL secretion (Wine, 2007;

Widdicombe and Wine, 2015; Ballard and Inglis, 2004; Baniak et al., 2012), suggesting that CF airway would fail to respond to inhaled insults (Sun et al., 2010; Joo et al., 2010; Joo et al., 2002; Ianowski et al., 2007). It has therefore been proposed that CF airway may fail to secrete ASL in response to bacterial inhalation, thus reducing the amount of antimicrobial compounds and mucin available in the airway, compromising mucociliary clearance and facilitating infection and inflammation (Pezzulo et al., 2012; Joo et al., 2010; Joo et al., 2002; Ianowski et al., 2007; Baniak et al., 2012; Marten et al., 2011; Ianowski et al., 2008). However, whether inhalation of bacteria triggers ASL secretion and whether this response is abnormal in CF lungs, has never been tested. We used $CFTR^{-/-}$ swine (gut-corrected $CFTR^{-/-}$, see "Materials and Methods" section) to study how CF airway respond to inhalation of bacteria *in vivo*, where all components of the regulatory mechanisms are intact, i.e., autonomic (Wine, 2007), sensory efferent (Widdicombe and Wine, 2015), and immune signals (Ballard and Inglis, 2004; Baniak et al., 2012). Our results show that there are a basal and a bacteria-triggered TLRs-related ASL secretory responses in the airway of wild-type swine. Both responses are missing in $CFTR^{-/-}$ swine, which do not display basal secretion nor respond to inhalation of *Pseudomonas aeruginosa*. The results suggest the missing ASL secretory responses in CF airway leads to bacteria clearance failure, which further results in facilitating infection and inflammation.

3.3 Materials and Methods

Animals

We used gut-corrected $CFTR^{-/-}$ swine purchased from Exemplar Genetics (Iowa, USA) and wild-type swine from Prairie Swine Center (University of Saskatchewan) that served as

controls.

A sow implanted with cloned embryos with the gut-corrected CFTR$^{-/-}$ genotype (CFTR$^{-/-}$;*TgFABP* > *p*CFTR pigs) (Stoltz et al., 2013) was purchased from Exemplar Genetics. The sow was housed at the Western College of Veterinary Medicine Animal Care Unit, University of Saskatchewan, for 4 weeks before due date to allow the sow to acclimate to the new environment and reduce stress during delivery. To reduce exposure to bacteria in the birth canal and to minimize the stress of natural birth on the piglets, the delivery was done through a cesarean section performed by a specialized veterinary surgeon team to ensure minimal exposure of the piglets to anesthetics.

The sow delivered 11 male piglets of normal weight (Table 3.S1). Each newborn animal was identified with a number and monitored 24 h a day. Food intake, urination, passing and consistency of feces, temperature, weight, respiratory function, O_2 saturation, body condition, and responsiveness were recorded for each piglet (Table 3.S1). Animal number 11 showed reduced O_2 saturation at birth that did not improve. Thus we decided to image it (this data was not included in our data set), and euthanized the animal 12 h after birth. Animals 3, 4, 5, 7, and 10 started to display deterioration of health status 48 h after birth, so we decided to image the animals and euthanized them. Animals 2, 6, and 8 displayed health deterioration 5 days after birth; thus, we imaged and euthanized the animals. Animals 1 and 9 reached the end of the experimental period at day 7 after birth. The control experiments were performed using 7 days old wild-type swine 3– 5 kg in weight (Prairie Swine Center, University of Saskatchewan). For *ex vivo* experiments, tracheas from CFTR$^{-/-}$ and wild-type animals where dissected within 15-30 minutes of euthanasia, clamped, and placed in ice-cold Krebs-Ringer solution (mM): 115

NaCl, 2.4 K_2HPO_4, 0.4 KH_2PO_4, 1.2 $CaCl_2$, 1.2 $MgCl_2$, 25 $NaHCO_3$, 10 glucose (pH=7.4) equilibrated with 95% O_2, 5% CO_2 until used. All experiments were performed within 18 h after euthanasia. All of the experiments were performed under the approvals of the Canadian Light Source and the Animal Ethics Committee of the University of Saskatchewan.

Analysis of CFTR expression in the gut

The CFTR expression correction in the gut of gut-corrected $CFTR^{-/-}$ swine piglets was tested by qPCR analysis as described before (Stoltz et al., 2013). Gut tissue (from pig #7 and a wild-type pig) was dissected, flash frozen in liquid nitrogen, and stored at -80^{o}C. The samples were later thawed in RNA-Ice (Ambion Cat # AM7030) overnight. Approximately 120-150 mg of the thawed tissue was used to extract total RNA using the Purelink RNA mini kit (Ambion Cat# 12183025). RNA quality was checked on a BioAnalyzer (Agilent) to ensure that RNA templates used in downstream applications had a RIN > 8.0 and was not contaminated with genomic DNA. First strand cDNA was synthesized from approximately 1µg of total RNA using random primers provided in the Superscript IV First Strand Synthesis Kit (ThermoFisher Cat# 18091050). RT-qPCR reactions were carried out using Taqman expression assays and probes (CFTR: Ss3389420_m1, β actin: Ss03376160_u1, ThermoFisher) previously used to measure CFTR mRNA levels in the $CFTR^{-/-}$ pigs (Stoltz et al., 2013). qPCRs were done on a CFX96 thermocycler (BioRad) and analyzed using the CFX manager software. Samples were run in quadruplicates.

qPCR results showed that CFTR mRNA levels (normalized to *β-actin*) in the gut of pig#7 was 23.29% that of wild-type (Fig 3,S1), which is consistent with what has been previously

reported (Stoltz et al., 2013).

Pathology analysis of CFTR$^{-/-}$ swine

After euthanasia, the carcasses were subjected to pathology analyzes by a board-certified veterinary pathologist. Gross examinations were conducted on each carcass. Tissues included brains (pigs #4, 5, 7, 10, and 11 only), eyes (pigs #4, 5, 7, 10, and 11, only), hearts, spleens, kidneys, livers, and pancreas (pigs #8 and 11 only), small and large intestines were fixed in 10% formalin for haematoxylin and eosin staining and histological examination.

On gross examination (Table 3.S2), the colon and cecum in 7 out of 10 pigs were distended by feces that was firmer than normal (Fig. 3.S2A). Four pigs that were euthanized later in the experiment showed cranioventral consolidation of the lung. Four pigs had gallbladders that were small (hypoplasia) on gross examination. In pig #10, the common bile duct was blocked by a thick mucus plug. Two pigs had increased amount of mucus in their nasal cavities compared to the other pigs (Fig. 3.S2B). On histological examination, the pancreases were hypoplastic (Fig. 3.S2C). Three pigs had evidence of cholestasis. The pneumonia was characterized by severe infiltration of neutrophils mixed with many bacteria in the alveoli and bronchiole (Fig. 3.S2D). Brains, eyes, hearts, spleens, kidneys, small and large intestines were normal histologically.

X-ray Imaging

Experiments were performed at the BioMedical Imaging and Therapy (BMIT) facility, Canadian Light Source (CLS), Saskatchewan, Canada (Wysokinski et al., 2007). All imaging

was done using the Bending Magnet (BM) beamline 05B1-1 endstation. The experimental hutch was located 25.5 meters from the storage ring. Monochromatic x-rays (33.5 keV, λ=0.037 nm for live swine experiments, and 20 KeV, λ=0.062 nm for isolated trachea experiments) were selected using a standard double-crystal monochromator. At the imaging station, the beam size was approximately 100.0 mm horizontal x 6.0 mm vertical. A propagation (sample-to-detector) distance of ~115 cm (*in vivo*) and ~ 65 cm (*ex vivo*) were chosen to enhance the air/ASL layer interface. Images were captured using a charge-coupled device (CCD) detector (C9300-124 Hamamatsu Photonics) with a high resolution X-ray converter (AA-60 Hamamatsu Photonics). The pixel size of the captured image was 8.75 x 8.75 μm. The exposure time for each image ranged from 400 to 600 ms depending on the storage ring current so as to maximize signal-to-noise ratio for image capturing.

Evaluation of agarose beads-epithelium interaction

We used agarose beads as "measuring rods" to determine the height of the ASL layer. ASL height was measured as the distance between the air/ASL interface and the edge of the agarose bead touching the surface epithelia. The validity of our measurement relies on the fact that the agarose beads instilled in the ASL do indeed come into physical contact with the airway surface epithelium and are immobilized (Luan et al., 2014). We therefore conducted a series of experimental tests and theoretical analysis to test whether the beads are in fact immobilized on the surface of the airway epithelia.

Agarose beads immersed in the airway surface liquid are subjected to two major forces that determine the stability of the beads: gravity and the surface tension created by the ASL. At

the dorsal (bottom, in supine position) surface of the trachea, both gravity and surface tension force the beads towards the surface epithelium (see Fig. 3.2c in main text); as a result, the beads are forced against the airway surface epithelium as long as the bead diameter is larger than the ASL thickness.

For the beads placed on the ventral (top) surface of the trachea, gravity acts to pull the bead away while ASL surface tension forces the bead towards the surface epithelium. In this case, the net force on the bead determines whether the bead would come into contact with the airway surface epithelium. We thus decided to produce a mathematical model of the bead-ASL/epithelium interaction to determine whether the beads were in contact with the epithelium under our experimental conditions.

The adhesion force due to surface tension and capillary forces on the bead (Fig. 3.1) can be calculated as: (Schurch et al., 1990; Rapacchietta et al., 1977).

$$F_\gamma = 2\pi R\gamma \sin\phi \sin(\theta + \phi) \qquad 1$$

Where R is the radius of the agarose bead, γ is surface tension of ASL, δ is the height of the ASL layer in the trachea, z_0 is the meniscus depth of ASL due to the capillary effect of liquid around the agarose bead, θ is the contact angle between ASL and agarose.

$$\cos\phi = 1 - \frac{\delta}{R} - \frac{z_0}{R} \qquad 2$$

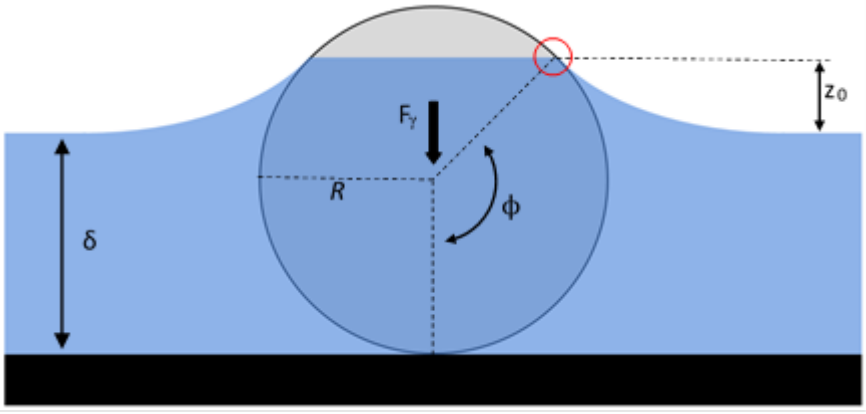

Fig. 3.1. Diagram of an agarose bead immersed in ASL. The diagram shows the force due to surface tension and the capillary forces acting on the bead, and the parameters relevant to Eq. (3). Where R is the radius of the agarose bead, γ is the surface tension of ASL, δ is the height of the ASL layer in the trachea, z_0 is the meniscus depth of the ASL due to the capillary effect of liquid around the agarose bead, θ is the contact angle between the ASL and the agarose. Our analysis shows that under our experimental conditions, the net effect of gravity and surface tension push the beads against the epithelium without causing significant tissue displacement.

From equation #1 and 2:

$$F_\gamma = 2\pi R\gamma \sin\left[\cos^{-1}\left(1-\frac{\delta+z_0}{R}\right)\right]\sin\left[\theta+\cos^{-1}\left(1-\frac{\delta+z_0}{R}\right)\right] \qquad 3$$

To resolve equation 3, we obtained airway fluid surface tension values (γ), previously reported to range from 30 to 34 mN/m (Hamed and Fiegel, 2013). We used the average value of 32 mN/m in our calculations. We measured the contact angle (θ) between the agarose and the ASL using a goniometer (Yuan and Lee, 2013). A droplet of swine trachea ASL was placed on a flat surface of 4% agarose, and the contact angle between the ASL and the 4% agarose was directly recorded to be $44° \pm 1.6°$.

Inputting these values to equation #3, we obtain:

$$F_\gamma = 2\pi R \cdot 32\ \mathrm{mN/m} \cdot \sin\left[\cos^{-1}\left(1-\frac{\delta+z_0}{R}\right)\right]\sin\left[44°+\cos^{-1}\left(1-\frac{\delta+z_0}{R}\right)\right] \qquad 4$$

We can assume for now that z_0 will be small compared to the thickness (averaging 93 μm) of the fluid layer. However, the thinner the ASL is, the more important z_0 becomes. And larger z_0 value would cause larger surface tension on the bead. Since z_0 would have minimal effect in our case, we simplified the force calculation to equation 5, where we underestimate the surface tension generated by ASL.

$$F_\gamma = 2\pi R \cdot 0.032\ \mathrm{N/m} \cdot \sin\left[\cos^{-1}\left(1-\frac{\delta}{R}\right)\right]\sin\left[44°+\cos^{-1}\left(1-\frac{\delta}{R}\right)\right] \qquad 5$$

Now there are only 2 variables; bead radius, R, and ASL layer height, δ.

Supplementary Fig. 3.S3 below shows the change in adhesion force, within the range of ASL thickness observed in swine trachea, 20 to 300 μm, with varying bead size and fluid thickness. The data show that negative adhesion, i.e. the bead would move away from tissue, occurs when the bead is fully submerged in the fluid. In that condition, the surface tension force would be considered nil, and gravity, $G = 4/3\rho\pi r^3$, would force the bead away from the

epithelium. The results show that beads with a range of diameters used in our experiments, 400 to 1000 μm, will touch the epithelium even with an ASL height as little as 2 μm (Supplementary Fig. 3.S3). Thus, under all our experimental conditions, the net effect of gravity and surface tension push the beads against the epithelium.

We also tested whether the forces acting on the agarose beads were strong enough to push the beads into the airway surface epithelium and deform the tissue, which would affect our measurements. The deformation of the trachea surface epithelia caused by the force applied on the tissue is related to the elasticity of the tissue (Van Vlierberghe et al., 2014).

We measured the elasticity of swine trachea by measuring the amount of force required to displace the tracheal tissue (Van Vlierberghe et al., 2014; Tay et al., 2006). The forces that cause varying displacement for trachea fall into a linear function, and the measured spring constant κ of swine trachea was 7.6 N/m. The displacement of tracheal epithelium by beads of varying sizes and and varying ASL layer thickness can be calculated from equation #6 .

$$d = F_{net}/\kappa \qquad 6$$

Where d is the displacement of trachea tissue, F_{net} is the net force on the agarose bead (for the beads at top of trachea, $F_{net} = F_\gamma - G$; for the beads at bottom of trachea, $F_{net} = F_\gamma + G$), and κ is the spring constant of swine trachea we measured.

The results indicate that displacement of airway epithelia by agarose beads would not be larger than 12 μm (Fig. 3.S4 and S5), which is within the range of the error of our measurments. Therefore, tissue displacement is unlikely to affect our measurements of ASL height.

We conducted experimental tests to determine whether the agarose beads in our experiments are in contact with the surface epithelia. Our results show that, as indicated by our

mathematical model, the beads indeed contact the epithelia. Initially, we placed agarose beads in an ASL sample collected from isolated trachea and placed it on the underside of a glass slide. The agarose beads were forced against the glass surface, indicating that the surface tension from the ASL is stronger than gravity and forces the beads up against the glass surface, as predicted by the mathematical model (Fig. 3.S6).

Histological evidence also supports the fact that the agarose beads are in direct contact with the surface epithelia. Agarose beads were instilled into freshy harvested trachea of 1 week old wild-type piglets. The preparations were flash frozen in liquid nitrogen and stored at -80^{o}C. Then, the trachea preparations were cryo-sectioned into 20 μm sections and stained with Nuclear Fast Red (Sigma) for 1 minute, which delineated the airway tissue. The sections were imaged on a light microscope. Histological images (n=11) clearly showed that the agarose beads were indeed in contact with the airway surface epithelium (Fig. 3.S7).

We also tested the prediction that tissue displacement by beads does not affect our measurements of the ASL height. First, if displacement of the tissue by beads did affect our ASL height measurements, one would expect that the ASL heights measured from beads located at the top part of the trachea, where gravity and surface tension act in opposite directions, would be smaller than those obtained from beads located at the bottom part of the trachea, where both gravity and surface tension push the beads into the tissue. Our analysis of the data collected shows that ASL measurements obtained from top and bottom of the trachea were not significantly different (Fig. 3.S8).

In addition, since the tissue displacement depends on bead size (Figs. 3.S4 and S5), we would expect that, if tissue displacement affects our measurements, bead size would influence

the ASL height measured. A small bead would cause less tissue displacement than a larger bead. As such, we should expect a correlation between bead size and the ASL height measured (Fig. 3.S9) or the change in ASL in 30 min (Fig. 3.S10). However, our data showed no such correlations between ASL height or change in ASL and bead size. Indicating that tissue displacement does not affect our ASL measurements.

Thus, using a range of theoretical and experimental evidence, we confirm that beads instilled in the ASL experience sufficient surface tension force that immobilize them against the airway, without significantly deforming the epithelium or affecting ASL measurement.

Preparation of agarose beads

Agarose beads were made in sterile conditions with 4% agarose in PBS as described elsewhere (Luan et al., 2014; Cash et al., 1979; Chmiel et al., 2002). Agarose beads were not only used as vehicles to deliver bacteria into trachea but were also used as "measuring rods" to determine the height of the ASL layer. Insoluble $BaSO_4$ or CuI (1 M) was loaded into the agarose beads to make them visible in x-ray imaging without affecting the osmotic pressure of the beads (Luan et al., 2014). Bacteria-free agarose beads were made from sterile PBS alone; and bacteria-laden agarose beads were made by adding 10% v/v of bacterial stock solution.

P. aeruginosa stock solution was made with a clinical isolate, *P. aeruginosa* (NH57388) (Hoffmann et al., 2005), generously provided by Dr. John Gordon at the University of Saskatchewan. Clinical isolates of *H. influenzae* and *S. aureus* were generously provided by Dr. Joseph Blondeau at the Royal University Hospital, Saskatoon, Saskatchewan, Canada. *E.*

coli DH5-α was provided by Dr. Gordon at the University of Saskatchewan, and *B. subtilis* was purchased from Cedarlane (Burlington, Ontario, Canada).

Aliquots of the *P. aeruginosa* clinical isolate, the *P. aeruginosa* PAK and PAKΔfliC strains, *S. aureus* clinical isolate, and *E. coli* DH5-α were inoculated in Erlenmeyer flasks containing growth media, and incubated for ~24 h at 37ºC with shaking at 170 rpm in an aerobic environment. An aliquot of the *H. influenzae* clinical isolate was incubated for ~24 h at 37ºC with shaking at 170 rpm in an anaerobic environment, and an aliquot of *B. subtilis* was incubated for ~24 h at 26ºC with shaking at 170 rpm in an aerobic environment. All bacterial cultures except *E. coli* and *B. subtilis* were then heat killed (by incubating at 80ºC for 30 min), concentrated by centrifuging, and then stored at -20ºC. Prior to use, pathogen concentrates were thawed and mixed with agarose; whereas non-pathogens (*E. coli DH5-α* and *B. subtilis)* were directly concentrated from bacterial culture aliquots before use.

Experimental set-up

For the *in vivo* experiments, the animal was placed in supine position on a warming pad and anesthetized with 2-2.5% isoflurane in pure medical O_2 through a face mask at an air flow rate of 1 liter per min. Throughout the experiment, the animals breathe spontaneously. Respiratory rate, heart rate, body temperature, and O_2 saturation level as well as the plane of anesthesia were monitored. The agarose beads with diameters ranging from 400 to 1000 μm where instilled into the trachea of the animal using an endotracheal tube. Before inserting the endotracheal tube, the larynx was sprayed with lidocaine to prevent a reflex response to

intubation. The agarose beads were then blot-dried and placed in the endotracheal tube. The endotracheal tube was placed at the opening of the larynx into the trachea and the beads were blown with a puff of air out of the tube and into the trachea, after which the endotracheal tube was immediately removed. Images were taken at 5 and 35 min after the agarose beads were placed in the trachea.

For *ex vivo* experiments (Luan et al., 2014), tracheas were dissected from recently euthanized animals and placed in a custom-built chamber wherein the tissue was immersed in Krebs solution plus 1 μM indomethacin at 35ºC and equilibrated with 95% O_2 and 5% CO_2. The trachea was sealed so that the lumen remained free of the solution but it was accessible for introduction of beads. Agarose beads ranging ~400 to 1000 μm in diameter were blotted dry and placed in the lumen of the airway.

The air-ASL interface can be detected only at the ventral (top) and at the dorsal (bottom) of the trachea, where the direction of the x-rays propagation is parallel to the plane of the air-ASL interface because only these regions generate x-ray phase shifts that produce a strong signal in phase contrast x-ray imaging (Fig. 3.1b). We therefore used a computer-controlled motorized stage to rotate the animal to ensure the beads were positioned appropriately before imaging. The ASL height was measured 5 and 35 min after instillation of the beads. The measurements made at 5 min were interpreted as the original state of ASL, i.e. before exposure to bacteria. We labeled the first time point as 5 min (instead of 0) to reflect the time delay between instillation of the beads and acquisition of the first image.

Both bacteria-free and bacteria-laden beads were instilled in each experiment (*in vivo* and *ex vivo*) to control for differences in response among preparations. We distinguished

bacteria-laden beads from bacteria-free beads using K-edge subtraction that allows us to determine iodine from barium labeled beads (Rubenstein et al., 1986). Iodine K-edge subtraction imaging was performed using monochromatic 33.20 keV and 33.35 keV beams. Barium K-edge subtraction imaging was performed using monochromatic 37.50 keV and 37.65 keV beams.

Secretion assays

A sample of trachea was cut along the trachealis muscle, and the airway submucosa containing the glands was dissected from the cartilage (Luan et al., 2014). This submucosa preparation was placed in a custom built chamber with the serosal side bathed in Krebs solution containing 1 μM indomethacin (Joo et al., 2001). The preparation was maintained at 37ºC and equilibrated with warm, humidified 95% O_2 and 5% CO_2 gas (TC-102, Medical Systems Corp., Greenvale, NY, US). The mucosal side was cleaned, dried with a stream of air, and coated with ~5 μl mineral oil. The ASL secreted by the submucosal glands formed a spherical droplet under the mineral oil. Cytokines interleukins 6 or 8 were added to the serosal side. The droplets of ASL secreted by the glands were imaged every 120s and stored for offline analysis using ImageJ 1.43u (NIH). The volumes of the secreted droplets were calculated assuming a spherical shape ($V = 4/3\pi r^3$) (Joo et al., 2001). The secretion rate was calculated by fitting the volume versus time plots with straight lines using linear regression, and the slopes were taken as the secretion rates using at least four points (Joo et al., 2002).

Surgical removal of the submucosal glands

The cartilage was removed from a tracheal preparation using a scalpel and a blunt-ended elevator (Luan et al., 2014). Once the cartilage was removed, the submucosal glands and other tissue in the submucosa were dissected out by "shaving" with a breakable scalpel blade (Fine Science Tools, Vancouver, Canada). As described previously (Luan et al., 2014), Ussing chamber and secretion assay experiments showed that our procedure allowed us to remove 90% of glands from the trachea without damaging the surface epithelia.

Reagents

CFTRinh-172, SQ22536, and flagellin from *Salmonella typhimurium* were obtained from Cedarlane Labs (Burlington, ON, CA). Atropine and lipopolysaccharide from *P. aeruginosa* were purchased from Sigma-Aldrich; tetrotoxin was purchased from Alomone labs (Jerusalem, Israel); lidocaine hydrochloride 12mg/metered dose was obtained from Odan Laboratories LTD (Montreal, Canada). Stock solutions of CFTRinh-172, SQ22536, and were dissolved in DMSO. The final concentration of DMSO was less than 0.1%. Atropine, flagellin and lipopolysaccharides were dissolved in milli-Q water.

Statistics

Data are presented as mean ± SEM. The data sets that met the assumption of normality and homogeneity of variances where analyzed with parametric tests, ANOVA or Student's t-test. For those that did not, we performed non-parametric tests, Wilcoxon match-pairs signed

rank test or Mann–Whitney U-test, using GraphPad Prism 5 (GraphPad Software Inc., San Diego, CA, USA), and $P < 0.05$ was considered significant. Preliminary experiments showed that a sample size of 6 was sufficient to ensure adequate power to detect the effects of treatment on ASL secretion. Animal #11 was not included in the study because it never recovered from the stress of delivery. We did not exclude any data collected from any of the animals studied from our analysis.

Data availability

The authors declare that all the data supporting the findings of this study are available within the article and its Supplementary Information files.

3.3 Result

Synchrotron-based x-ray phase contrast imaging

The main challenge in studying airway secretion *in vivo* is the lack of an imaging method with sufficient contrast and resolution to observe the thin ASL layer (93 ± 8 μm thick, see Fig. 3.2) that is constantly cleared out of the airway through mucociliary clearance. We developed a synchrotron-based x-ray imaging technique to measure the ASL layer *in vivo*. The technique exploits the large difference in x-ray refractive index between the air and the ASL layer, which generates a strong signal at the air/ASL interface under x-ray phase contrast imaging (PCI) (Fig. 3.2b) (Luan et al., 2014; Lewis et al., 2005). Because PCI does not allow us to observe the ASL/tissue interface, we used agarose beads instilled into the swine airway as ‘measuring rods’ to measure the ASL height by determining the position of the tissue with respect to the air/ASL

interface (Fig. 3.2b, c, see “Materials and Methods” section). A researcher blinded to the experimental conditions measured ASL height as the distance between the air/ASL interface and the edge of the agarose bead touching the surface epithelium (Fig. 3.2b). The surface tension of the ASL immobilizes the beads onto the surface of the epithelium (“Materials and Methods”). The liquid secreted by the airway, which would normally be cleared out by mucociliary clearance, is retained around the static bead, allowing us to measure the accumulation of the ASL secreted by the airway (Luan et al., 2014). Another advantage of agarose beads is that they can be used as a pathogen delivery system by loading the beads with CF relevant bacteria, such as *P. aeruginosa*.

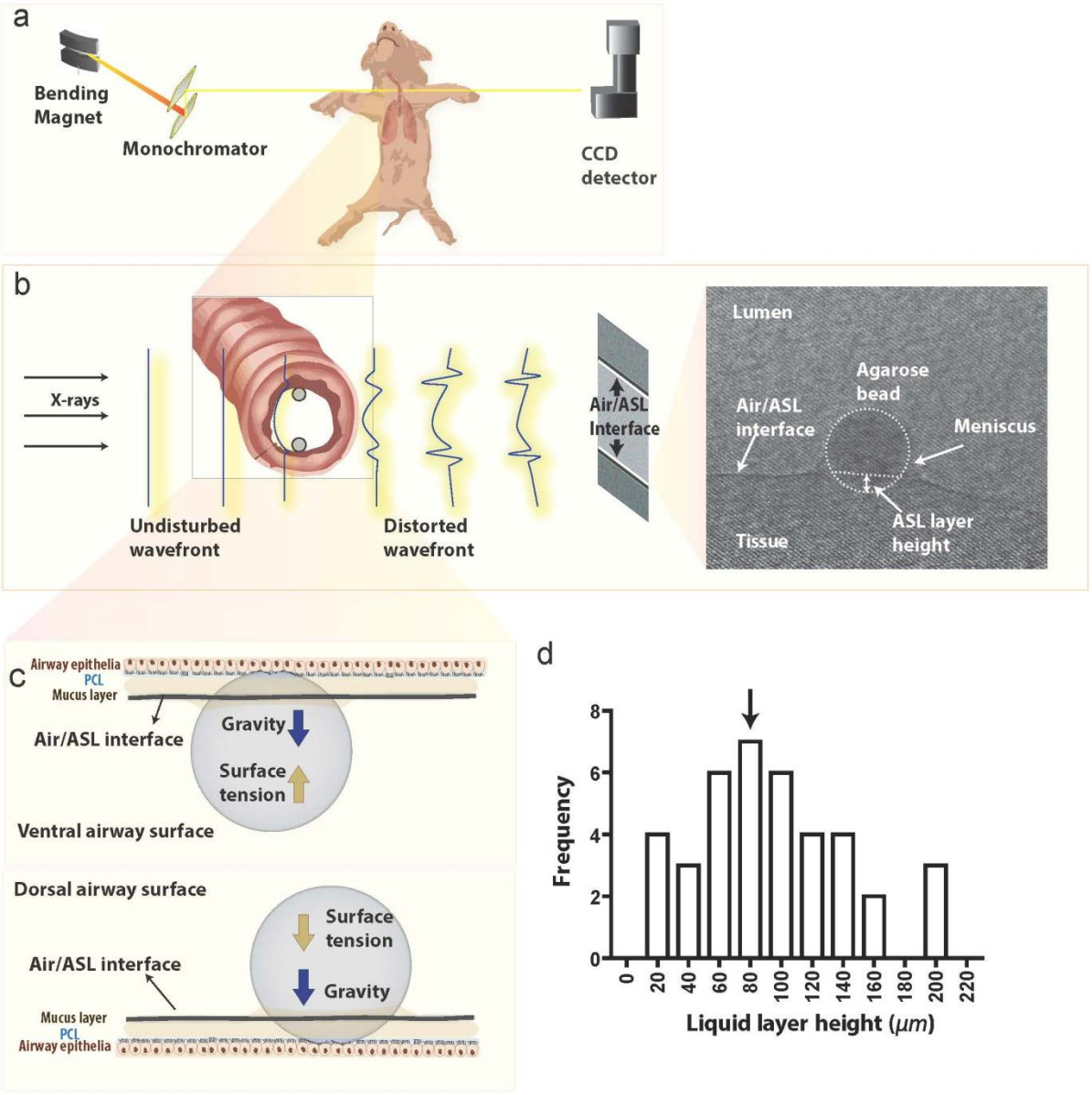

Fig. 3.2. Synchrotron-based phase contrast imaging. a) Schematic of the *in vivo* imaging set up. b) Detection of the air/ASL layer interface in the lumen of swine trachea *in vivo*. When x-ray (undisturbed) pass through the trachea, the difference in refractive index between the ASL and the air in the lumen results in a phase shift of the x-ray (distorted wavefront), which is detected by phase contrast imaging (PCI). PCI cannot resolve the ASL/tissue interface because the ASL refractive index is very similar to that of the tissue. Thus we used agarose beads as "measuring rods" to determine the position of the tissue with respect to the air/ASL interface. In the phase contrast image obtained *in vivo* (grayscale image on right panel), the air/ASL interface is clearly observable as a dark line

(highlighted with dotted line). The edge of the agarose bead is outlined by the dotted circle. The distance from the bottom of the agarose bead to air/ASL interface is used to measure the height of the ASL layer. Note that the air/ASL interface is below the level of the meniscus formed by the ASL on the agarose bead. Scale bar represents 500 μm. c) Schematic diagram illustrating the forces acting on the agarose bead (surface tension and gravity) and the bead–tissue interaction. d) Frequency distribution and mean (93 ± 8 μm, indicated by arrow) of ASL height in wild-type swine trachea exposed to bacteria-free agarose beads *in vivo* (n = 39 agarose beads obtained from 24 wild-type live pigs).

Absent ASL secretion in response to inhaled bacteria in CF

We studied airway ASL secretory response to inhaled bacteria in anesthetized, 2–7-days-old $CFTR^{-/-}$ and wild-type swine. Our analyses indicate that the trachea of wild-type animals have a basal level of ASL secretion that increased by 100% after instillation of *P. aeruginosa*-laden agarose beads (Fig. 3.3a–c). In contrast, exposure to *P. aeruginosa*-laden beads failed to increase ASL secretion in $CFTR^{-/-}$ swine (Fig. 3.3d–f). These results show that ASL secretion is indeed upregulated by bacterial inhalation, revealing a previously unknown component of the airway's innate immune response. This response is absent in CF airways, which would result in reduced bacterial clearance, thus facilitating infection.

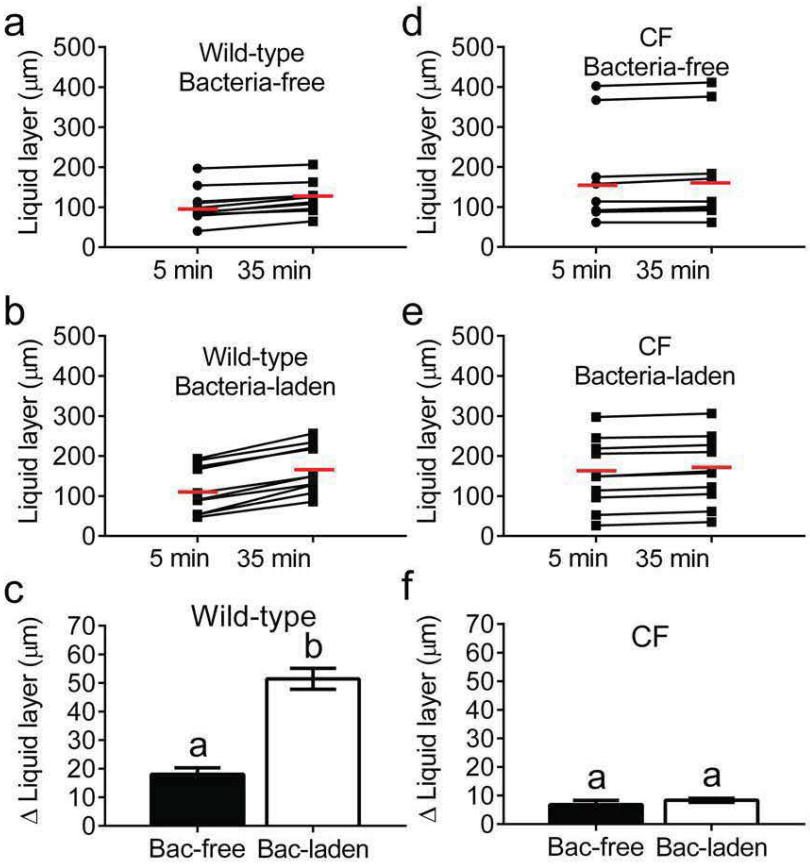

Fig. 3.3. CFTR$^{-/-}$ swine fail to respond to *Pseudomonas aeruginosa in vivo*. Scatter plot and median (red line) of the effect of a) bacteria-free and b) bacteria-laden agarose beads on the ASL layer of wild-type swine. Bacteria-free beads trigger an ASL increase from 105 to 123 µm ($p < 0.05$, n=10 from 7 pigs, Wilcoxon match-pairs signed rank test) while bacteria-laden beads triggered a height increase from 117 to 168 µm ($p < 0.05$, n=10 from 6 pigs, Wilcoxon match-pairs signed rank test). c) Increase in ASL height triggered by bacteria-laden (n=10) and bacteria-free (n=10) agarose beads ($p < 0.0001$, t=7.76 df=18, unpaired Student's t test). Effect of d) bacteria-free and e) bacteria-laden agarose beads on the ASL layer of CFTR$^{-/-}$ swine. Bacteria-free beads trigger an ASL increase from 172 to 178 µm ($p < 0.05$, n=9 from 6 pigs, Wilcoxon match-pairs signed rank test) while bacteria-laden beads triggered a height increase from 150 to 158 µm ($p < 0.05$, n=11 from 8 pigs, Wilcoxon match-pairs signed rank test). f) The increase in ASL height triggered by bacteria-laden (n=11) and bacteria-free (n=9) agarose beads were not significantly different in CFTR$^{-/-}$ swine ($p = 0.4943$, unpaired Mann-Whitney test). Data is presented as mean ± SEM and columns labeled with different letters differ significantly.

To understand the lack of response in CF lungs, we investigated the mechanism(s) underlying *P. aeruginosa*-mediated ASL secretory response. Pathogen detection in the airway requires the activation of Pattern Recognition Receptors (PRRs), which in turn trigger more specific innate immune responses (Kawai and Akira, 2010). For instance, in CF15 cells, the response to *P. aeruginosa* is mediated by the activation of Toll-Like Receptor (TLR) 5 by the bacterial protein flagellin, and bacteria strains that lack flagellin (i.e. PAKΔfliC) fail to elicit any response (Hybiske et al., 2004). Similarly, our results show that PAKΔfliC bacteria fail to trigger ASL secretion *in vivo*, whereas beads loaded with flagellin alone produced the same stimulatory effect as *P. aeruginosa* (Fig. 3.4a). These data suggest that airway response to *P. aeruginosa* is primarily mediated by stimulation of PRRs by flagellin. Because other relevant CF pathogens such as *Staphylococcus aureus* and *Haemophilus influenzae* do not express flagellin, we tested whether these pathogens stimulate ASL production. We found that *S. aureus*- and *H. influenzae*-laden beads also stimulated ASL secretion in wild-type swine (Fig. 3.4b). In addition, beads loaded with lipopolysaccacharide (LPS), a common PRR stimulating endotoxin present in *S. aureus* and *H. influenzae,* also triggered similar ASL secretory responses in wild-type trachea (Fig. 3.4b). Interestingly, introducing beads loaded with the non-pathogenic bacteria *Escherichia coli* (DH5-α) and *Bacillus subtilis* failed to stimulate airway ASL secretory response (Fig. 3.4c). These data indicate that bacteria triggered-ASL secretion is an innate immune response specific to pathogens and occurs via the activation of TLRs, which would lead to the production of proinflammatory cytokines, e.g. interleukin (IL) 1β, TNFα, 6 and 8 that stimulate ASL secretion (Baniak et al., 2012; Luan et al., 2014; Illek et al., 2008; Mohamed et al., 2012; Reiniger et al., 2007). In CF airways, pathogen inhalation would

stimulate TLRs and trigger proinflammatory signals (Bartlett et al., 2016); however, IL-1β, and TNF-α (Baniak et al., 2012), IL-6, and IL-8 (Fig. 3.4d and f) fail to trigger ASL secretion and clear pathogens, thus facilitating infection and inflammation.

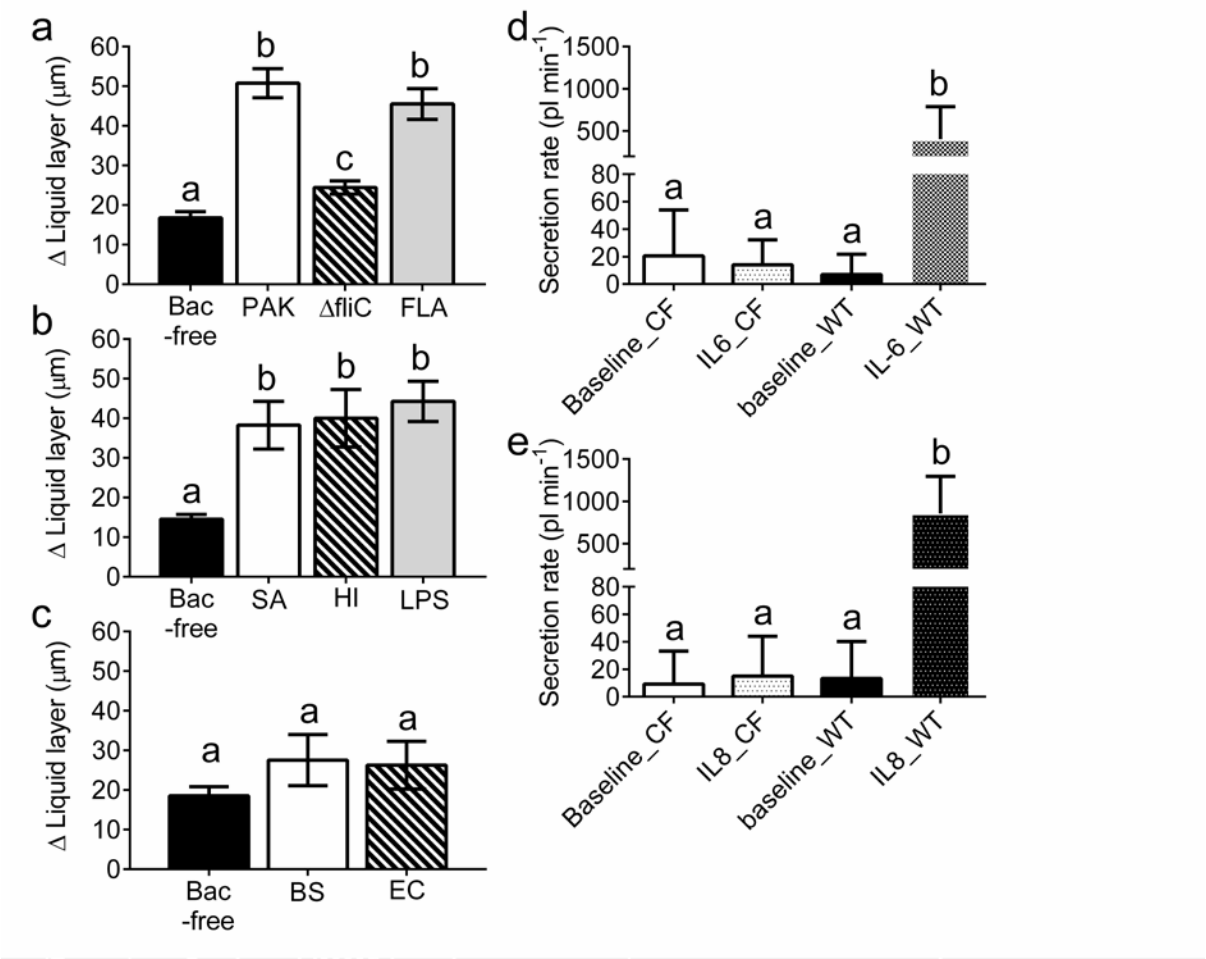

Fig. 3.4. Stimulation of pattern recognition receptors trigger ASL secretion in wild-type swine *in vivo*. a) *P. aeruginosa* PAK strain-laden agarose beads (PAK) significantly stimulates ASL secretion. PAKΔfliC-laden agarose beads (ΔfliC), which lacks flagellin, induce much less ASL secretion. Flagellin-laden (10 ng/ml) agarose beads (FLA) triggered a similar response as PAK beads (n = 11 bacteria-free from 6 pigs, n = 10 PAK from 6 pigs, n = 10 ΔfliC from 7 pigs, and n = 8 FLA from 5 pigs; $p < 0.0001$, $F (3, 35) = 36.59$, ANOVA and Tukey's multiple comparison test). b) *S. aureus*-(SA) and *H. influenzae*-laden (HI) agarose beads stimulate ASL secretion in wild-type swine. Similarly, LPS (20 μg/mL)-laden beads produce a similar effect (n = 10 bacteria-free from 7 pigs, n = 7 *S. aureus* from 4 pigs, n = 7 *H. influenzae* from 4 pigs, and n = 7 LPS from 5 pigs; $p =0.0003$, $F (3, 27) = 8.79$, ANOVA and Tukey's multiple comparison test). c) The non-pathogenic *B. subtilis* (BS)- and *E. coli* (EC)-laden agarose beads failed to trigger ASL secretion in wild-type swine (n = 10 bacteria-free from 6 pigs, n = 7 *E. coli*

DH5-α from 5 pigs, and n = 7 *B. subtilis* from 6 pigs; p =0.3369, F (2, 21) = 0.40, ANOVA and Tukey's multiple comparison test). Secretion assay data showed that d) IL-6 (50 ng/mL, n =16 preparations from 7 $CFTR^{-/-}$ animals and n = 9 preparations from 4 wild-type animals, $p < 0.0001$, F (3, 60) = 12.79, ANOVA and Tukey's multiple comparison test) and f) IL-8 (50 ng/mL, n =15 for $CFTR^{-/-}$ airway tissue from 7 pigs and n = 10 for wild type tissue from 4 pigs, $p < 0.0001$, F (3, 56) = 13.09, ANOVA and Tukey's multiple comparison test) failed to trigger submucosal gland secretion in CF tissue, but stimulated ASL secretion in wild-type airway. Data is presented as mean ± SEM and columns labeled with different letters differ significantly.

Reduced basal ASL secretion in CF

The ability of CF airways to clear pathogens may also be compromised by a reduction in basal ASL secretion, i.e., background ASL production independent of bacteria inhalation. Indeed, using bacteria-free agarose beads, we detected a basal ASL secretion rate both in wild-type and CFTR swine *in vivo*, however, the basal ASL secretion by CFTR swine was significantly smaller (Fig. 3.5a). Therefore, we decided to study the source of this secretion and its regulation. Our results show that basal ASL secretion is produced by submucosal glands, and surgical removal of over 90% of the submucosal glands from wild-type *ex vivo* tracheal preparations significantly reduced ASL secretion (Fig. 3.5b). These results are consistent with previous reports that more than 90% of ASL produced in the upper airway is secreted by the submucosal glands (Ballard and Inglis, 2004). Treatment of wild type *ex vivo* tracheal preparations with the CFTR inhibitor, CFTRinh172, blocked basal ASL secretion (Fig. 3.5c), reinforcing that CFTR-mediated glandular secretion is the source of basal ASL production in the trachea.

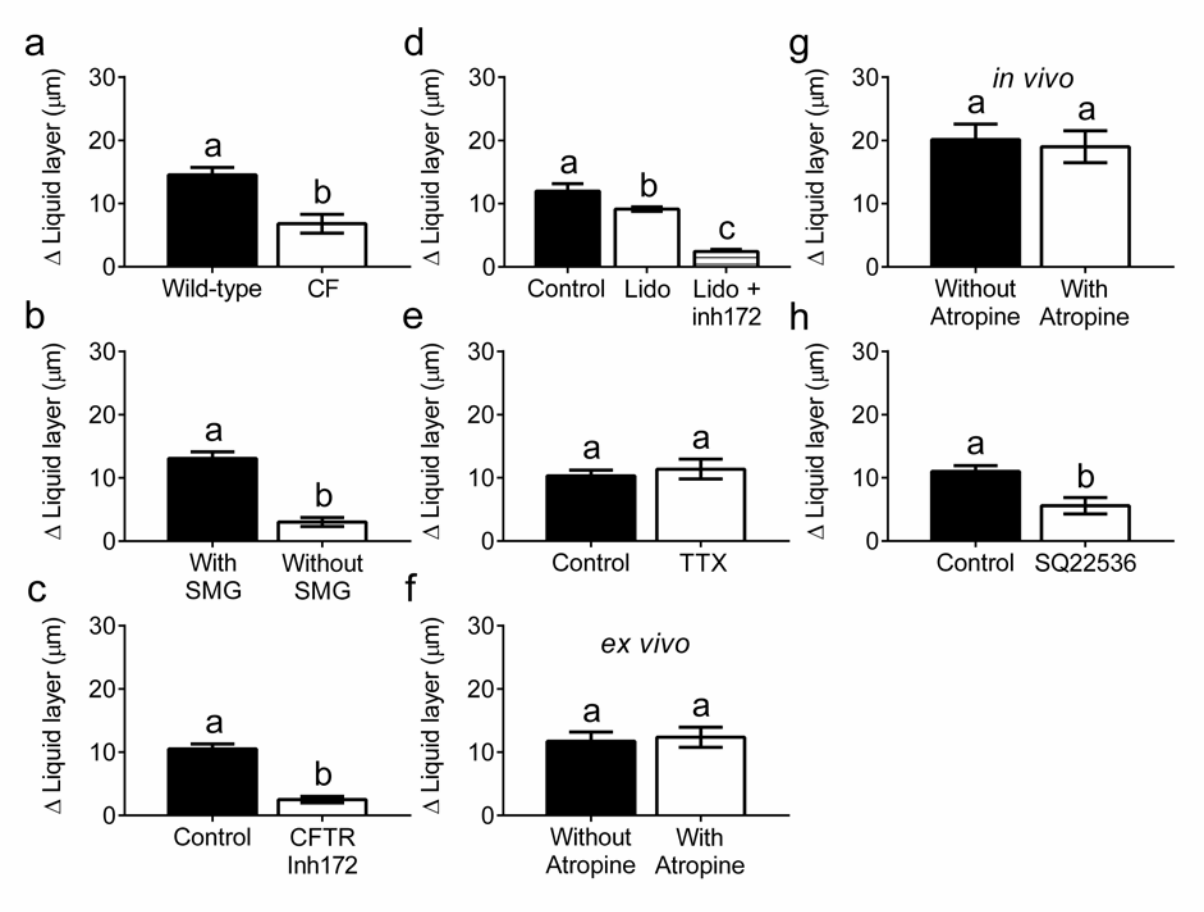

Fig. 3.5. CF tissue fail to produce basal ASL secretion. a) $CFTR^{-/-}$ swine (CF, n=9 from 6 animals) display significantly lower basal ASL secretion than wild-type swine (n=10 from 7 animals, mean ± SEM, p =0.0010, unpaired Mann-Whitney test). b) Wild-type *ex vivo* preparations with surgically removed submucosal glands (SMG) produced significantly lower basal ASL (n=12 with SMG from 6 preparations and n=13 without SMG from 6 preparations, p <0.0001, unpaired Mann-Whitney test). c) Wild-type *ex vivo* preparations incubated with the CFTR anion channel blocker, CFTRinh172 (100 μM), produced significantly lower basal ASL than non-treated preparations (Control, n=6 from 4 preparations for control, and n=14 from 5 preparations for CFTRinh172, p <0.0001, unpaired Mann-Whitney test). d) Inhibition of sensory neurons with topical application of lidocaine (Lido) had a small effect on basal ASL secretion. Simultaneous treatment with the CFTR inhibitor (Lido + inh172) completely blocked basal ASL secretion (mean ± SEM, n=13 control from 5 preparations, n=21 Lido from 8 preparations, and n=16 Lido+inh172 from 7 preparations; p < 0.0001, F (2, 47) = 59.35, ANOVA and Tukey's

multiple comparison test). e) Blocking neuronal function with tetrodotoxin (1μM, TTX) treatment had no effect on basal ASL secretion (mean ± SEM, n=18 control from 8 preparations, and n=11 TTX from 4 preparations, p=0.5820, unpaired Mann-Whitney test). Blocking cholinergic receptors with atropine had no effect on basal ASL secretion in f) *ex vivo* preparations (10μM, n=8 without Atropine from 3 preparations and n=8 with Atropine from 4 preparations, p=0.7656, t=0.3040 df=14, unpaired Student's t test) or g) *in vivo* wild-type swine (treated with 0.04mg/kg IM 2-10 minutes following induction of anesthesia, n=8 without Atropine from 6 animals, and n=10 with Atropine from 7 animals, p=0.7538, t=0.3191 df=16, unpaired Student's t test). h) Inhibiting cAMP production with the adenylyl cyclase inhibitor, SQ22536 (0.5 mM), blocked basal ASL secretion (n=10 control from 4 preparations and n=11 SQ22536 from 4 preparations; p =0.0003, unpaired Mann-Whitney test). Data is presented as mean ± SEM and columns labeled with different letters differ significantly.

It is possible that spontaneous ASL secretion could be a reactive response of sensory neurons to the presence of agarose beads. We tested this by blocking sensory neurons in *ex vivo* trachea preparations with the topical anesthetic lidocaine, which caused a slight reduction in basal secretion, but not to the extent that would explain loss of secretion in CF tissues (Fig. 3.5d). ASL secretion may also be stimulated by airway intrinsic neurons (Widdicombe and Wine, 2015). Thus, we treated preparations with tetrodotoxin, a Na^+ channel blocker that inhibits airway intrinsic neuron function (Allen and Burnstock, 1990), which had no discernible effect on basal ASL secretion (Fig. 3.5e). We also tested whether parasympathetic tonic stimulation may drive basal secretion by treating airways with the cholinergic antagonist, atropine (Ueki et al., 1980). The treatment had no effect on secretion *in vivo* or *ex vivo* (Fig. 3.5f and g), indicating that basal secretion is independent of neuronal activation (i.e. parasympathetic, sensory efferent, and airway intrinsic neurons). However, blocking cAMP production with the adenylate cyclase blocker, SQ22536, significantly reduced basal secretion *ex vivo* (Fig. 3.4h), suggesting that a cAMP-mediated regulatory mechanism modulates basal secretion that is independent of the nervous system.

3.4 Discussion

This study provides evidence of previously unknown components of the airway innate immune response to pathogens. We describe a basal level of ASL secretion that perhaps performs a "housekeeping" function (Wine, 2007) by ensuring a basal presence of mucins and antimicrobial compounds in the airway, which may be the only protection against non-pathogenic particles. In addition, the airway has a pathogen-triggered ASL secretion response

at the site of infection through paracrine stimulation of ASL secretion by cytokines (Joo et al., 2010; Joo et al., 2002; Ianowski et al., 2007; Wine, 2007; Baniak et al., 2012; Martens et al., 2011; Ianowski et al., 2008). The lack of basal secretion in CF airway would result in reduced ASL availability to deal with inhaled particles, which combined with the lack of response to pathogens would severely undermine the innate immune system's ability to protect the airway from inhaled insults. Instead, pathogens would activate PRRs and production of proinflammatory signals, thus favoring inflammation (Pezzulo et al., 2012; Sun et al., 2010; Cho et al., 2011). Finally, our results suggest that treatments which improve the basal ASL secretion, such as hypertonic saline nebulization, or treatments that protect the airway from inhaled bacteria, such as prophylactic antibiotics, would slow the progression of CF airway disease.

3.6 Supplemental data

Table 3.S1. Summary of clinical histories of the gut-corrected CFTR$^{-/-}$ piglets.

Pig#	Vital signs at birth				Treatments	Euthanasia	
	Wt	HR	O_2	Temp	some offered more than once	Age	Reason
1	1.13	158	99	37.6	1ml enema (oil)	7 days	elective
2	1.43	172	99	37.8	2.5ml enema (water-oil)	5 days	IC, RS.
3	1.14	149	96	36.7	5% dextrose IP 5cc	2 days	IC
4	1.47	136	96	35.6	5% dextrose IP 5cc	2 days	IC
5	1.18	153	90	36.9	5% dextrose IP 5cc, 2.5ml enema (water-oil)	2 days	IC
6	1.47	176	92	38.2	1ml enema (oil)	5 days	IC, RS.
7	1.25	193	95	37.2	5% dextrose IP 5cc, 2.5ml enema (water-oil)	2 days	RS
8	1	198	88	37.7	2.5ml enema (water-oil)	5 days	IC
9	1.37	170	85	37.8	1.5 ml enema (oil)	7 days	elective
10	1.55	171	93	37.3	2.5ml enema (water-oil)	2 days	IC
11	1.26					12 h	RS

Wt- Weight kg. HR- Heart rate. O_2- % oxygen saturation. Temp- Temperature in degree Celsius. IC- Intestinal complications. RS- Respiratory Symptoms.

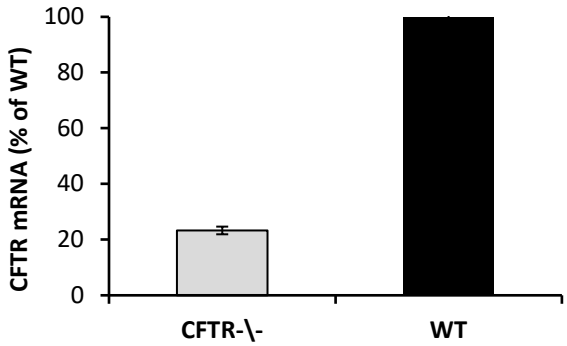

Fig. 3.S1. CFTR mRNA levels (relative to *β-actin*) in CF gut corrected ($CFTR^{-/-}$) and Wild-type (WT) pigs.

Values are shown as percentage mRNA levels relative to the wild-type. Samples were run in quadruplicates. qPCR results showed that CFTR mRNA levels (normalized to β-actin) in the gut of pig#7 was 23.29% that of wild-type, which is consistent with what has been previously reported (Stoltz et al., 2013).

Pig ID	Distended colon and cecum with firmer than normal feces	Hypoplastic gall bladder	Common bile duct blocked by thick bile	Suppurative pneumonia	Notable excessive mucous in nasal cavity	Prominent bile stasis	Pancreatic hypoplasia
1	-	+	-	+	-	-	NA
2	+	+	-	+	-	+	NA
3	NA	NA	NA	NA	NA	NA	NA
4	+	-	-	-	-	-	NA
5	+	+	-	-	-	-	NA
6	+	-	-	+	-	-	NA
7	-	-	-	-	-	-	NA
8	+	+	-	-	+	+	+
9	-	+	-	+	+	-	NA
10	+	-	+	-	-	+	NA
11	+	-	-	-	-	-	+

Table 3.S2. Summary of gross and histological findings

+: present, -: absent, NA: observation not available

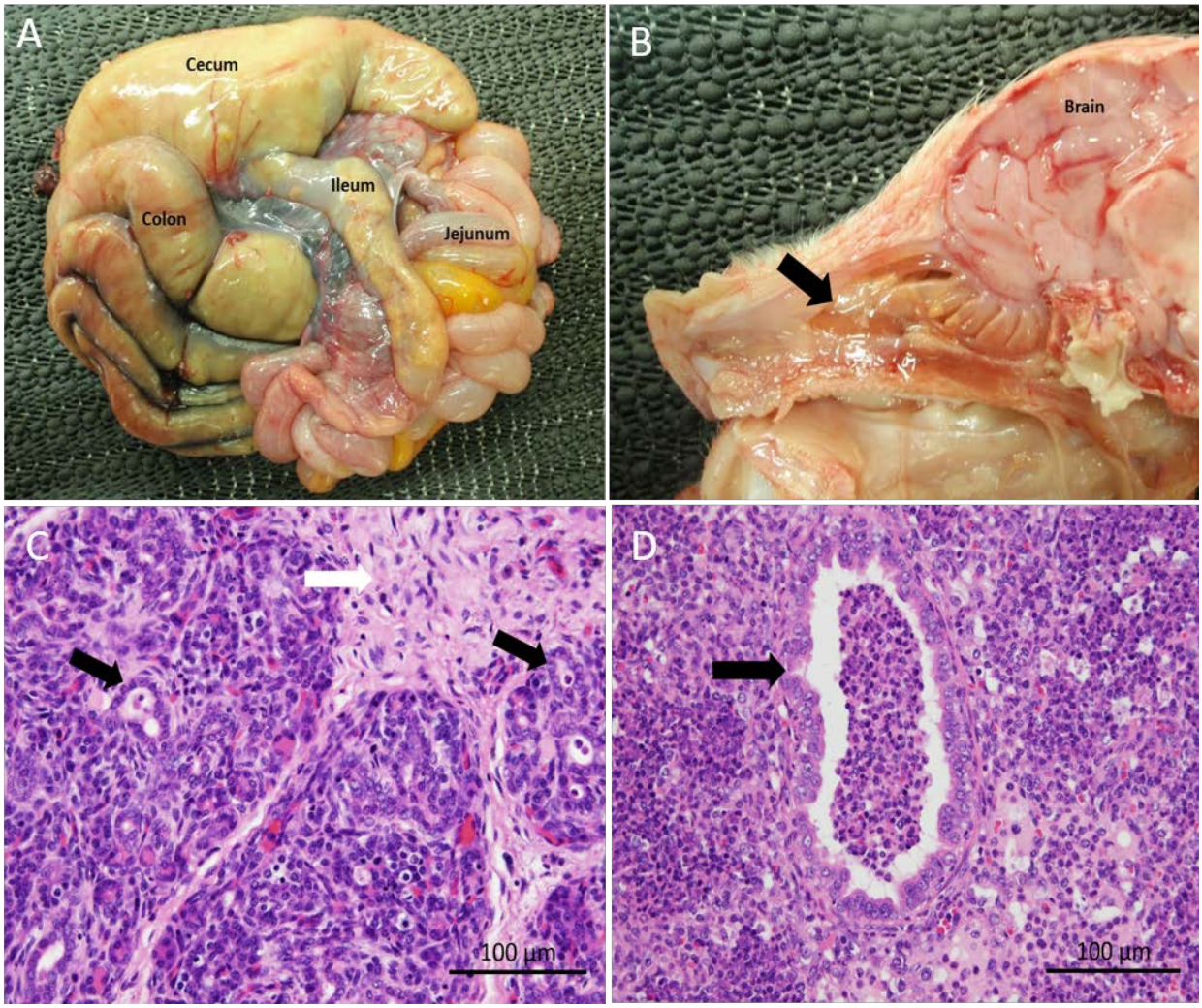

Fig. 3.S2. Pathology analysis of gut-corrected CFTR$^{-/-}$ swine. The carcasses of 10 animals were subjected to pathology analyses by a board-certified veterinary pathologist. A) Intestines: The cecum and spiral colon are severely distended by feces. B) Head: The nasal cavity contains excessive mucous (arrow). C) Pancreas: The acini (black arrows) are mostly devoid of zymogen granules, and the interstitium contain increase amount of fibrous tissues (white arrows). D) Lung: The bronchiole (arrow) and alveoli are filled with many inflammatory cells, mostly neutrophils. Scale bars indicate 100 µm.

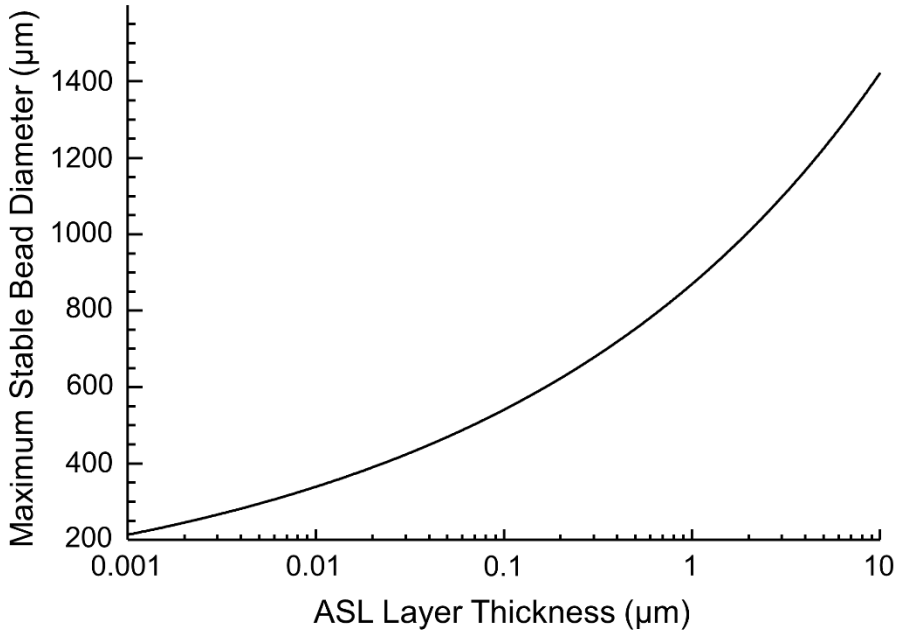

Fig. 3.S3. Maximum diameter of beads that will be forced against the epithelium at the top of the trachea at a given range of ASL layer thickness. The data shows the change in adhesion force, within the range of ASL thickness (20 to 300 μm) observed in swine trachea, with varying bead size and fluid thickness as calculated from equation 5.

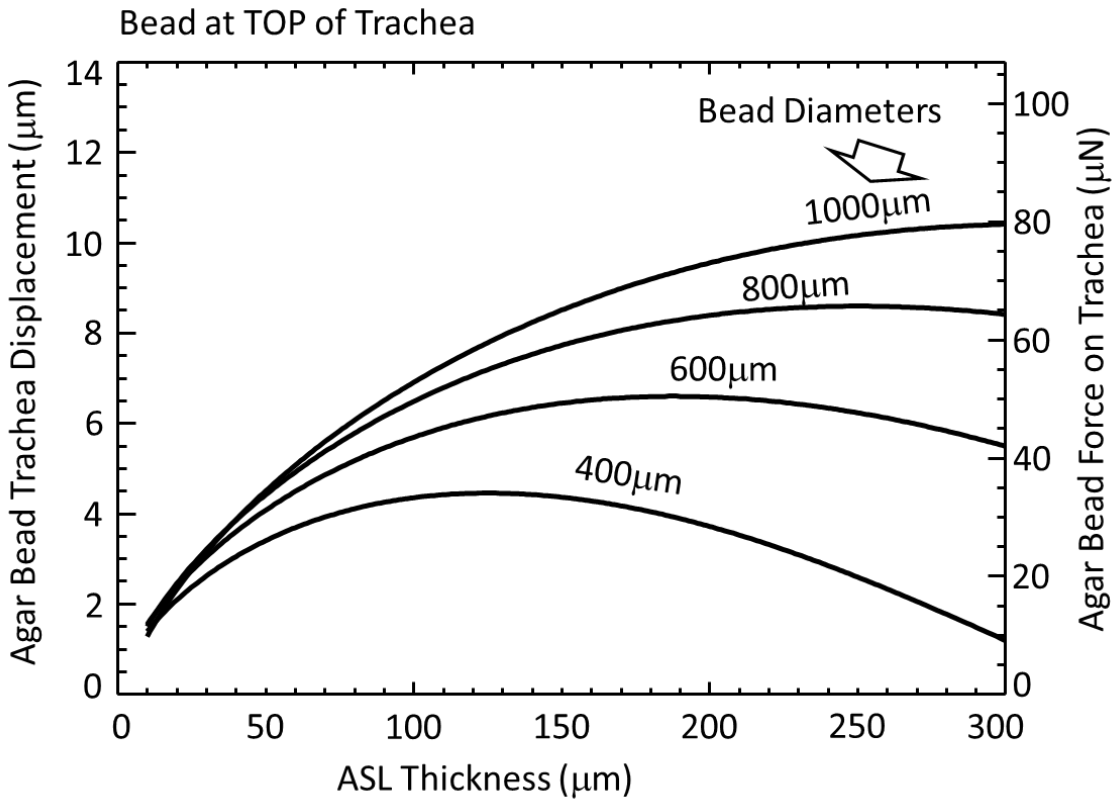

Fig. 3.S4. Tissue deformation in the top part of the trachea for given ASL thicknesses and bead diameters.

The displacement of tracheal epithelium by beads of varying sizes and under varying ASL layer thicknesses can be calculated from equation 6 . Tissue displacement is negligible compared to the height of the ASL layer in live swine trachea.

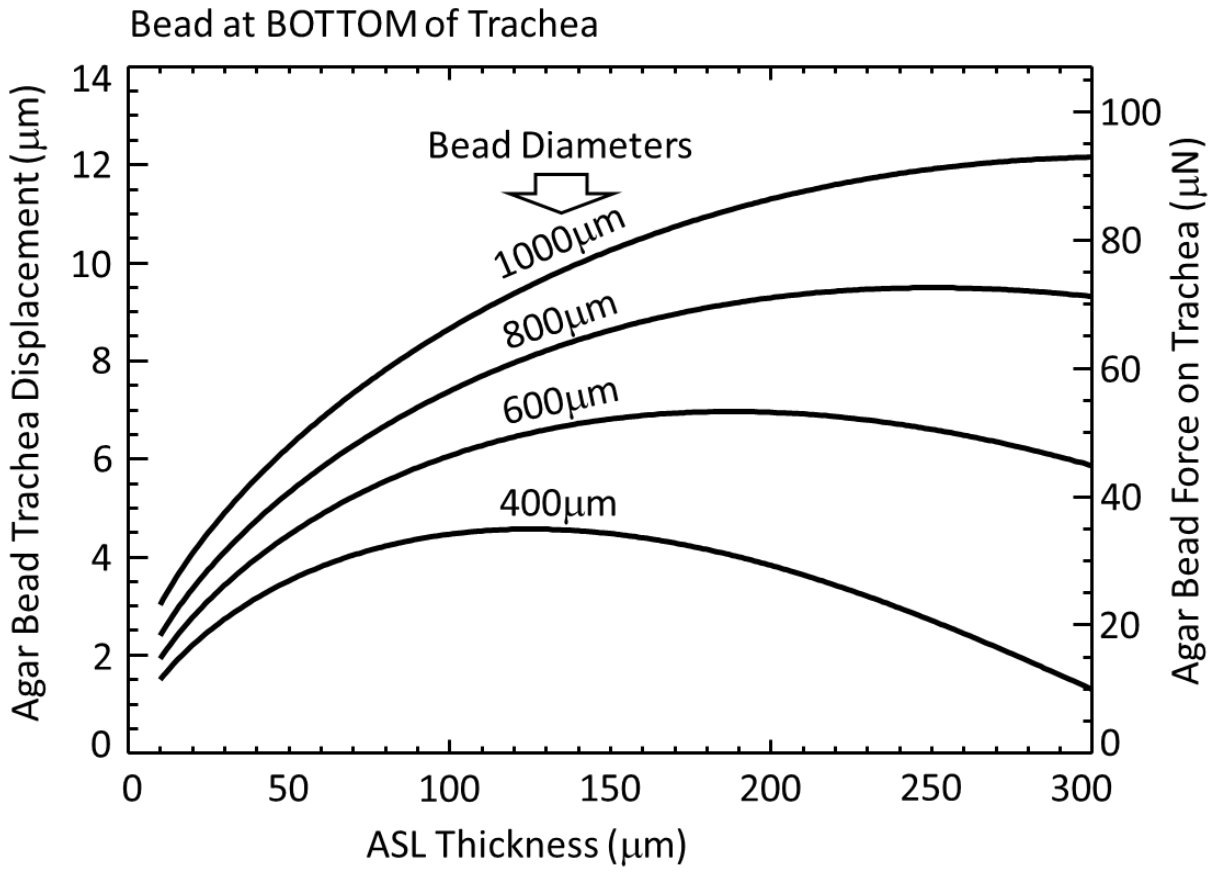

Fig. 3.S5. Tissue deformation of the bottom part of the trachea for given ASL thicknessnes and bead diameters. The displacement of tracheal epithelium by beads of varying sizes and under varying ASL layer thicknesses can be calculated from equation 6 . Tissue displacement is negligible compared to the height of the ASL layer in live swine trachea.

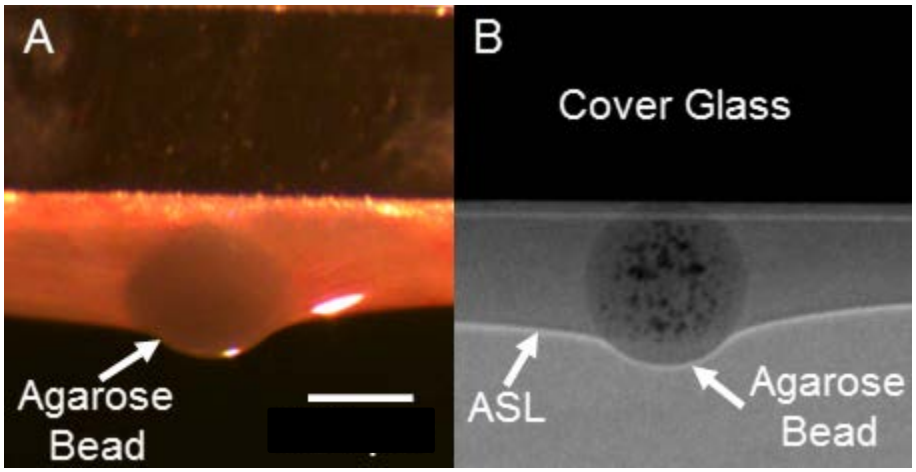

Fig. 3.S6. Surface tension force the beads against the glass slide. We placed agarose beads in an ASL sample collected from isolated trachea and placed it on the underside of a glass slide. The agarose beads were forced against the glass surface, indicating that the surface tension from the ASL is stronger than gravity and it forces the beads up against the glass surface, as predicted by the mathematical model A) Light, and B) phase contrast images of the same bead immersed in ASL(Luan et al., 2014). Scale bar represents 500 µm. `

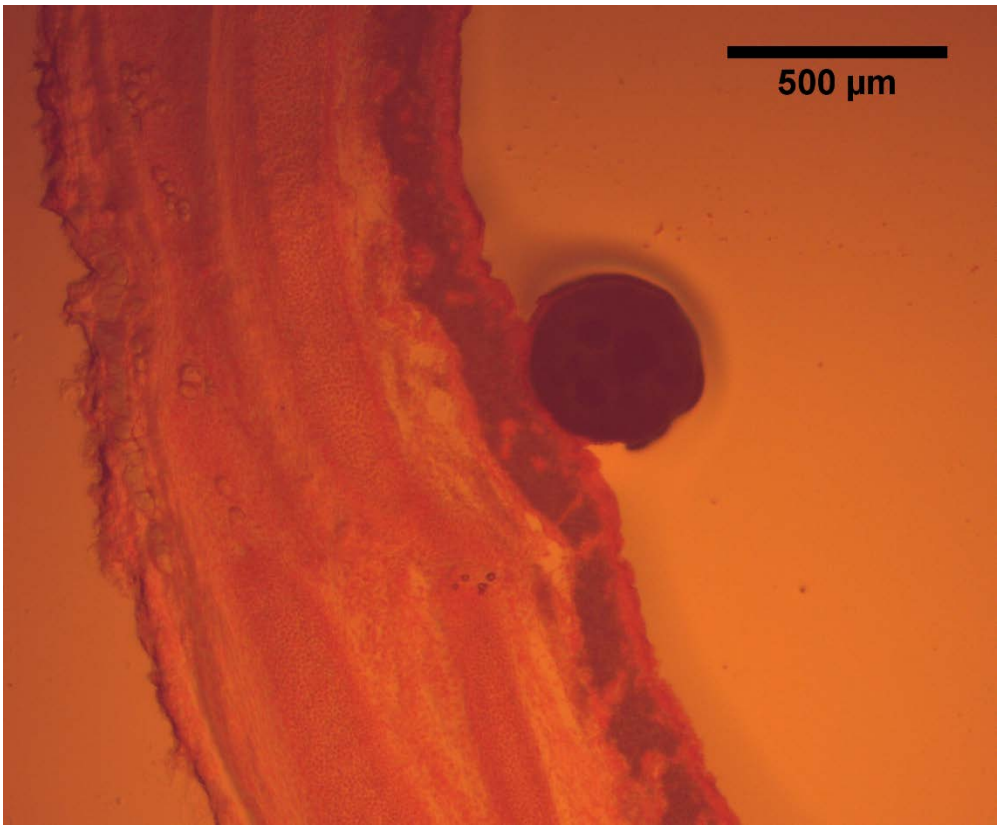

Fig. 3.S7. Cryo-section of a tracheal preparation showing an agarose bead in contact with airway surface epithelia. Agarose beads were instilled into freshly harvested trachea of 1 week old wild-type piglets. The preparations were flash frozen in liquid nitrogen and stored at -80 °C. Then, the trachea preparations were cryo-sectioned into 20 µm sections and stained with Nuclear Fast Red (Sigma) for 1 minute, which delineated the airway tissue. The sections were imaged on a light microscope. Histological images (n=11) clearly showed that the agarose beads were indeed in contact with the airway surface epithelium. Scale bar represents 500 µm

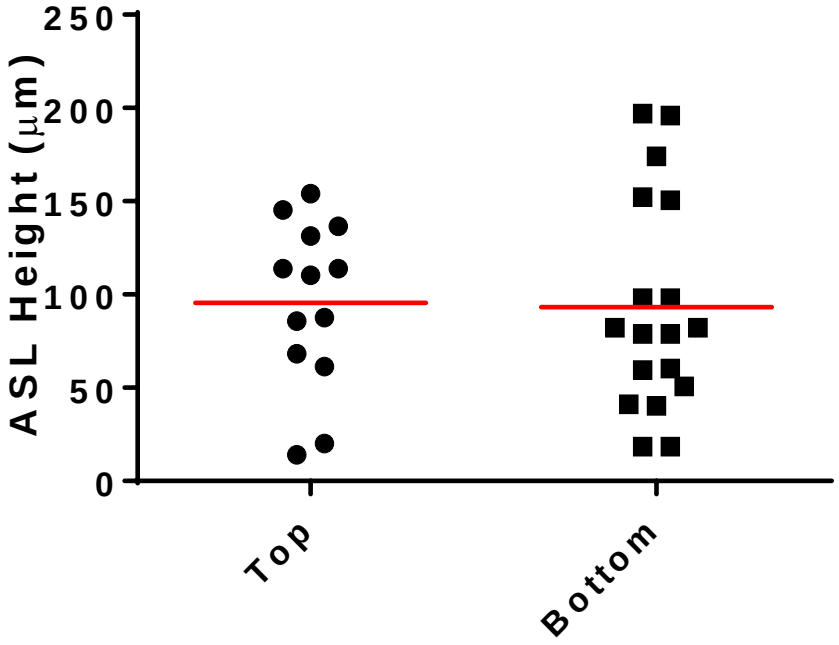

Fig. 3.S8. Scatterplot and mean (red lines) ASL height measured with beads placed at the top and bottom parts of live swine trachea (n = 13 for top and n = 18 for bottom; t = 0.1239, df = 29, p = 0.90, Students' t-test)**.**

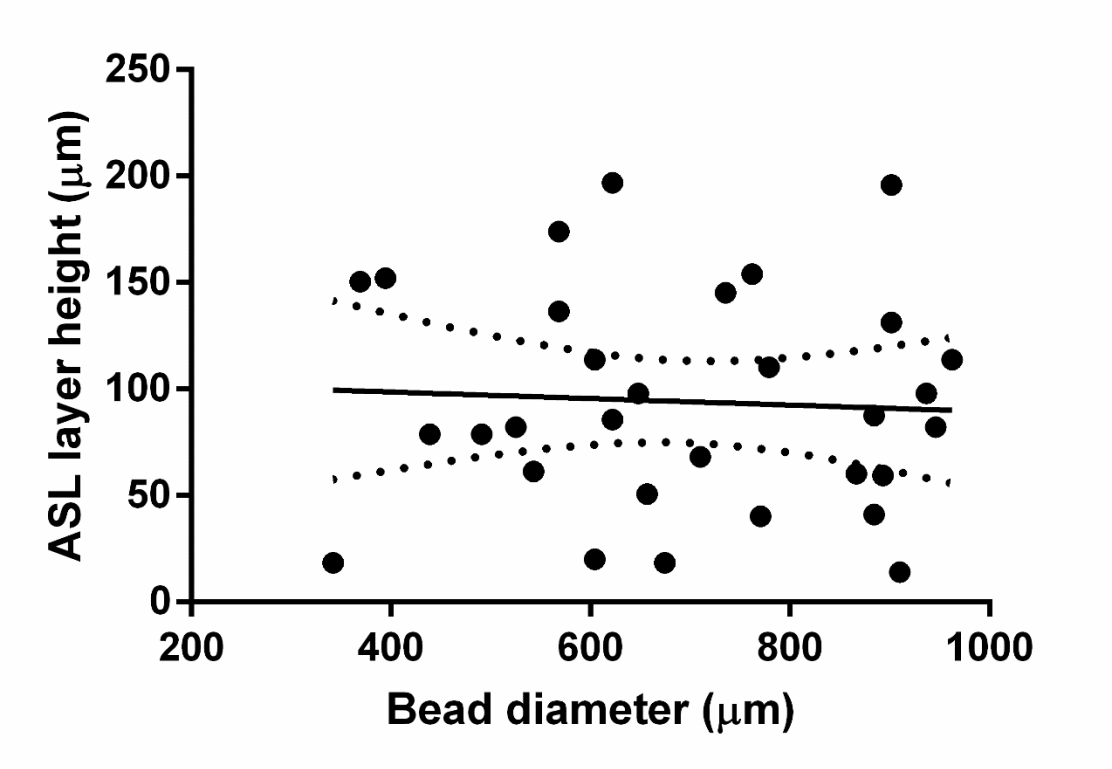

Fig. 3.S9. Scatterplot and linear regression of bead diameter vs ASL height measured 5 min after incubating tissues with bateria-free beads. The linear regression was not significant ($p = 0.77$, $F = 0.087$, $DFn = 1$, $DFd = 29$; $r^2 = 0.003$)

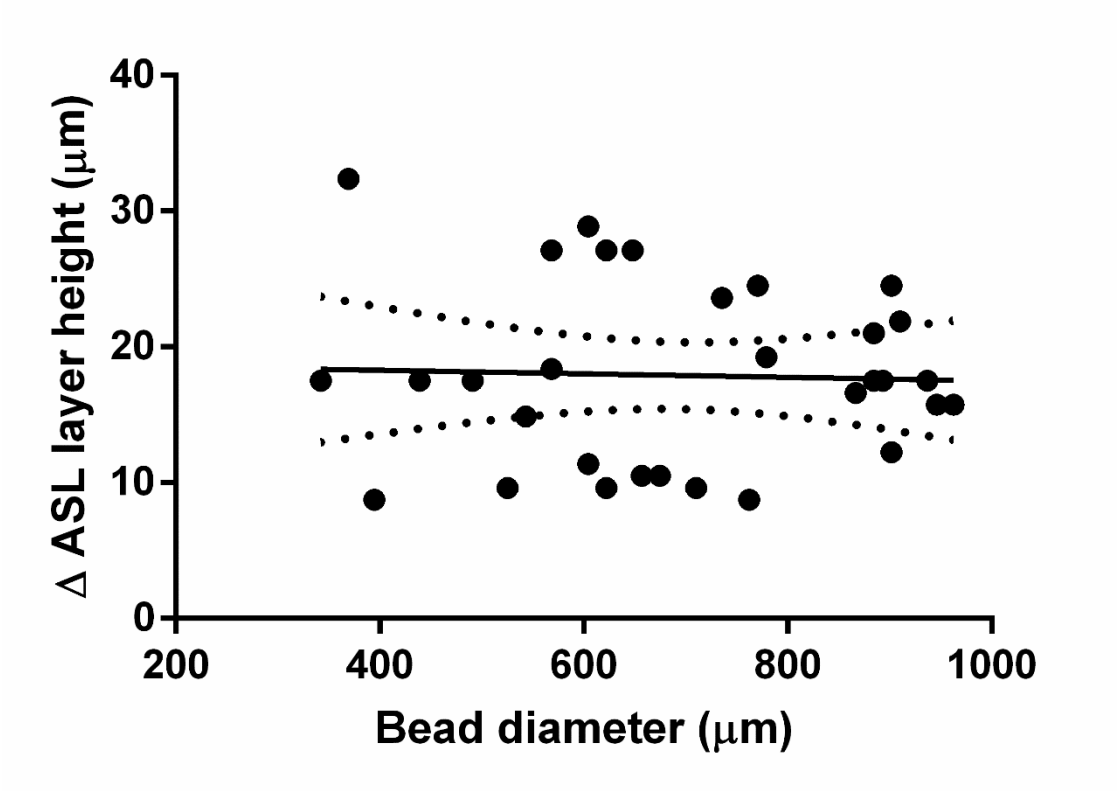

Fig. 3.S10. Scatterplot and linear regression of bead diameter vs change in ASL height after 30 min of incubation with bacteria-free beads. The linear regression was not significant ($p = 0.84$, $F = 0.038$, $DFn = 1$, $DFd = 29$; $r^2 = 0.001$).

Chapter 4

Nebulized hypertonic saline triggers active liquid secretion by airway epithelia in swine

4.1 Abstract

Background: Inhaled hypertonic saline (HTS) treatment is used to improve lung health in patients with cystic fibrosis. However, the mechanisms underlying the effect of this treatment are not fully understood, which makes it difficult to develop procedures to modulate the duration and intensity of the treatment to improve outcomes. The current consensus is that the treatment generates an osmotic gradient that draws water into the airways and increases the airway surface liquid (ASL) volume. However, there is evidence that hypertonic saline may also stimulate active secretion of ASL by airway epithelia through the activation of sensory neurons.

Objective: We tested the contribution of the nervous system and airway epithelia on HTS-stimulated ASL production using a novel synchrotron-based method to visualize and measure ASL in isolated swine trachea.

Results: We found that blocking the nervous system with tetrodotoxin and lidocaine reduced HTS-stimulated ASL secretion by 50%. Similarly, incubating the preparations with blockers known to inhibit ion transport across the airway epithelia; i.e. CFTRinh172, bumetanide and niflumic acid in bicarbonate free saline; resulted in a 50% decrease in response to HTS treatment.

Conclusion: Hypertonic saline treatment of the airway epithelia triggers both neuron-mediated ASL secretion and osmotically driven fluid production. It might be possible to

modulate the duration and intensity of HTS treatment by pharmacologically altering the function of airway neurons and epithelia.

4.2 Introduction

Inhaled hypertonic saline (HTS) is a well-established treatment for patients with cystic fibrosis (Donaldson et al., 2006; Elkins et al., 2006; Wark and McDonald, 2009). HTS treatment has been shown to improve mucociliary clearance, forced expiratory volume in 1 s, frequency of exacerbations, days on antibiotics, and well-being (Donaldson et al., 2016, Elkins et al., 2006; Tildy and Rogers, 2015; Reeves et al., 2015). Recent analyses of lung clearance index and spirometry data for patients under long-term HTS treatment suggest that HTS treatment may be able to halt the progression of mild CF lung disease (Ellemunter et al., 2016).

The exact mechanism of action of HTS is not understood (Tildy and Rogers, 2015), which makes it difficult to develop procedures to modulate the duration and intensity of the treatment to improve outcomes (Tang et al., 2016; Cazzarolli et al., 2016; Bennett et al., 2015). The current consensus on the mechanism of action of HTS inhalation is that the treatment generates an osmotic gradient that draws water into the airways. This increases the volume of airway surface liquid (ASL), improves mucus rheological properties, and accelerates mucus transport rates (Tildy and Rogers, 2015; Reeves et al., 2015).

However, there is evidence that HTS may also stimulate sensory nerves in the airways, triggering neurogenic inflammation and stimulating ASL secretion by airway epithelia. In rat airways, treatment with HTS stimulates neurogenic inflammation, specifically through the local release of inflammatory mediators by sensory-efferent pathways (Umeno et al., 1990;

Barnes, 2001; Barnes, 1998; Maggi et al., 1995). In guinea pig airways, HTS treatment activates airway afferent nerves including Aδ and C fibers both *in vitro* and *in vivo* (Pedersen et al., 1985; Fox et al., 1995). Treatment of the nasal cavity with HTS in healthy volunteers stimulates nociceptive nerves and glandular mucus exocytosis (Baraniuk et al., 1999). In addition, HTS induces robust reflex responses in the nose and larynx of guinea pigs, similar to that evoked by capsaicin, and evokes coughing when applied topically to the tracheal or laryngeal mucosa (Chou et al., 2008). Furthermore, neurogenic inflammation triggers ASL secretion by airway submucosal glands (Widdicombe and Wine, 2015; Ianowski et al., 2008), and in ferret trachea, HTS stimulates the production of two markers of gland secretion, mucins and lysozyme (Kishioka et al., 2003).

We thus tested the role of airway neurons in HTS-stimulated ASL production in tracheas isolated from pigs using a novel synchrotron-based imaging method, which we developed to measure and quantify ASL secretion in isolated intact tracheas (Luan et al., 2014). Our results show that HTS-stimulated ASL production is partially blocked, i.e. ~50% reduction, by inhibiting either neuronal function or epithelial ASL secretion. These results suggest that part of the ASL produced by HTS treatment is the result of the sensory-efferent stimulation of epithelial ASL secretion.

4.3 Materials and Methods

Tracheas were obtained from 4-week-old juvenile female and male pigs (15 to 25 kg) purchased from the Prairie Swine Centre, University of Saskatchewan. The tracheas were dissected within 30 minutes of euthanasia, clamped at both ends to prevent liquid entering the

lumen and placed in ice-cold Krebs-Ringer saline solution containing 115 mM NaCl, 2.4 mM K_2HPO_4, 0.4 mM KH_2PO_4, 1.2 mM $CaCl_2$, 1.2 mM $MgCl_2$, 25 mM $NaHCO_3$ and 10 mM glucose (pH 7.4), equilibrated with 95% O_2 and 5% CO_2 until use. For the bicarbonate-free Krebs-Ringer saline solution, 25 mM $NaHCO_3$ was replaced with 24 mM NaCl and 1 mM HEPES, pH 7.4, equilibrated in O_2 (Wine et al., 2011). Both solutions had similar osmotic pressures of 270 ± 0.7 and 269 ± 0.5 (n = 6).

Synchrotron-based x-ray imaging set-up

Experiments were performed using the BioMedical Imaging and Therapy-Bending Magnet (BMIT-BM) beamline 05B1-1, at the Canadian Light Source (CLS), Saskatchewan, Canada. The experimental hutch is located 25.5 meters away from the storage ring. Phase contrast imaging (PCI) was performed using monochromatic 20 keV (λ=0.062 nm) x-rays, selected using a standard double-crystal monochromator. The beam size was 100.0 mm (wide) x 8.0 mm (vertical). The distance between the sample and the detector was 65 cm. Images were captured using a high-resolution x-ray converter (AA-60, Hamamatsu Photonics, San Jose, CA, USA) with a charge-coupled device (CCD) detector (C9300-124, Hamamatsu Photonics, San Jose, CA, USA). The converter used a 10 μm-thick scintillator (Gd2O2S:Tb) to convert x-rays to visible light, which was then directed to the CCD. The pixel size of the image was 8.75 x 8.75 μm. Exposure time ranged from 600 to 900 ms.

Agarose bead preparation

We used agarose beads as ‘measuring rods’ to determine the height of the ASL layer,

which was measured as the distance between the air/ASL interface and the edge of the agarose bead touching the surface epithelia (Fig. 4.1, see supporting information). Agarose beads were made in sterile conditions with 4% agarose in PBS (Luan et al., 2014; Cash et al., 1999; Chmiel et al., 2002). All solutions used in the process of making agarose beads were autoclaved at 250°C for at least 20 min. Warm (50-55°C) 4% agarose solution was made in PBS. The agarose solution was mixed with warm (50-55°C) heavy paraffin oil and stirred rapidly, achieving a vortex 2 cm in depth. The agarose/oil mixed solution was left in a beaker for 11 min, and then ice was slowly added around the beaker for 7 min. After 7 min of cooling, the agarose/oil solution was poured into a separatory funnel containing warm (50-55°C) 0.5% w/v sodium deoxycholate in PBS to wash the mineral oil from the beads. The agarose beads were allowed to settle and then washed 3 times with PBS at room temperature to wash away the sodium deoxycholate. The upper one third of agarose beads at the bottom of the separatory funnel were then taken and used for the experiments.

In order to make the beads visible by x-ray, we added $BaSO_4$ (nominal 1 M) as contrast agents to the PBS. This salt was chosen because it is insoluble in water and thus does not contribute to the osmotic pressure of the bead. The osmolarity of the beads solution were 278 ± 0.1 and 276 ± 0.3 for PBS and PBS plus 1M $BaSO_4$, respectively (Luan et al., 2014).

Experimental set-up

The trachea preparation was clamped at both ends so that the lumen was filled with air. The cartilage was removed with the aid of a scalpel and a fine blunt-ended elevator to improve access of the drugs to the epithelia and nervous tissue. The trachea preparation was placed in a

custom-built chamber. The tissue was immersed in Krebs solution plus 1 μM indomethacin at 35ºC and equilibrated with 95% O_2 and 5% CO_2. The lumen of the trachea preparation remained free of solution and sealed, yet was accessible to the researchers to introduce the agarose beads. Agarose beads (~200 to 800 μm in diameter) were blotted dry and placed in the lumen of the preparation using a cotton swab. Each bead was placed at a location where the air/ASL interface is parallel to the x-rays penetrating the sample, i.e. the top or bottom of the preparation (Fig. 4.1) (Luan et al., 2014), using a motorized computer-controlled experimental stage. Hypertonic (7% NaCl solution w/v) and isotonic (0.9% NaCl solution w/v) saline treatments were administered using a nebulizer (705-445, AMG Medical Inc, Montreal, Quebec, Canada), which produces liquid aerosols with a median diameter of 4 μm. The nebulizer was connected to a ventilator (687 mouse ventilator, Harvard Apparatus, St. Laurent, Quebec, Canada) that delivered the aerosols to the tracheal preparation for a period of 90 s with a frequency of 40 strokes per minute. Each stroke was 30 ml. Hypertonic saline or ITS treatment began at time 0. Images were captured 3 minutes before treatment (-3 min), and 6, 12, and 18 minutes after treatment.

Reagents

The drugs were obtained from Sigma-Aldrich unless otherwise stated. CFTRinh172 was purchased from Cedarlane Labs (Burlington, ON, CA), tetrodotoxin was obtained from Alomone labs (Jerusalem, Israel), and lidocaine hydrochloride spray was acquired from Odan Laboratories LTD (Montreal, Canada). Stock solutions of CFTRinh172, atropine, bumetanide, niflumic acid, and L-703606 were dissolved in DMSO. The final concentration of DMSO was

less than 0.1%. Tetrodotoxin was directly dissolved into purified water.

Statistics

Data are presented as mean ± SEM. The two-way ANOVA analysis and Tukey's multiple comparisons test was done using GraphPad Prism 5 (GraphPad Software Inc., San Diego, CA, US), with $p < 0.05$ considered significant.

Study approval

All experiments were performed with the approval of the Canadian Light Source and the Animal Ethics Committee at the University of Saskatchewan.

4.4 Results

We have developed a synchrotron-based imaging method to measure and quantify ASL secretion in intact airways (Luan et al., 2014). We exploited the large refractive index difference between the air and the airway surface liquid (ASL) layer, which produces a strong signal at the air/ASL interface using phase contrast imaging (PCI) (Fig. 4.1A) (Donnelley et al., 2014; Morgan et al., 2013). Because PCI does not allow us to observe the ASL/tissue interface to determine the ASL height, we determined the position of the tissue with respect to the air/ASL interface using agarose beads as "measuring rods". The agarose beads are instilled in the ASL and come into direct contact with the surface epithelium due to the force generated by the surface tension of the ASL (see supporting information). The surface tension of the ASL immobilizes the beads on the surface of the epithelium (i.e. beads are not cleared away by

airway cilia), and the liquid secreted by the airway, which would normally be cleared from the airway due to mucociliary clearance, is retained around the static bead, allowing us to measure the accumulation of the ASL produced by fluid secretion. A researcher blinded to the experimental conditions measures the height of the ASL layer as the distance between the air/ASL interface and the edge of the agarose bead touching the surface epithelium (Fig. 4.1B) (Luan et al., 2014).

Tracheal preparations had the cartilage removed to expose the submucosal glands and the nervous tissue to the bathing fluid, and the preparations were fitted to a custom-built chamber that maintained the tissue immersed in Krebs solution bath while the lumen of the trachea preparation remained free of solution and accessible to the researchers. The preparation was attached to a ventilator connected to a nebulizer. Hypertonic (7%) or isotonic (0.9%) saline was applied to the lumen of the preparation using the nebulizer and ventilator arrangement (Fig. 1A). The height of ASL layer was measured 3 min before treatment and 6, 12, and 18 min after nebulization (time 0) (Fig. 4.1C).

As expected, treatment of swine airway with HTS significantly increased ASL production when compared to preparations nebulized with isotonic saline (ITS) and preparations without treatment (control) (Fig. 4.1D). HTS caused a significant increase in ASL secretion within 6 minutes after treatment that persisted for the remainder of the experiment. The ASL layer also increased in both the ITS and control groups, but the difference between the groups was not significant. This would suggest that there is a basal level of ASL secretion in the isolated airway.

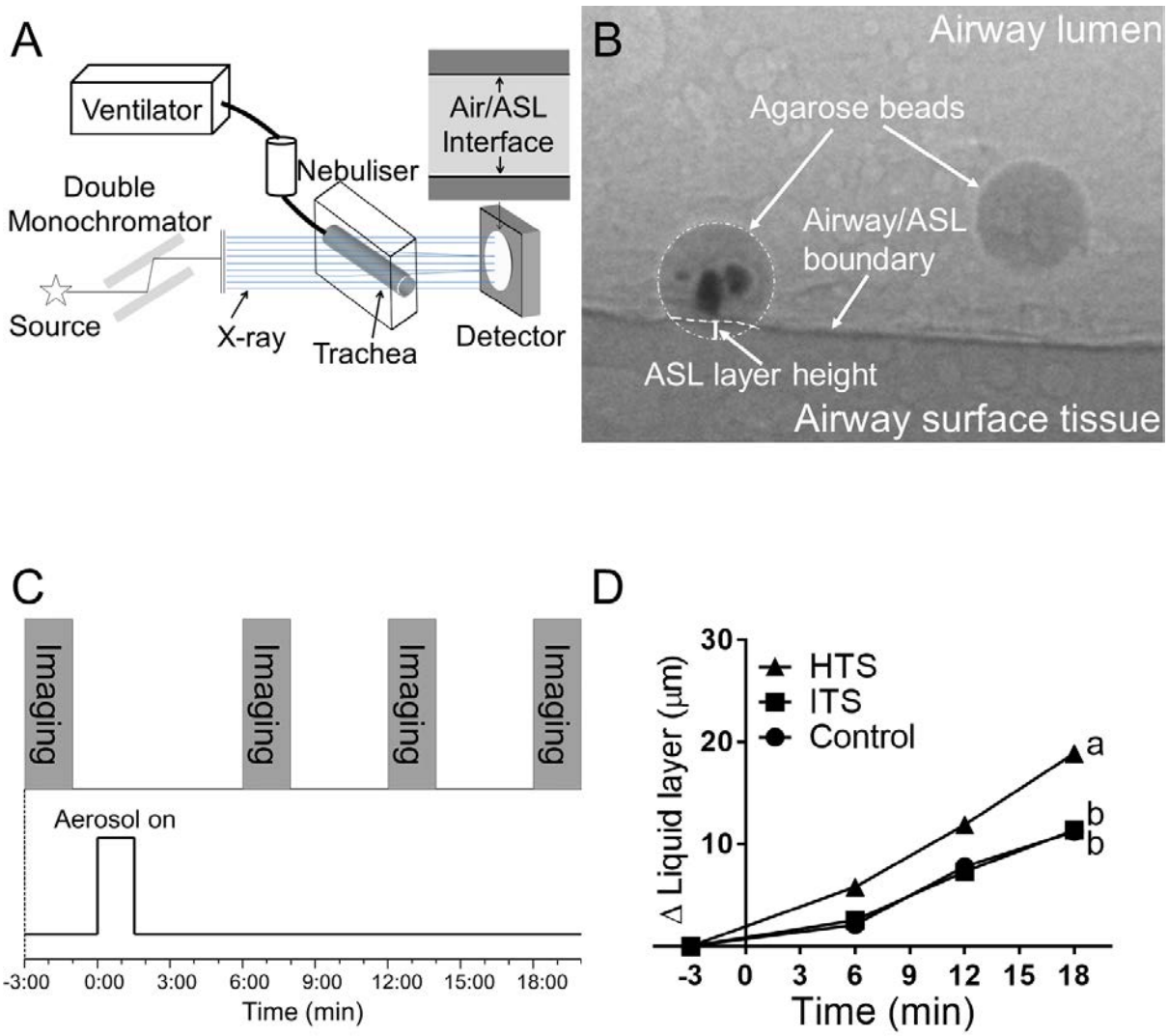

Fig. 4.1. Experimental design and phase contrast imaging using synchrotron x-rays. (A) Schematic showing the set up for the detection of air-ASL interface in the lumen of an intact trachea using phase contrast imaging. When x-rays pass through the preparation, the difference in refractive index between the ASL and the air results in a phase shift of x-rays that causes a distinct interference pattern detected as variations in x-ray intensities on the CCD. The trachea preparation was set up in a custom build chamber that was connected to a nebulizer and a ventilator apparatus. (B) Synchrotron-based phase contrast imaging measurement of ASL height in an isolated swine trachea. (C) HTS or ITS aerosol were delivered at time 0 for 90 seconds, and images were acquired at time -3, 6, 12, and 18 minutes. (D) Treatment with HTS stimulated higher ASL secretion compared to preparations treated with ITS and control preparations (HTS, n = 45 beads from 15 tracheas; ITS, n = 49 beads from 14 tracheas;

control, n = 12 beads from 5 tracheas). Data is presented and the statistical analyses were performed on an individual bead measured value basis. Data is presented as mean ± SEM and were analyzed by two-way ANOVA and Tukey's multiple comparison test. The error bars are small and hidden behind the symbols. Data sets labeled with different letters differ significantly, $p < 0.05$.

HTS-triggered ASL secretion is partially mediated by the nervous system

Since previous reports indicated that HTS stimulates neurogenic inflammation (Umeno et al., 1990), we tested the effect of blocking the nervous system in airways treated with HTS. Incubating airways in tetrodotoxin (TTX, 1μM) and lidocaine (luminal spray of 80 mg/ml solution) blocks both the voltage-dependent sodium channels (Scholz et al., 1998; Brau et al., 2000) expressed by neurons intrinsic to the airways and the TTX-independent sodium channels expressed by sensory neurons of the airways (Widdicombe and Wine, 2015; Wine, 2007). These results show that blocking neuronal function with lidocaine+TTX reduces the effect of HTS treatment by ~50% (Fig. 4.2A). In contrast, lidocaine+TTX treatment had no effect on ITS-treated preparations (Fig. 4.2A). We also tested whether lidocaine may have non-specific inhibitory effects on epithelial cells. It has shown that exposure to bacteria stimulated ASL secretion independently of the nervous system (Luan et al., 2017). Using similar procedures (Luan et al., 2014), we determined that lidocaine-treated preparations showed no reduction in bacteria-stimulated ASL response (data not shown), rejecting any non-specific inhibitory effects of lidocaine on epithelial function. These results suggest that blocking neuronal function specifically abrogates HTS-triggered ASL production, which is consistent with the hypothesis that neurogenic inflammation plays a role in the response to HTS treatment.

To evaluate the effect of HTS treatment in CF airways, we used the CFTR blocker CFTRinh172 (100 μM) to model airways without CFTR function (Melis et al., 2014). HTS treatment in preparations incubated with CFTRinh172 (HTS+172) was less effective in stimulating ASL production than preparations not incubated in CFTR blocker (HTS). However, it still stimulated higher ASL production than ITS treatment (ITS+172, Fig. 4.2B). This result

concurs with previous experiments showing that HTS treatment improves ASL hydration in CF patients (Robinson et al., 1996; Robinson et al., 1997). Interestingly, CFTRinh172 treatment reduced ASL secretion in ITS-treated samples (ITS+172) below that of ITS treatment in control preparations (ITS, Fig. 4.2B), suggesting that the trachea has a basal level of CFTR-dependent ASL secretion.

Preparations incubated with CFTRinh172 suffered a reduction in the response to HTS treatment when neuronal function was blocked with lidocaine+TTX (Fig. 4.2C). In contrast, ITS-treated preparations were not affected by lidocaine+TTX (Fig. 4.2C). These results suggest that HTS treatment, but not ITS, increases ASL secretion through stimulation of sensory and/or airway intrinsic neurons in CF airways.

Since there is evidence that HTS treatment triggers substance P (SP) release (Baraniuk et al., 1999), and that SP can stimulate ASL secretion by airway epithelia in the trachea of several species (Ianowski et al., 2008; Choi et al., 2009; Khansaheb et al., 2011), we tested the effect of a SP receptor (neurokinin 1 receptor, NK-1) blocker, L-703606 (1 μM) on HTS-stimulated ASL production. The results show that treatment with L-703606 (HTS + NK-1 Blocker) significantly reduced HTS-triggered ASL production, but had no effect on the ITS treatment group (ITS + NK-1 Blocker, Fig. 4.2D). However, HTS treatment of preparations incubated with CFTRinh172 was unaffected by the NK-1 blocker (Fig. 4.2E), indicating that the SP-mediated HTS-triggered effect is CFTR dependent and may be absent in CF airways.

We then tested the possible role of muscarinic stimulation on HTS-triggered ASL secretion. Blocking muscarinic receptors with atropine (1μM) reduced HTS-triggered ASL secretion but had no effect on ITS treated samples (Fig. 4.2F). Atropine also reduced the

response to HTS treatment in preparations incubated with the CFTR blocker, CFTRinh172, but had no effect on ITS-treated preparations. These results suggest that in CF airways, HTS treatment stimulates neuronal release of cholinergic signals and the production of active ASL secretion by airway epithelia.

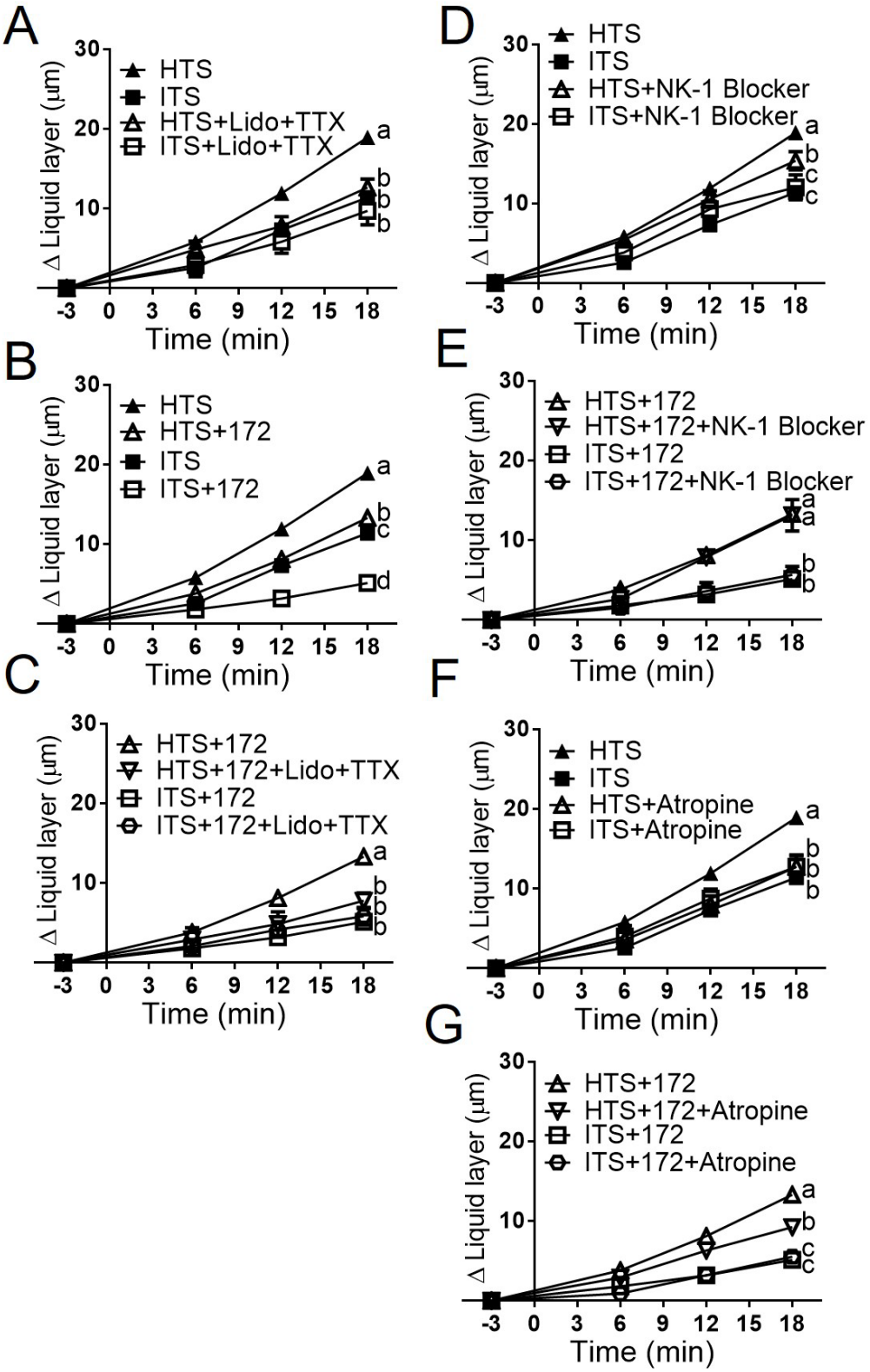

Fig. 4.2. HTS stimulates ASL secretion via activation of sensory neurons and release of acetylcholine in CF airways. (A) Treatment with lidocaine (Lido, 80mg/ml aerosol) plus tetrodotoxin (TTX, 1μM) blocked HTS-triggered ASL secretion but had no effect in ITS-treated preparations (HTS, n = 45 beads from 15 tracheas; ITS,

n = 49 beads from 14 tracheas; HTS+Lido+TTX, n = 18 beads from 4 tracheas; ITS+Lido+TTX, n = 9 beads from 4 tracheas). (B) Incubation with CFTRinh172 (172, 100μM) reduced the effect of HTS treatment. However, HTS treatment still produced more ASL than ITS treatment (HTS, n = 45 beads from 15 tracheas; ITS, n = 49 beads from 14 tracheas; HTS+172, n = 59 beads from 12 tracheas; ITS+172, n = 29 beads from 8 tracheas). (C) Incubation with lidocaine plus TTX blocked the response of CFTRinh172-treated airway to HTS, but had no effect on ITS treated preparations (HTS+172, n = 59 beads form 12 tracheas; HTS+172+Lido+TTX, n = 9 beads from 4 tracheas; ITS+172, n = 29 beads form 8 tracheas; ITS+172+Lido+TTX, n = 21 beads from 6 tracheas). (D) The substance P receptor blocker, L-703606 (NK-1 Blocker, 1μM), reduced the response to HTS treatment but had no effect on ITS treated samples (HTS, n = 45 beads from 15 tracheas; ITS, n = 49 beads form 14 tracheas; HTS+NK-1 Blocker, n = 36 beads form 12 tracheas; ITS+NK-1 Blocker, n = 16 beads from 5 tracheas). (E) CFTRinh172-treated preparations did not respond to the NK-1 blocker (HTS+172, n = 59 beads from 12 tracheas; HTS+172+NK-1Blocker, n = 10 beads from 4 tracheas; ITS+172, n = 29 beads from 8 tracheas; ITS+172+NK-1 blocker, n = 17 beads from 6 tracheas). (F) Blocking muscarinic receptors with atropine (1 μM) significantly reduced the effect of HTS treatment but had no effect on ITS treated preparations (HTS, n = 45 beads from 15 tracheas; ITS, n = 49 beads form 14 tracheas; HTS+Atropine, n = 22 beads from 5 tracheas; ITS+Atropine, n = 11 beads from 4 tracheas). (G) Atropine (1 μM) blocks the effect of HTS treatment but does not affect ITS treatment in preparations incubated in CFTRinh172 (HTS+172, n = 59 beads from 12 tracheas; HTS+172+Atropine, n = 18 beads from 5 tracheas; ITS+172, n = 29 beads from 8 tracheas; ITS+172+Atropine, n = 19 beads from 5 tracheas). Data is presented and the statistical analyses were performed on an individual bead measured value basis. Data are presented as mean ± SEM and were analyzed by two-way ANOVA and Tukey's multiple test. The error bars are small and hidden behind the symbols. Data sets labeled with different letters differ significantly, $p < 0.05$.

HTS treatment triggers active secretion of ASL by airway epithelia

To further test the possible role of active epithelial ASL secretion in response to HTS treatment, we tested pharmacological agents that block epithelial ASL production. If HTS triggers neuron-stimulated epithelial ASL secretion, one would expect to block the effect of HTS by blocking ion transport by epithelial cells. However, if the effect of HTS is entirely mediated by an osmotic effect, then an ion transport blocker treatment should have little effect. As most of the ASL in the upper airways (i.e. down to about the 10^{th} bronchial generation, where airway lumen is ~1–2 mm in diameter) is produced by submucosal glands (Tos, 1966; Wine and Joo, 2004), we tested blockers known to abrogate gland secretions on HTS-triggered ASL production (Baraniuk et al., 1999; Wine and Joo, 2004): the CFTR blocker CFTRinh172, the Na^+:K^+:2Cl^- cotransporter blocker bumetanide (100 µM) (Wine and Joo, 2004), and a Ca^{2+}-activated Cl^- channel blocker niflumic acid (100 µM) (Wine and Joo, 2004), and in HCO_3^--free saline solution (Joo et al., 2002).

HTS treatment of preparations incubated in the CFTR inhibitor alone produced a higher level of ASL secretion compared with preparations incubated in the cocktail of blockers (i.e. CFTRinh172, bumetanide, and niflumic acid in HCO_3^--free bath), suggesting that HTS triggers active ASL production by the airway epithelia in a CFTR-independent manner (Fig. 4.3A). In contrast, there was no difference in ASL production by ITS-treated preparations incubated with CFTR inhibitor alone or the blocker cocktail (Fig. 4.3B), indicating that the blocker cocktail specifically blocks the effect of HTS treatment. These results suggest that the CF airway responds to HTS treatment by triggering active ASL secretion independent of CFTR, by the airway epithelia. To estimate the proportion of ASL produced by active ASL secretion by CF

epithelia, we incubated preparations in CFTRinh172, bumetanide, and niflumic acid in HCO_3^--free saline and treated them with HTS or ITS (Fig. 4.3C). Since these preparations are unable to produce ASL through epithelial secretion, the difference in ASL produced by HTS and ITS treated preparations must be driven by the osmotic effect alone generated by the hypertonic treatment. The results show that ~50% of the ASL produced by HTS treatment in CF preparations (i.e. incubated in CFTRinh172) is generated by active ASL secretion by airway epithelia.

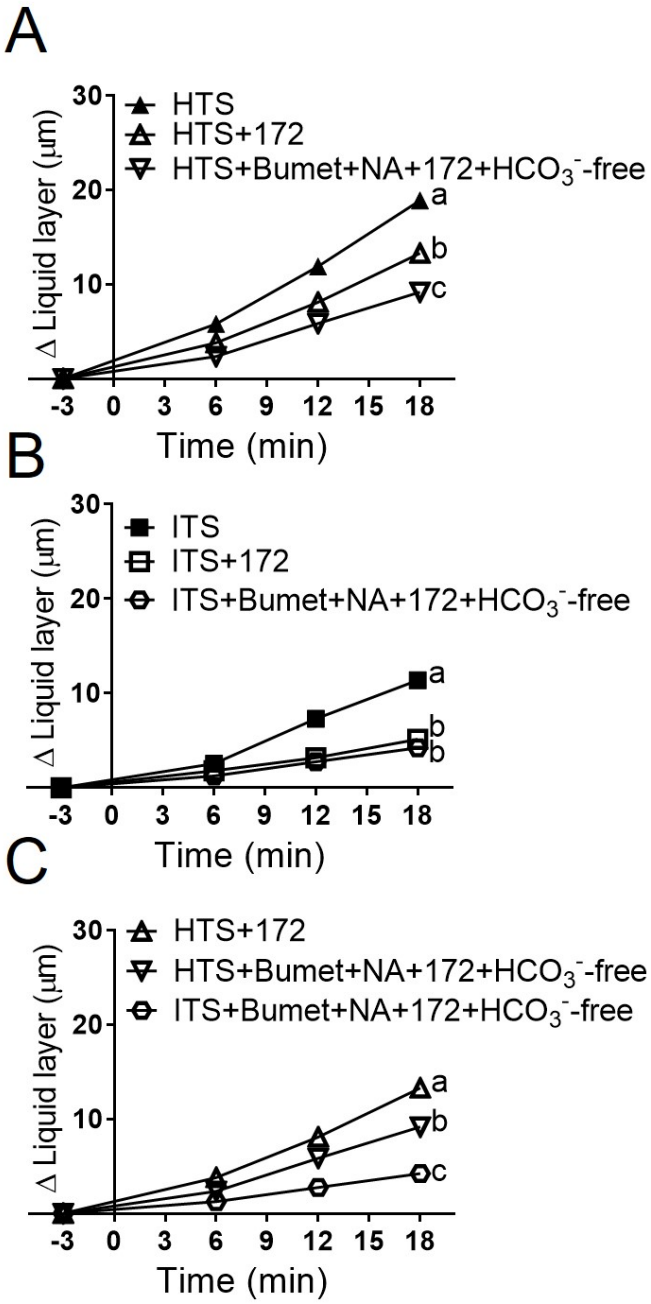

Fig. 4.3. HTS treatments stimulate active ASL production by airway epithelia. (A) Treatment with the CFTR blocker CFTRinh172 (100 μM) reduced HTS-triggered ASL production. However, treatment with CFTRinh172, bumetanide (100 μM), and niflumic acid (100 μM) in HCO_3^--free saline solution bath reduced HTS-triggered ASL production even further (HTS, n = 45 beads form 15 tracheas; HTS+172, n = 59 beads form 12 tracheas; HTS+Bumet+NA+172+HCO_3^--free, n = 24 beads form 7 tracheas). (B) In ITS-treated preparations incubation with the ion transport blocker cocktail (CFTRinh172, bumetanide, and niflumic acid in HCO_3^--free

bath) has a similar effect as CFTRinh172 alone (ITS, n = 49 beads form 14 tracheas; ITS+172, n = 29 beads from 8 tracheas; ITS+ Bumet+NA+172+HCO_3^--free, n = 18 beads form 7 tracheas). (C) Approximately 50% of the ASL produced by HTS in airways without CFTR function is the result of the osmotic effect. After blocking all ion transport with CFTRinh172, bumetanide, and niflumic acid in HCO_3^--free saline, HTS produced ~50% less ASL secretion than that produced by preparations incubated with CFTRinh172 alone (HTS+172, n = 59 beads form 12 tracheas; HTS+ Bumet+NA+172+HCO_3^--free, n = 24 beads form 7 tracheas; ITS+ Bumet+NA+172+HCO_3^--free, n = 18 beads form 7 tracheas). Data is presented and the statistical analyses were performed on an individual bead measured value basis. Data is presented as mean ± SEM and was analyzed by two-way ANOVA and Tukey's multiple comparison test. The error bars are small and hidden behind the symbols. Data sets labeled with different letters differ significantly, $p < 0.05$.

4.5 Discussion

The key finding in this study is that HTS treatment triggers ASL production, not only through an osmotic effect that draws water from the serosal surface into the ASL, but also through the stimulation of the nervous system, which triggers active ASL secretion by airway epithelia. The presence of hypertonic saline may be detected by Aδ and C fibers (Pedersen et al., 1985; Fox et al., 1995), probably as a change in osmolality or ion concentration in the sensory neurons (Pedersen et al., 1985), which triggers the local release of neurotransmitters that stimulate ASL secretion from airway submucosal glands (Wine and Joo, 2004), and possibly modulates surface airway epithelia ion transport (Joo et al., 2016). Aδ and C fibers are more frequent in the larger airways (Chou et al., 2008), which may explain the recent unexpected finding that HTS treatment has a stronger effect on mucociliary clearance in the larger airways than in small ones (Cazzarolli et al., 2016).

The contribution of the nervous system to HTS-triggered ASL secretion may be larger *in vivo*, where the nervous system is intact and nebulization with HTS may trigger central reflexes and more vigorous epithelia secretion (Chou et al., 2008). A large number of nervous signals, including cholinergic, neurokinins, and vasoactive intestinal peptides may stimulate epithelial ASL secretion and also can have additive or synergistic effects (Widdicombe and Wine, 2015). In our *ex vivo* preparation, we detected substance P and cholinergic mediated stimulation of ASL secretion, however, only cholinergic stimulation had an effect on preparations without functional CFTR, suggesting that the contribution of the nervous system on HTS-triggered ASL secretion would be different in CF and in non-CF airways (Cazzarolli et al., 2016; Widdicombe and Wine, 2015).

Our results also indicate that it may be possible to modulate the duration and intensity of HTS treatment by pharmacologically modulating the contribution of the nervous system to ASL secretion by using agonists, such as capsaicin, or by using blockers, such as lidocaine. Finally, our results highlight that the use of HTS formulations, which include blockers of epithelial ASL reabsorption (e.g. ENaC blockers) may reduce the effect of HTS treatment if they interfere with epithelial ASL secretion (Donaldson et al., 2006).

Chapter 5

Ion transport anomalies by the collecting and ciliated ducts contribute to airway surface liquid secretion deficient by submucosal glands in cystic fibrosis swine

5.1 Abstract

The upper airway is protected by an efficient innate defence mechanism that relies on the airway surface liquid (ASL) to trap, kill, and clear pathogens from the lungs. Most of the ASL required for host defence in the upper airway is secreted by submucosal glands. In CF, the function of airway submucosal glands is abnormal, resulting in the production of ASL with lower pH, reduced antimicrobial properties, and abnormal rheological properties. The glands' abnormal function contributes to the failure of bacterial clearance from the lungs. This failure triggers a cycle of infection and inflammation that may eventually result in respiratory failure. These abnormalities are attributed to anomalies in ion transport across the epithelia lining the different section of the gland, each of which function coordinately to produce the ASL. However, the ion transport properties of each individual segment of the gland (i.e. serous acini, mucous tubules, collecting duct and ciliated duct) are unknown, and there is controversy regarding what segments express CFTR. This makes it difficult to determine the nature of glandular abnormalities that may contribute to CF lung disease and to identify targets for treatment. Using a self-referencing ion selective electrode technique, we characterized Cl^- and Na^+ transport properties in all four segments of the submucosal glands, and we identified how they are anomalous in CF swine. Our results show that in normal airway, the serous acini and collecting duct secreted Cl^- and Na^+ into the lumen in response to carbachol and forskolin

stimulation. The ciliated duct also transported Cl^- and Na^+ but in the opposite direction, i.e. reabsorption from the ASL, which may contribute to lowering Na^+ and Cl^- concentrations in the glandular secretion relative to the plasma. In $CFTR^{-/-}$ airway the serous acini, collecting duct, and ciliated duct fail to execute their function after forskolin stimulation, which results in abnormal ASL production with reduced pH but normal Cl^-, Na^+ and K^+ concentration.

5.2 Introduction

Cystic fibrosis (CF) is an autosomal recessive genetic disorder caused by mutations in the gene encoding the anion channel Cystic Fibrosis Transmembrane conductance Regulator (CFTR). Most of the morbidity and mortality suffered by CF patients arises from lung disease (Stoltz et al., 2015) that results from chronic bacterial infections and inflammation. However, the sequence of events that result in lung disease from CFTR mutations is not fully understood. Data accumulated over the last few years show that the first consequence of CFTR mutation is an impaired ability to eradicate bacteria from the lungs.

Lungs from CF animal models (F508del and $CFTR^{-/-}$ pigs) (Ostedgaard et al., 2011; Stoltz et al., 2010) fail to clear bacteria as effectively as wild-type littermates before the development of inflammation (Stoltz et al., 2010; Stoltz et al., 2013). This suggests that impaired bacterial elimination is the pathogenic event initiating a cascade of inflammation and pathology in CF lungs (Stoltz et al., 2010). Research in neonate animal models of CF suggest that the failure to clear bacteria may be the result of abnormal airway surface liquid (ASL) secretion by airway submucosal glands (Luan et al., 2014; Luan et al., 2017). The ASL produced by $CFTR^{-/-}$ swine has low pH and bacteria killing properties (Stoltz et al., 2010;

Pezzulo et al., 2012; Joo et al., 2006; Joo et al., 2010; Ballard et al., 2016). The ASL rheological properties of the ASL are also abnormal, causing ASL to be retained within the glands, which reduces the rate and efficiency of mucociliary clearance (Hoegger et al., 2014; Ballard et al., 2016; Tang et al., 2016; Jayaraman et al., 2001; Roy et al., 2014). Thus, it has been proposed that abnormal ion transport by submucosal gland is the pathogenic event that inhibits the innate immune function of the airway, and triggers a cycle of infection and inflammation that may eventually lead to respiratory failure in CF patients (Joris et al., 1993; Smith et al., 1996; Choi et al., 2009; Wine and Joo, 2004, Widdicombe and Wine, 2015). Unfortunately, we have a poor understanding of how the properties of the ASL are regulated. We also do not understand the function(s) of the different cell types and anatomical regions of the gland. Thus, we do not know how they malfunction in CF.

Submucosal glands are complex organs comprised of four distinct segments – the serous acini, the mucous tubule, the collecting tube, and the ciliary duct (Meyrick et al., 1969), as shown in Fig. 5.1. The serous acini have been well studied and are known to be the primary site of fluid secretion (Mayerick and Reid, 1970). The fluid then flows into the mucous tubules and hydrates the gel-forming mucins secreted by mucus cells (Widdicombe and Wine, 2015; Wine and Joo, 2004). The mucous tubules feed into the collecting duct, and the fluid is then transported through the ciliated duct and released onto the airway surface. It is not known whether the duct cells contribute to ASL formation (Wine and Joo, 2004). The anatomical characteristics of the duct cells as well as reports of CFTR expression in duct epithelia suggested that they may be involved in ion transport and modulation of ASL properties and may malfunction in CF (Meyrick et al., 1969; Englehardt et al., 1992; Wine and Joo, 2004;

Kedra et al., 2005; Jiang and Engelhardt, 1998). However, to date, there is no direct evidence of the ion transport properties of each segment of the gland. We thus do not how their functions are altered in CF. A key reason for this lacuna is the lack of a technique that has sufficient resolution to measure ion transport within each of the subunits of the submucosal gland.

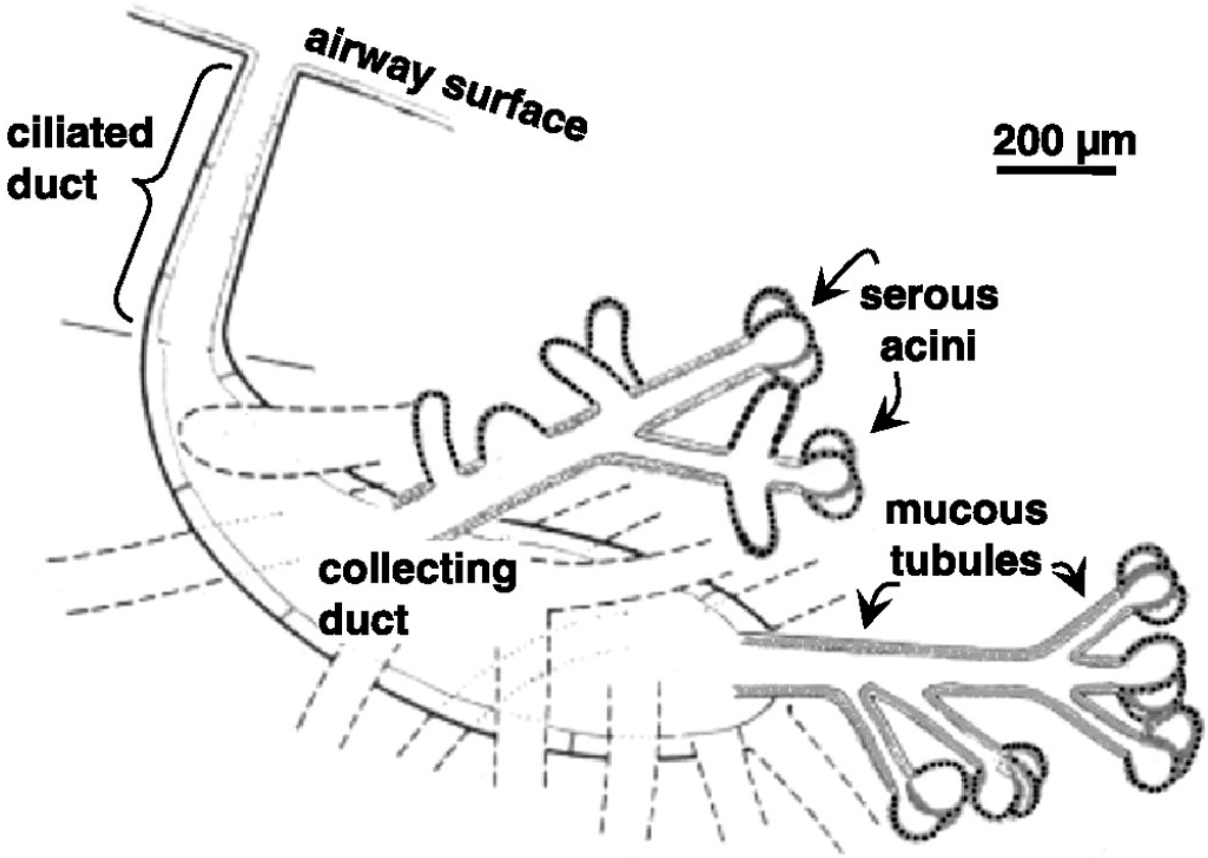

Fig. 5.1 Segmentation model of airway submucosal gland. (adapted from Wu et al., 2007)

In this study, we use a self-referencing ion selective microelectrode technique capable of spatial resolution unparalleled by previous studies, to measure the ion transport properties of the different segments of the airway submucosal glands in wild-type and in $CFTR^{-/-}$ swine. Our results show that stimulating wild-type airway submucosal glands with the intracellular cAMP elevating agent, forskolin, or the cholinergic agonist, carbachol, activated Na^+ and Cl^- transport by the serous acini, the collecting duct, and the ciliated duct. Quite interestingly, we found that the ciliated duct reabsorbs NaCl from the lumen of the gland, which may explain the reduced NaCl concentration in glandular secretion. In $CFTR^{-/-}$ swine glands, the serous acini, collecting duct, and ciliated duct fail to respond to forskolin stimulation, and the pH of glandular secretion was acidic.

5.3 Materials and Method

All procedures were approved by the Animal Care Committee of the University of Saskatchewan. The full detail of experimental methods can be found in the supplemental methods section

Tracheal preparation and dissection of submucosal glands

Swine airways and lungs were harvested from wild-type juvenile female and male pigs weighing 20-23 kg or one week old, and from $CFTR^{-/-}$ swine aged from 2-7 days. The trachea and major bronchi were dissected within 15-30 minutes of euthanasia and placed in ice cold Krebs–Ringer bicarbonate buffer (mmol l^{-1}): 115 NaCl, 2.4 K_2HPO_4, 0.4 KH_2PO_4, 1.2 $CaCl_2$, 1.2 $MgCl_2$, 25 $NaHCO_3$, 10 glucose (pH=7.4) equilibrated with 95% O_2, 5% CO_2. Since the

viability of the tissue declines with time we did not keep the tissue for more than 30h after euthanasia. To minimize tissue exposure to endogenously generated prostaglandins during tissue preparation, mounting, and experimentation, 1 μmol l^{-1} indomethacin was present in the bath throughout.

Dissected pieces of airway (~3 cm^2) were pinned mucosal side up. The mucosa containing submucosal glands was dissected from the cartilage and pinned onto the petri dish with the serosal side up.

Construction of ion-selective microelectrodes

The liquid membrane ion-selective microelectrodes were fabricated from borosilicate unfilamented capillary glass (WPI, Sarasota, USA). The capillary glass was washed for 10 min in nitric acid, then rinsed with deionized water and baked on a hot plate at 250°C for at least 30 min. The capillaries were then removed from the hotplate and pulled on a vertical micropipette puller (PC-10, Narishige, Japan). The diameters of microelectrodes tip were about ~5 μm. Retention of the hydrophobic ionophore cocktails requires salinization of the interior of the capillary. For this purpose, the capillaries were placed on a hot plate at 250 °C and cover by a glass petri dish with approximately 500 μl of dimethyldichlorosilane (Fluka), whose vapors salinize the interior of the capillary. The capillaries were baked for overnight at 250°C. Finally, a short column of liquid ion-selective cocktail of ~250 μm was introduced into the capillary and it was backfilled with the appropriate solution.

Sodium microelectrodes were made with Na^+ Ionophore II-Cocktail A (Fluka) and backfilled with 100 mmol l^{-1} NaCl solution. These electrodes were calibrated using 15 mmol l^-

^{1} NaCl + 135 mmol l^{-1} LiCl and 150 mmol l^{-1} NaCl solutions. The change in voltage measure for a tenfold change in ion activities (i.e. slope) was 52.7 $\pm$ 0.2 mV.

Potassium microelectrodes were made with K^{+} Ionophore I-Cocktail B (Fluka) and backfilled with 100 mmol l^{-1} KCl solution. These electrodes were calibrated using 15 mmol l^{-1} KCl + 135 mmol l^{-1} NaCl and 150 mmol l^{-1} KCl solutions. The change in voltage measured for a tenfold change in ion activities (i.e. slope) was 52.3 $\pm$ 0.6 mV.

Chloride microelectrodes were made with Cl^{-} Ionophore I-Cocktail A (Fluka) and backfilled with 1 mol l^{-1} KCl solution. These electrodes were calibrated using 10 mmol l^{-1} KCl and 100 mmol l^{-1} KCl solutions. The change in voltage measure for a tenfold change in ion activities (i.e. slope) was 57.0 $\pm$ 0.6 mV.

Measurement of ion flux

We used the Scanning Ion-selective Electrode Technique (SIET, Forestdale, MA, USA) and the automated scanning electrode technique (ASET 2.0) software (Science Wares Inc. East Falmouth, MA, USA) to measure ion flux across the different segments of submucosal glands. SIET permits non-invasive measurements of ion flux in isolated epithelia (Doughty and Langton, 2001; Smith and Trimarchi, 2001; Messerli et al., 2009) or in *in-situ* preparations (Boudko et al., 2001). The gland preparation was mounted in a temperature-controlled (37°C) custom-build chamber. The sites of interest (2 sites in each segment per gland) was identified and the electrode was programed to measure ion flux 3 times in each site. Thus, for each gland, we report the ion transport properties of a single region (e.g. serous acini) that is calculated as the average of 2 different sites and 3 repetitions per site.

The electrode was repeatedly moved between two measuring points within the unstirred layer that were separated by 50 µm (determined as optimal in preliminary experiments) using computer-controlled stepper motors. After each movement the system waited for 3s to ensure that electrode movement did not disturb the unstirred layer before measuring the voltage for 1s. The average of three repetitive measurements at each site was used to calculate the ion flux. The reference electrode was Ag/AgCl connected via a salt bridge (3 M KCl with 3% agar inside 1.5 mm diameter borosilicate glass capillary) in a fixed place in the bath 30 to 50 mm away from the stepping ion selective microelectrodes. Baseline potential differences were established at locations in the bath 1.5 mm away from the specimen where there is no detectable unstirred layer. All measurements at the specimen are referred to baseline readings taken periodically during the experiment.

The voltage gradients obtained from the ASET software was used to calculate concentration gradients:

$$\Delta C = C_B \times 10^{\frac{\Delta V}{S}} - C_B$$

Where, ΔC, in µmol l^{-1} cm^{-3}, is the concentration gradient between two points 50 µm apart. C_B is the measured background ion concentration in µM. ΔV is the voltage gradient obtained from ASET in µV, and S is the slope of the microelectrode obtained from the calibration curve. The ion concentration gradient was then converted into ion flux using Fick's law of diffusion:

$$J_I = \frac{-D_I(\Delta C)}{\Delta x},$$

Where J_I is the net flux of the ion in pmol cm^{-2} s^{-1}. D_I is the diffusion coefficient of the ion (1.55×10^{-5} cm^2 s^{-1} for Na^+ and Cl^- and 1.92×10^{-5} cm^2 s^{-1} for K^+). ΔC is the concentration

gradient in pmol cm^{-3} and Δx is the distance between the two points, 50 µm, expressed in cm. Negative values indicate that ions are moving into the lumen of the serous acini and positive flux value indicate that ions are moving from the lumen of the serous acini to the bath.

The experimental saline solution used for SIET experiments were modified from the normal Krebs solution to maximize the signal. For Na^+ measurements, the bathing solution contained 50 mmol l^{-1} Na^+ (mmol l^{-1}): 25 NaCl, 2.4 K_2HPO_4, 0.4 KH_2PO_4, 1.2 $CaCl_2$, 1.2 $MgCl_2$, 25 $NaHCO_3$, 10 glucose, 90 NMDG-Cl^- (pH 7.4). For Cl^- measurements, the bathing solution contained 65 mmol l^{-1} Cl^- (mmol l^{-1}): 65 NaCl, 2.4 K_2HPO_4, 0.4 KH_2PO_4, 1.2 Ca Gluconate, 1.2 Mg Gluconate, 25 $NaHCO_3$, 10 glucose, 50 Na Gluconate (pH 7.4). For K^+ measurement, normal Krebs solution was used (see above). Isolated submucosal glands were placed in dishes with the different saline solutions for at least 15 minutes before starting measuring. All the experiments were performed around 36°C.

The detail procedure to measure the efficiency and spatial resolution of ion selective electrode is described elsewhere (Rheault and O'Donnell, 2001; Pineros et al., 1998; Somieski and Nagel, 2001). We used 1 M NaCl with 0.5% (w/v) agar with tip size about 5 µm as the artificial Na^+ sources to determine the efficiency and space resolution of our SIET setup.

To determine the efficiency of the ion selective electrode, the ratio between the experimental and theoretical slopes of ion concentration change versus distance from the source are measured. As shown in Fig 5.2b and c, experimental measurements (open circles) were made by vibrating the microelectrode through an amplitude of 50 µm at each distance and theoretical values (filled circles) were calculated according to the following equation:

$$\Delta V = S[(-U\Delta r)/(C_B r^2 + Ur)]/2.3$$

where ΔV is the change (mV) over the vibration excursion, S is the slope of the electrode, r is the distance from the source, Δr is the amplitude of the vibration, C_B is the background activity of Na^+ and U is an empirical constant.

To calculate the empirical constant U, a plot of ion activity values at different distances from ion source versus the inverse of the distance from the Na source (1/r) yields were measured, and the slope of the plot indicated the empirical constant U, as described in the following equation:

$$C=C_B+U/r$$

where C_B is the background activity of Na^+.

The efficiency of our SIET Na^+ flux measurement was 78%, which is consistent with previous reports the performance Na^+ electrode.

To estimate the spatial resolution of our Na^+ electrode, the ability to resolve two Na^+ point sources was tested (Fig. 5.2d). Two Na^+ sources were placed 35 µm apart, and the Na^+ flux was measured at both point source and the space surrounding and between the sources every 5 µm per step (Fig. 5.2e). The data shows that SIET can easily resolve the two Na^+ point sources, suggesting that the space resolution of our SIET system allow us to study different segments of airway submucosal gland.

Secretion assay

We used the secretion assay developed by Quinton (1979) as explained elsewhere (Ianowski et al., 2007). Briefly, the mucosal layer from trachea or primary bronchus, with underlying glands, was dissected from the cartilage. A piece of tissue of about 1 cm^2 was pinned

mucosal side up and mounted in a 35-mm-diameter plastic Petri dish lined with Sylgard (Dow Corning Corp). The serosal side was immersed in a bathing solution (~1 ml volume) and the mucosa was in air. Before experimentation, the mucosal surface was gently cleaned and blotted dry with cotton swabs and further dried with a stream of air, after which 20–30 μl of water-saturated mineral oil was placed on the surface. The preparation was then placed in a temperature controlled chamber (TC-324B, Warner Instruments, Hamden, CT, USA) maintained at 37°C and equilibrated with warmed, humidified 95% O_2 and 5% CO_2. Pharmacological agents were diluted to final concentrations with warmed bath solution equilibrated with 95% O_2 and 5% CO_2. They were added to the serosal side by complete bath replacement.

Fluid secreted by individual submucosal glands formed droplets under oil. Images of the lumen of the trachea were taken at 2 min intervals using a digital camera (MiniVid, LW Scientific, Lawrenceville, GA, USA) and stored for off-line analysis. Stored images were analyzed using ImageJ 1.32J (NIH). Secretion volumes were calculated, as previously described, by assuming the mucus droplet to be spherical. Then $V=4/3\pi r^3$, where r is the radius (Joo et al., 2001). The following inclusion criteria for individual droplets were used: (a) circular outline so that a spherical shape could be assumed; (b) clear edges to allow accurate measurement of the radius; and (c) no fusion with neighboring droplets. Viability of the preparation was tested at the end of each experiment by measuring the response to carbachol. Non-responding glands (<5%) were excluded from the analysis. The secretion rate was calculated by fitting the volume versus time plots using linear regression using at least 4 points and the slopes were taken as the secretion rates. The r^2 value for such linear fits was > 0.8.

Reagents

CFTR Inhibitor-172 was obtained from Cedarlane Labs (Burlington, ON, CA); all other compounds were obtained from Sigma (St Louis, MO, US). The solution of carbachol was dissolved directly in Krebs solution. Stock solutions of CFTR Inhibitor-172 and forskolin were dissolved in DMSO and the final concentration of DMSO was less than 0.1%.

Statistics

SIET ion flux data are presented as means $\pm$ SEM obtained from the average of three repeated measurements at the same site. Sample size (n) is the number of glands. The data were analyzed using ANOVA, with $P < 0.05$ considered significant. Data analysis was done using GraphPad prism 5 (GraphPad Software Inc., San Diego, CA, US).

5.4 Results and Discussion

We studied the Na^+ and Cl^- transport properties of the different segments of the airway submucosal gland using the Scanning Ion-selective Electrode Technique (SIET, Fig. 5.2, see methods, Shipley and Feijó, 1999; Kunkel et al., 2006). SIET takes advantage of the ion concentration gradient generated by an ion transporting epithelium, i.e. the unstirred layer adjacent to the cells (Fig. 5.2a). The intensity of this unstirred layer is proportional to the epithelial transport rate (Barry and Diamond, 1984). Hence, it is possible to map and measure patterns of Na^+ or Cl^- flux across an epithelium by measuring the Na^+ or Cl^- concentration gradient in the unstirred layer. SIET uses a computer-controlled ion selective microelectrode

(ISE, Fig. 5.2a) positioned at two sites within the unstirred layer to measure the ion concentration gradient (Fig. 5.2b). We then use Fick's law of diffusion to calculate the diffusion rate of the ions within the unstirred layer, which in steady state, matches net epithelial ion transport (Kuhtreiber and Jaffe, 1990). Thus, SIET directly measures ion (i.e. Na^+, K^+ and Cl^-) transport rate regardless of the transport pathway (transcellular or paracellular) or whether it is passive or active. Another advantage of SIET is the remarkably high temporal and spatial resolution of the technique, which may be in the order of seconds and spatial resolution of ~10 µm (Smith et al., 1999; Piñeros et al., 1998; Somieski and Nagel, 2001, see Methods). We tested the spatial resolution of our electrodes and sampling protocol using two point sources of NaCl separated by 35µm (Fig. 5.2d and e, Somiesk and Nagel, 2001, see methods) and showed that SIET easily resolved the two point sources, indicating sufficient spatial resolution to discriminate the different segments of the glands.

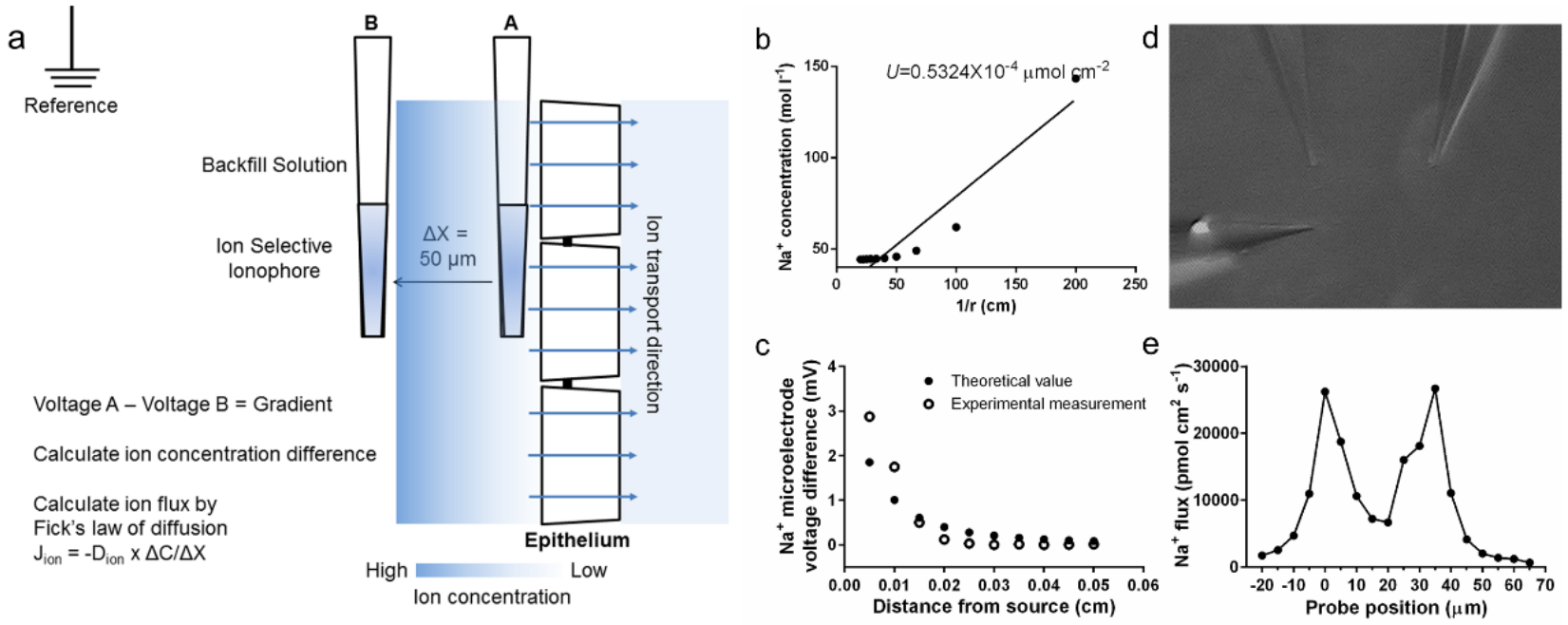
a
Reference
B
A
Backfill Solution
Ion Selective
Ionophore
ΔX =
50 µm
Ion transport direction
Epithelium
Voltage A – Voltage B = Gradient
Calculate ion concentration difference
Calculate ion flux by
Fick's law of diffusion
$J_{ion} = -D_{ion} \times \Delta C/\Delta X$
High
Low
Ion concentration
b
U=0.5324X10^{-4} µmol cm^{-2}
Na$^+$ concentration (mol l^{-1})
1/r (cm)
c
Theoretical value
Experimental measurement
Na$^+$ microelectrode voltage difference (mV)
Distance from source (cm)
d
e
Na$^+$ flux (pmol cm^{-2} s^{-1})
Probe position (µm)

Fig. 5.2. SIET demonstration. a) Schematic diagram showing an ion selective electrode in an experimental setup. The electrode records the ion concentration difference between two points and calculates the ion flux across the epithelium. b and c) Experimental measurements (open circles) were made by vibrating the microelectrode through an amplitude of 50 µm at each distance. Theoretical values (filled circles) were calculated according to the following equation: $\Delta V=S[(-U\Delta r)/(C_B r^2+Ur)]/2.3$, where ΔV is the change (mV) over the vibration excursion, S is the slope of the electrode, r is the distance from the source, Δr is the amplitude of the vibration, C_B is the background activity of Na and U is an empirical constant. b shows the calculation of the empirical constant U. Static measurements were made at a series of distances from the source, and the millivolt outputs were then converted to activity values. A plot of these activity values versus the inverse of the distance from the Na source (1/r) yields a line with a slope of U, according to the equation: $C=C_B+U/r$, where C_B is the background activity of Na and U ($mmolcm^{-2}$) defines the diffusion characteristics of the gradient source. Electrode efficiency (78 %) was calculated as the ratio of the slope of the experimental data to the slope of the theoretical data. d and e) the performance Na electrode in the vicinity of two Na souces about 35 µm apart.

Ion transport properties of the serous acini

We measured transepithelial flux of Na^+, K^+ and Cl^- across the serous acini of submucosal glands from wild-type and $CFTR^{-/-}$ swine. At baseline conditions (i.e. without any treatment) serous acini from wild-type airway submucosal glands displayed little Na^+, K^+ and Cl^- transport (Fig. 5.3a). However, treatment with forskolin (10 μM), an intracellular cAMP elevating agent that stimulates CFTR-dependent gland secretion, triggered serous acini epithelia to transport Na^+ and Cl^- ions from the bath into the lumen, i.e. generating negative values for Na^+ and Cl^- flux measurement (Fig. 5.3). Serous acini preincubated with CFTRinh172 (100μM) - a CFTR anion channel blocker – failed to trigger forskolin-stimulated Na^+ and Cl^- flux (Fig. 5.3). On the other hand, stimulation with the cholinergic agonist carbachol (1μM), with or without CFTRinh172, triggered serous acini cells to move Na^+ and Cl^- ions from the basolateral bath into the apical lumen side at a rate similar to that observed after forskolin stimulation (Fig. 5.3a, b and f).

In contrast, K^+ ion flux does not seem to contribute to fluid production since it remained unaltered and did not significantly differ from zero both before and after forskolin or carbachol treatment (data not shown). These data suggest that Na^+ is the main cation involved in fluid secretion by serous cells.

We characterized the function of the serous acini in CF airway submucosal glands isolated from 2 to 7 days old $CFTR^{-/-}$ swine by measuring Na^+ flux. These Na^+ flux measurements are surrogates for NaCl and/or $NaHCO_3^-$ transport across the epithelia since Na^+ transport rate must be matched by a counter-ion (i.e. Cl^- or HCO_3^-) to maintain electroneutrality. Thus, abnormal Cl^- transport would also cause abnormal Na^+ transport, which would be

detected by SIET. Our results show that baseline Na^+ transport levels in $CFTR^{-/-}$ swine were unperturbed even after treating preparations with forskolin. This is consistent with what is expected when tissues lack functional CFTR channels. However, like wild-type glands, the $CFTR^{-/-}$ serous acini showed bath to lumen Na^+ transport after carbachol treatment (Fig. 5.3e and h). Similar results have been reported previously using secretion assays (Joo et al., 2010). These data reinforce previous reports suggesting that the serous acini are the primary source of CFTR-mediated ASL secretion and their dysfunction contribute to CF pathogenesis.

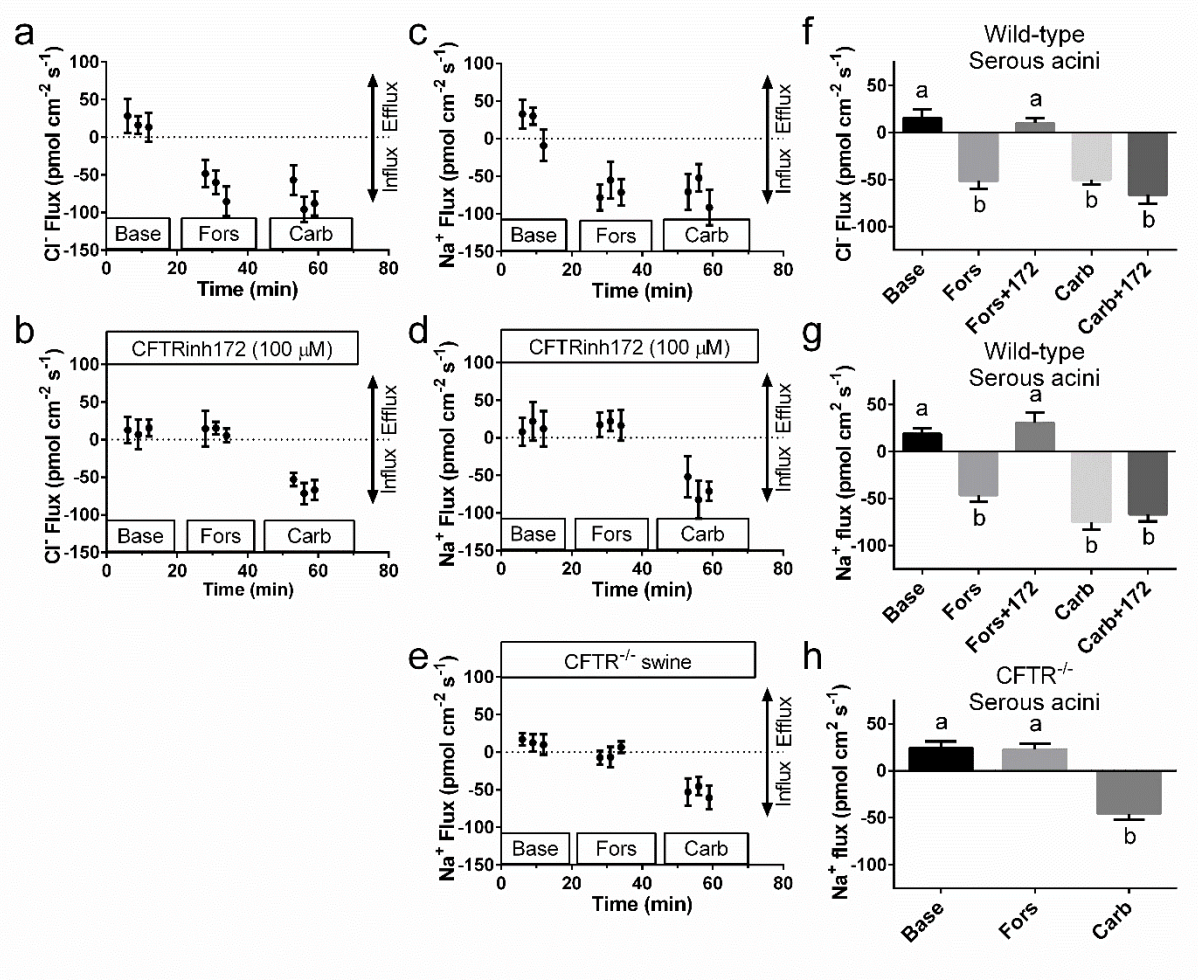

Fig. 5.3. Cl^- and Na^+ fluxes across the serous acini measured by SIET in normal and CF swine tissue. a) Sample trace of Cl^- flux across serous acini of wild-type tissue at baseline condition, Forskolin-treated (10 μM), and Carbachol-treated (1 μM) conditions. b) Sample trace of Cl^- flux across serous acini of wild-type tissue with CFTRinh172 (10 μM) at baseline condition, Forskolin-treated (10 μM), and Carbachol-treated (1 μM) conditions. c) Sample trace of Na^+ flux across serous acini of wild-type tissue after different treatments. d) Sample trace of Na^+ flux across serous acini of wild-type tissue with CFTRinh172 (10 μM) after different treatments. e) Sample trace of Na^+ flux across $CFTR^{-/-}$ serous acini. f) Summary of Cl^- flux changes across serous acini during baseline condition, Forskolin, Forskolin + CFTRinh172, Carbachol, and Carbachol + CFTRinh172 in wild-type tissue (n = 13 glands from 6 animals for baseline, Forskolin, and Carbachol, and n = 11 glands from 6 animals for Forskolin+172 and Carbachol+172). g) Summary of Na^+ flux changes across serous acini during baseline

condition, Forskolin, Forskolin + CFTRinh172, Carbachol, and Carbachol + CFTRinh172 in wild-type tissue (n = 16 glands from 7 animals for baseline, Forskolin, and Carbachol, and n = 12 glands from 7 animals for Forskolin+172 and Carbachol+172). h) Summary of Na^+ flux changes across serous acini during baseline condition, Forskolin, and Carbachol in $CFTR^{-/-}$ tissue (n = 10 glands from 7 animals for baseline, Forskolin, and Carbachol). The statistical analyses were performed on an individual gland measured value basis. (Different letters indicate statistical difference, $p<0.05$, one way ANOVA, Student-Newman-Keuls multiple comparison test).

Ion transport properties of the mucus tubule

The mucous tubules showed low Na^+ and Cl^- movement at baseline conditions and were not increased by forskolin simulation. However, the mucous tubule responded to cholinergic stimulation (carbachol 1μM) by triggering Na^+ and Cl^- fluxes from the basolateral side to the apical side, thus contributing to ASL secretion (Fig. 5.4a and d).

In the presence of CFTRinh172, the mucous tubule segment did not behave any differently, suggesting that this response is independent of CFTR. Furthermore, the mucous tubules from $CFTR^{-/-}$ swine showed the same ion transport pattern as that of wild type swine (Fig. 5.4b and c). This is consistent with the finding that mucous tubules do not seem to express CFTR protein (Engelhardt et. al., 1992; Jiang and Engelhardt, 1998). To our knowledge, this is the first evidence that mucous tubule, in addition to secreting mucins (Finkbeiner et al., 2011), may also contribute ions and fluid transport to the ASL produced by airway submucosal glandular, after cholinergic stimulation.

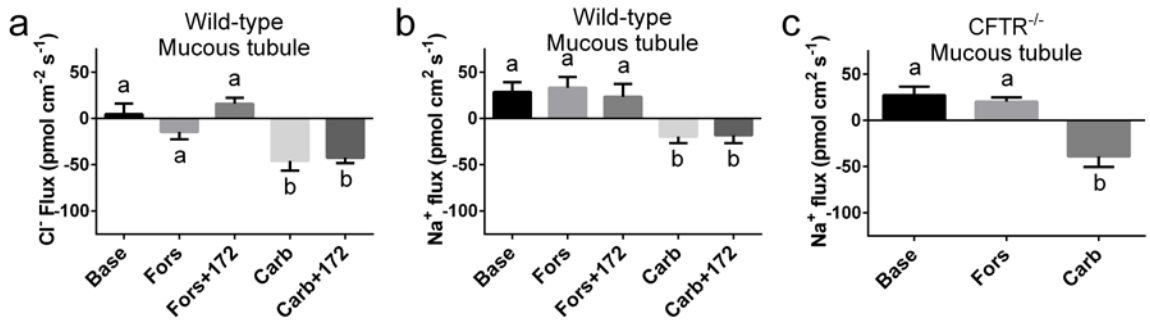

Fig. 5.4. Cl^- and Na^+ fluxes across the mucous tubule measured in normal and CF swine tissue. a) Measurements of Cl^- fluxes across mucous tubule during different treatments (untreated baseline, Forskolin, Forskolin + CFTRinh172, Carbachol, and Carbachol + CFTRinh172) in wild-type gland (n = 10 glands from 6 animals for baseline, Forskolin, and Carbachol, and n = 8 glands from 6 animals for Forskolin+172 and Carbachol+172). b) Measurements of Na^+ fluxes across mucous tubule during different treatments (untreated baseline, Forskolin, Forskolin + CFTRinh172, Carbachol, and Carbachol + CFTRinh172) in wild-type gland (n = 11 glands from 7 animals for baseline, Forskolin, and Carbachol, and n = 8 glands from 6 animals for Forskolin+172 and Carbachol+172). c) Measurements of Na^+ fluxes across mucous tubule during different treatments (untreated baseline, Forskolin, and Carbachol) in $CFTR^{-/-}$ gland (n = 8 glands from 6 animals for baseline, Forskolin, and Carbachol). The statistical analyses were performed on an individual gland measured value basis. (Different letters indicate statistical difference, $p<0.05$, one way ANOVA, Student-Newman-Keuls multiple comparison test).

Ion transport properties of the collecting duct

The collecting duct cells displayed a basal level of Na^+ and Cl^- transport that was not different than 0 flux (Fig. 5.5). Upon stimulation with forskolin both Cl^- and Na^+ increased transepithelial flux from the bath into the lumen, contributing to ASL production. Treatment with the CFTR inhibitor, CFTRinh172 (100μM), blocked the effect of forskolin on Na^+ and Cl^- transport, suggesting that it is CFTR dependent. On the other hand, carbachol (1 μM) stimulated Na^+ and Cl^- ions transport into the lumen of the collecting duct from the surrounding saline bath, and this response was not affected by CFTRinh172 (Fig. 5.5a and b).

In $CFTR^{-/-}$ swine airway submucosal glands, the collecting duct did not respond to forskolin stimulation, but increased Na^+ flux after carbachol treatment (Fig. 5.5c). These results are the first direct evidence that the collecting duct contributes to production of ASL and their function is abnormal in CF.

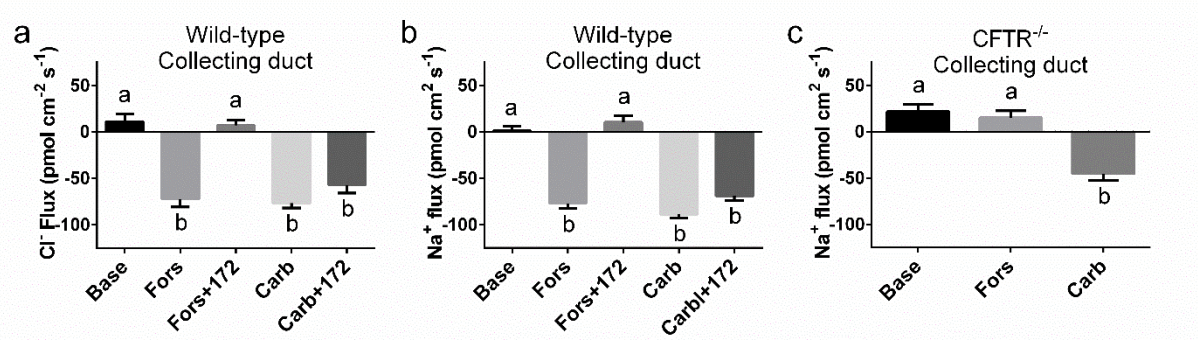

Fig. 5.5. Cl^- and Na^+ fluxes across the collecting duct under different stimulations in normal and CF swine tissue. a) Changes of Cl^- flux across collecting duct during baseline condition, Forskolin-challenge, Forskolin + CFTRinh172- challenge, Carbachol-challenge, and Carbachol + CFTRinh172-challenge in wild-type gland (n = 8 glands from 5 animals for baseline, Forskolin, and Carbachol, and n = 7 glands from 5 animals for Forskolin+172 and Carbachol+172). b) Changes of Na^+ flux across collecting duct during baseline condition, Forskolin-challenge, Forskolin + CFTRinh172- challenge, Carbachol-challenge, and Carbachol + CFTRinh172-challenge in wild-type gland (n = 11 glands from 7 animals for baseline, Forskolin, and Carbachol, and n = 7 glands from 4 animals for Forskolin+172 and Carbachol+172). c) Changes of Na^+ flux across collecting duct during baseline condition, Forskolin-challenge, Carbachol-challenge in $CFTR^{-/-}$gland (n = 7 glands from 5 animals for baseline, Forskolin, and Carbachol). The statistical analyses were performed on an individual gland measured value basis. (Different letters indicate statistical difference, $p<0.05$, one way ANOVA, Student-Newman-Keuls multiple comparison test).

Ion transport properties of the ciliated duct

Like the collecting duct, the ciliated duct epithelia did not have a basal ion transport level. After forskolin stimulation, the ciliated duct cells increased Na^+ and Cl^- transport, but interestingly, transport occurred in the opposite direction than what is observed in the serous acini, mucus tubule and collecting duct cells. The cells lining the ciliated duct transported Na^+ and Cl^- from the lumen of the glands back into the blood side of the tissue, i.e. removing ions form the ASL. Thus, depending the water permeability of this epithelium, the ciliated duct may either reduce the volume of ASL (high water permeability) or reduce the ion strength and osmotic pressure of the ASL (low water permeability). The effect of forskolin was blocked by incubation with the CFTR blocker, CFTRinh172, indicating CFTR-dependent ion transport in ciliated ducts (Fig. 5.6a and b).

Cholinergic stimulation of gland function triggered the ciliated ducts to transport Na^+ and Cl^- from the lumen into the bath, removing ions from the ASL (Fig. 5.6). This transport was not affected by blocking CFTR (Fig. 5.6). These are the first results directly demonstrating that the ciliated duct epithelium is involved in ASL formation, and is concordant with the finding that like airway surface epithelial cells, the ciliated ducts also express CFTR channels (Engelhardt et al., 1992; Kedra et al., 2005).

The ciliated ducts from $CFTR^{-/-}$ swine glands failed to respond to forskolin stimulation (Fig. 5.6c). However, the response to carbachol was similar to that observed in wild-type preparations. Thus, supporting the idea that in CF airway the ciliated epithelium would malfunction.

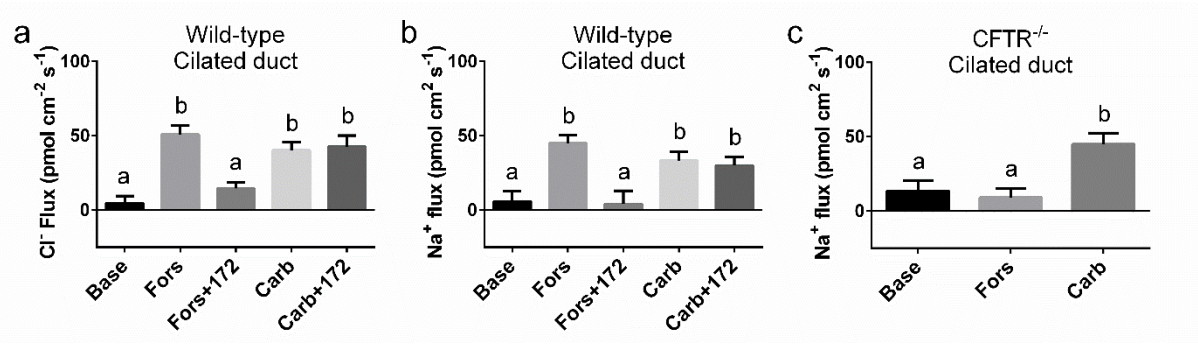

Fig. 5.6. Cl^- and Na^+ fluxes across the ciliated duct under different stimulations in normal and CF swine tissue. a) Summary of Cl^- flux changes across ciliated duct during baseline condition, Forskolin-treatment, Forskoline + CFTRinh172-treatment, Carbachol-treatment, and Carbachol +CFTRinh172-treatment in wild-type gland (n = 9 glands from 6 animals for baseline, Forskolin, and Carbachol, and n = 7 glands from 5 animals for Forskolin+172 and Carbachol+172). b) Summary of Na^+ flux changes across ciliated duct during baseline condition, Forskolin-treatment, Forskoline + CFTRinh172-treatment, Carbachol-treatment, and Carbachol +CFTRinh172-treatment in wild-type gland (n = 10 glands from 6 animals for baseline, Forskolin, and Carbachol, and n = 7 glands from 4 animals for Forskolin+172 and Carbachol+172). c) Summary of Na^+ flux changes across ciliated duct during baseline condition, Forskolin-treatment, and Carbachol-treatment in $CFTR^{-/-}$ gland (n = 7 glands from 5 animals for baseline, Forskolin, and Carbachol). The statistical analyses were performed on an individual gland measured value basis. (Different letters indicate statistical difference, $p<0.05$, one way ANOVA, Student-Newman-Keuls multiple comparison test).

Ion composition of wild-type and CFTR$^{-/-}$ submucosal gland secretions

To further study the role of CFTR and the effect of CFTR mutation on ASL secretion, we measured pH and Na^+, K^+, and Cl^- concentrations in secretions from individual airway submucosal glands. We collected secretions from individual glands using secretion assays in order to avoid potential alteration of fluid by airway surface epithelium. We then measured the ion composition using ion-selective microelectrodes. The concentrations of Na^+, K^+ and Cl^- were the same in basal, forskolin-stimulated, and carbachol-stimulated secretions. Interestingly the ion concentrations in the ASL was significantly lower than that of the fluid bathing the glands, thus suggesting that the ASL is hyposmotic with respect to the plasma (Table 5.1). This may be the result of ion reabsorption by the ciliated duct. Preincubation with the CFTR blocker, CFTRinh172, reduced the volume of ASL but had no effect in the Na^+, K^+, and Cl^- concentrations of the ASL in basal, forskolin-stimulated and carbachol-stimulated compared to untreated control glands (Table 5.1, Jayaraman et al., 2001).

Table 5.1 Na^+, Cl^-, and K^+ concentrations in the gland secretion bubble in health and CFTRinh172-treated pig tissue

	WT-Control			WT-CFTRinh172			Bath
Gland secretion	Baseline	Forskolin	Carbachol	Baseline	Forskolin	Carbachol	
Na^+ concentration (mM)	90.1 ± 3.1[a]	88.3 ± 6.2[a]	91.1 ± 5.9[a]	85.9 ± 6.5[a]	91.9 ± 8.1[a]	92.7 ± 8.9[a]	139.4 ± 5.5[b]
	(n=9)	(n=9)	(n=9)	(n=6)	(n=7)	(n=8)	(n=4)
Cl^- concentration (mM)	96.2 ± 7.0[a]	94.6 ± 6.8[a]	99.2 ± 8.3[a]	91.1 ± 8.9[a]	100.1± 9.4[a]	101.9 ± 11.3[a]	120.1 ± 7.0[b]
	(n=8)	(n=8)	(n=8)	(n=6)	(n=7)	(n=7)	(n=4)
K^+ concentration (mM)	10.2 ± 2.0[a]	13.2 ± 4.1[a]	12.9 ± 3.3[a]	9.5 ± 4.2[a]	9.2 ± 6.0[a]	8.9 ± 5.9[a]	5.17 ± 0.49[b]
	(n=6)	(n=6)	(n=6)	(n=6)	(n=6)	(n=6)	(n=4)

(Data is presented as mean ± SEM and the statistical analyses were performed on an individual gland measured value basis. Different letters in the same row indicate statistical difference, $p<0.05$, one way ANOVA, Student-Newman-Keuls multiple comparison test).

We also measured the pH in the glandular secretion under basal, forskolin-stimulated, and carbachol-stimulated conditions. We found ASL pH was 7.69 ± 0.05 and 7.72 ± 0.06 for basal and forskolin-stimulated glands, respectively, was not statistically different ($p>0.05$, n= 9 secretion essay preparations for baseline and n= 9 secretion essay preparations for forskolin, two-way ANOVA). However, after stimulation with carbachol the pH of glandular secretion increased to 8.25±0.08 ($p<0.05$, n= 10 secretion essay preparations two-way ANOVA, Tukey's multiple comparison test, Table 5.2). Treating the preparations with the CFTR inhibitor, CFTRinh172, significantly change the pH of the ASL secretion compared to untreated control glands ($p<0.05$, n= 5 secretion essay preparations for all baseline, forskolin, and carbachol, two-way ANOVA, Tukey's multiple comparison test, Table 5.2). Accordingly, the ASL produced by glands from $CFTR^{-/-}$ swine had a more acidic ASL at all basal secretion, after stimulation with forskolin, as well as after stimulation with carbachol ($p<0.05$, n= 6 secretion essay preparations for all baseline, forskolin, and carbachol, two-way ANOVA, Tukey's multiple comparison test, Table 5.2). This result is consistent with previous of low pH in ASL secretion by $CFTR^{-/-}$ glands (Pezzulo et al., 2012).

Table 5.2 pH measurements in health, CFTRinh172-treated, and CFTR$^{-/-}$ swine gland secretion

	WT-Control			WT-CFTRinh172			CFTR-/-			Bath	
Gland secretion	Baseline	Forskolin	Carbachol	Baseline	Forskolin	Carbachol	Baseline	Forskolin	Carbachol		
pH	7.69 ± 0.05[a]	7.72 ± 0.06[a]	8.25 ± 0.08[b]	7.49 ± 0.10[c]	7.59 ± 0.11[c]	7.95 ± 0.11[d]	7.34 ± 0.09[c]	7.51 ± 0.07[c]	7.87 ± 0.03[d]	7.47 ± 0.09[e]	
	(n=9)	(n=9)	(n=10)	(n=5)	(n=5)	(n=5)	(n=4)	(n=6)	(n=6)	(n=3)	

(Data is presented as mean ± SEM and the statistical analyses were performed on an individual gland measured value basis. Different letters in the same row indicate statistical difference, $p<0.05$, one way ANOVA, Student-Newman-Keuls multiple comparison test).

5.5 Conclusion

Most exocrine glands, such as submucosal glands, work in a similar fashion. A group of cells located at the distal most segment of the gland, produce a primary fluid that is later modified by the epithelia lining the tubular segments connected to the opening of the gland to produce secretion with varied properties, such as different pH, ion composition, protein content, etc (Humphrey and Williamson, 2001; Delporte, 2014; Quinton, 2007; Saga, 2002; Dartt, 2009). To understand how the airway submucosal glands determine the properties of the ASL and why they are abnormal in CF, we need to understand the function of each segment of the gland in health and disease. Our study is the first to directly measure ion transport properties across the different segments of the airway submucosal gland. The key finding is that in addition to the serous acini, the mucus tubule, collecting duct, and ciliated duct segments of the submucosal gland trigger ion transport after stimulation, and thus, may contribute to determining the ASL properties, e.g. pH, and rheological properties. Moreover, these segments malfunction in CF airway, which may contribute to the abnormal properties of the ASL in CF.

The ion transport properties of the serous acini indicate the existence of CFTR-dependent and CFTR-independent ion transport pathways, which is consistent with previous publications (Widdicombe and Wine, 2015). A novel finding is that both pathways display very similar Na^+, Cl^-, and K^+ transport, suggesting that both pathways produce fluid with similar ion composition. The fluid then enters the mucous tubules, which is believed to be mostly involved in mucin secretion (Audie et al., 1993; Aust et al., 1997; Widdicombe and Wine, 2015). One of the most unexpected results was the discovery that cholinergic stimulation, but not forskolin, triggers Na^+ and Cl^- transport from the bath into the gland lumen across the mucous tubules in both

wild-type and $CFTR^{-/-}$ preparation. These results indicate that the mucous tubule may contribute to the properties of the ASL by modulating the ion composition and volume of the ASL, in addition to producing mucin.

We also present the first ever evidence that the collecting and ciliated ducts are involved in ion transport as suggested by their anatomical characteristics and CFTR expression patterns in the epithelia cells of these segments (Kreda et al., 2005). Like the serous acini, the collecting duct transported Na^+ and Cl^- from the basolateral side (blood side) into the lumen of the gland, after stimulation with forskolin or carbachol. Since the cells lining the collecting duct express aquaporins (Kreda et al., 2001), the accumulation of NaCl in the lumen after stimulation of ion transport would drive water into the lumen, thus contributing to the volume and properties of the ASL secreted by the glands. In CFTR/airways, the forskolin-stimulated transport was absent, but cholinergic-stimulated transport was no different than wild-type., thus suggesting that the cAMP-mediated ion flux is dependent on CFTR and would be absent in CF. This indicates that abnormal collecting duct function may contribute to the abnormalities in ASL secretion in CF.

The ciliated duct also transports Na^+ and Cl^-, however, it does so in the opposite direction relative to the collecting duct, mucus tubule, and serous cells. The ciliated duct reabsorbs Na^+ and Cl^- from the lumen of the glands into the blood side. This transport may have two possible consequences, reducing the volume of ASL, or reduction of the Na^+ and Cl^- concentration of the ASL depending on the water permeability of the epithelia. The ion concentration measurements in the ASL excreted by glands (Table 5.1) show that the ASL has lower Na^+, K^+ and Cl^- concentration than the bathing solution. These results support the view that the ciliated duct reduces the ion concentration of the primary fluid produced by the upstream segments of

the gland.

The concentrations of Na^+, K^+ and Cl^- in the ASL were the same in all conditions, but the pH is significantly more acidic after forskolin stimulation compared to cholinergic stimulation in wild-type swine, suggesting that the regulation of pH may be different in these two stimulatory pathways (i.e. cholinergic vs. cAMP-dependent). Consistent with previous reports (Pezzulo et al., 2012), $CFTR^{-/-}$ swine produced acidic ASL. Treating wild-type glands with the CFTR blocker, CFTRinh172, resulted in secretion of a similarly acidic ASL, which is consistent with the hypothesis that acidic pH results from reduced HCO_3^- transport though CFTR. However, our data does not allow us to pinpoint which segment of the gland is responsible for the acidic pH.

Our results shed new light on the malfunction of the submucosal glands in CF. Dysfunctional CFTR channels would result in loss of cAMP-activated ion transport not only at the serous acini but also at the collecting duct, and ciliated duct. The resulting ASL has reduced volume and low pH. This may result in inadequate unpacking and hydration of mucins released by the mucus tubule. In addition, we show that basal and forskolin-stimulated ASL has low pH compared to cholinergic-stimulated ASL secretion, which suggests that CFTR-dependent and CFTR-independent ASL secretion may have different properties and functions. In addition, the pH of the ASL from $CFTR^{-/-}$ swine display lower pH compared to wild-type. Overall, our study suggests that loss of CFTR-dependent ion transport leads to reduced glandular ASL secretion, and results in lower ASL pH. The abnormal ASL properties may contribute to the failure of the airway defense against pathogens.

Appendix A

Using synchrotron-based phase contrast imaging to study early stage cystic fibrosis lung disease

A.1 Abstract

Evidence show that children with CF may develop structural damage in small airway at early stage of life. Moreover, studies on the recently developed CF swine model shows that newborn piglets display distal airway lesions without any obvious evidence of airway infection or inflammation, which suggests that the CF lung disease starts in the small airway. Unfortunately, conventional imaging methods, such as hospital computed tomography (CT) scan and magnetic resonance imaging (MRI), are unable to visualize small airway about 1mm in cross section making difficult to study early CF lung disease. We developed a new high-resolution imaging method to investigate early CF lung disease in the distal airway and to perform longitudinal studies to follow its progression. Our goal is to use synchrotron-based phase contrast CT to study the progression of the lung disease *in vivo* using $CFTR^{-/-}$ swine as CF model. Our experiments indicated that synchrotron-based phase contrast imaging CT scan allow us to visualize and investigate the distal airways in live swine. The combination of high energy monochromatic x-ray (70 keV), respiratory monitoring and gating system, and high-speed Fiber Optic x-ray camera allow us to perform CT scan in live swine at the desired point of the respiratory cycle (fully inflated lungs), with high resolution and low radiation dose. Our data indicates that we can observe distal airways with 100 μm in diameter.

A.2 Introduction

Cystic fibrosis (CF) is the most common fatal genetic disease affecting Caucasian populations. Most of the mortality arises from lung disease. Unfortunately, the events leading from gene mutation to lung disease are not fully understood, and there is controversy regarding the primary defect responsible for CF airway disease pathogenesis.

Until recently, there was consensus in the field that blockage of air flow in the airway of CF patients resulted from repeated cycles of infection and inflammation, which trigger airway remodeling and mucus accumulation that damaged airway (Ramsey et al., 2012; Baltimore et al., 1989; Hamutcu et al., 2002). However, recent studies showed that CF infants and newborn CF piglet suffer from lesions that appear as regions with obstructed airflow, in the distal airways, without any obvious evidence of airway infection or inflammation (Sly et al., 2009; Hall et al., 2011; Adam et al., 2013). These observations indicate that lesions may be independent of infection/inflammation cycle. Thus, the results raise questions about the nature of CF small airway lesions: whether the small airway obstruction caused by liquid infiltration due to inflammation and/or by mucus plug that blocking air flow.

The major difficulty for investigating the CF distal airway pathogenesis is the lack of an imaging method with sufficient resolution to observe the distal airway *in vivo*. Current imaging methods (such as CT and MRI) are unable to resolve small airway (~ 1millimeter diameter) and it is not possible to observe anything smaller than mainstem bronchi in piglets *in vivo* (Adam et al, 2013). In addition, it is difficult to determine if the lesions are filled with fluid (i.e. a sign of inflammation) or air (a sign of mechanical blockage with mucus or tissue). Therefore, we have developed a new imaging technique to investigate the relation between structural

changes and physiologic abnormalities observed in the distal airways of CF lungs (i.e. CFTR$^{-/-}$ swine) *in vivo*. We use synchrotron-based phase contrast imaging (PCI) to image the air/fluid/soft tissue interface in the lung and observe small airways. The large differences in refractive index between air, fluid, and soft tissue results in a strong refraction signature that is easily detected using phase-related imaging methods. We developed a new imaging method to visualize the small airway (~100 micrometer in diameter) and the content of the lesions in swine *in vivo*.

A.3 Materials and Methods

One week old wild-type piglets, weighing about 3 kg, were purchased from Prairie Swine Centre.

Synchrotron-based x-ray imaging set-up

Experiments were performed using the BioMedical Imaging and Therapy-Insertion Device (BMIT-ID) beamline 05ID-2, at the Canadian Light Source (CLS), Saskatchewan, Canada. The sample stage is located 58 meters away from the storage ring. Phase contrast imaging (PCI) was performed using monochromatic 70 keV (λ=0.018 nm) x-rays, selected using a standard double-crystal monochromator. The beam size was 200.0 mm (wide) x 8.0 mm (vertical). The distance between the sample and the detector was 200 cm. Images were captured by using Photonic Science Fiber Optic Camera X-ray SCMOS. The converter on camera used a 15 μm-thick scintillator (Gd2O2S:Tb) to convert x-rays to visible light. The pixel size of the image was 25.3 x 25.3 μm. Exposure time per image during CT scan was 25

ms.

Experimental set-up

One week old piglets were placed in a holder in an upright position. The animal was placed under anesthesia using 2-2.5% isoflurane. During the CT scan the custom-build animal holder limited the movement of the animal while allowing the pig to breath spontaneously throughout the experiment. Respiratory rate, heart rate, body temperature, and O_2 saturation level as well as the plane of anesthesia were monitored during the imaging process. A m2m BioVet system was used to monitor the respiratory movements of the animas by attaching the sensors to the lower abdomen. The system also monitored the cardiac function and produced an electrocardiogram (ECG). The BioVet system controlled the gating of the imaging by triggering the shutter of the beam based on both respiratory cycle and ECG signals. The gating process reduces the unnecessary x-ray exposure time for the piglets, which would lead to the lower radiation dose for the animal, and minimizes movement artifacts. We used a 600-projection CT scan protocol where the stage rotated 0.3 degree per step and the whole stage rotated 180 degrees in total.

Data analysis

CT scan data was processed by image J, CT reconstruction was done by NRECON and Avizo.

Study approval

All experiments were performed with the approval of the Canadian Light Source and the Animal Ethics Committee at the University of Saskatchewan.

A.4 Results and Discussion

Canadian Light Source BioMedical Imaging and Therapy (BMIT) Beamline provides a unique opportunity for our project. High energy x-ray generated by synchrotron source provides the ability of imaging large animals, such as swine, and high-resolution detector provide the ability to study the small airway, which are about 100 μm in diameter. High energy monochromatic x-ray (70 keV) was selected since the higher the x-ray energy, the lower the radiation dose delivered to the animal. Also, in order to provide a better signal-to-noise ratio, the sample to detector distance had been carefully chosen to highlight the distal airways but to avoid detecting the alveolus. To limit the radiation dose for the animal, we tightly control the exposure time and the number of projections during image acquisition for the CT scan. Our preliminary data shows that we can detect the small airways (less than 100 um in diameter) in piglets (Fig. A.1) with 600 projections CT scan and 25 ms exposure time, and the x-ray radiation dose for the one week old live piglet is ~400 mGy. Also, in order to test the functional imaging capabilities of the PCI CT, we mimic the condition of mucus plugging in the pig lung by injecting mucus in the lower bronchial of pig lung. In Fig. A.2, the presence of fluid in the small airway can be detected easily detected by PCI CT.

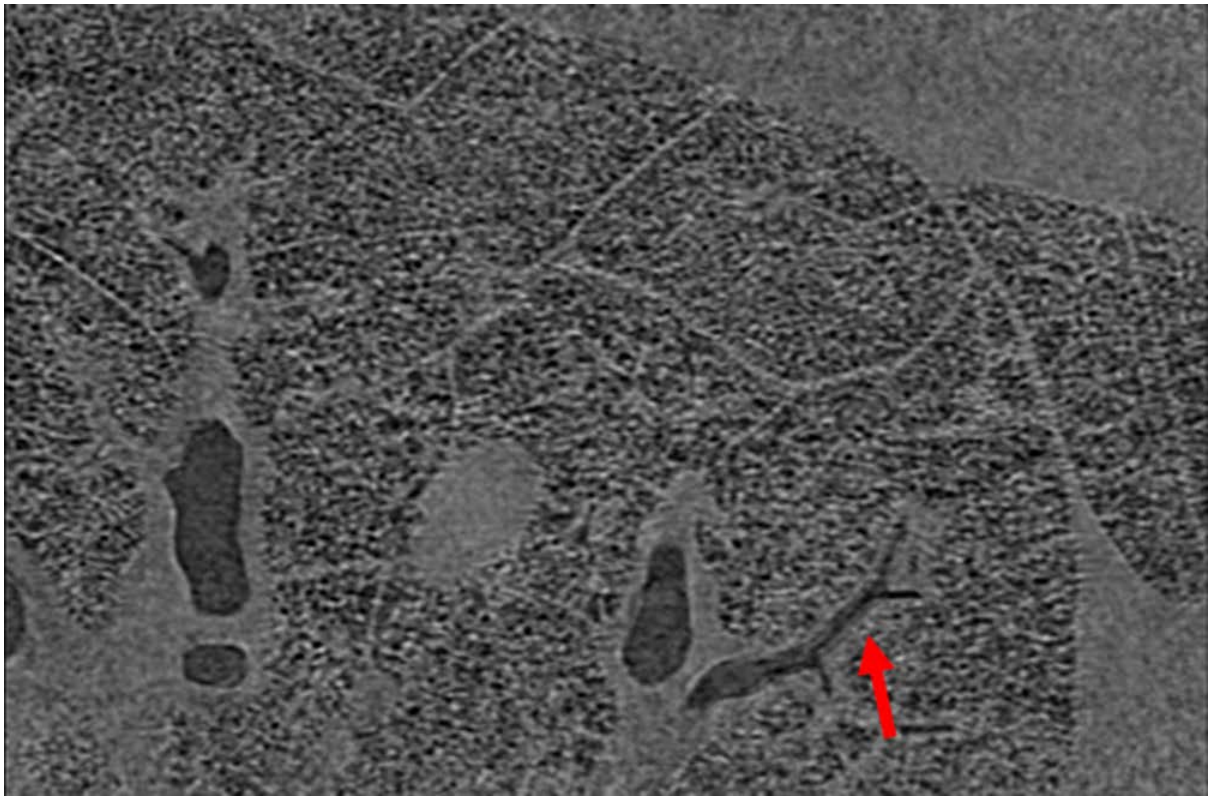

Fig. A.1. Re-sliced phase contrast CT lung image from *ex vivo* piglet scan acquired at ID beamline. The pixel size was 26 µm. Small airways (80 µm diameter) can be detected as indicated by red arrow. (Adapted from Wysokinski et al., 2016).

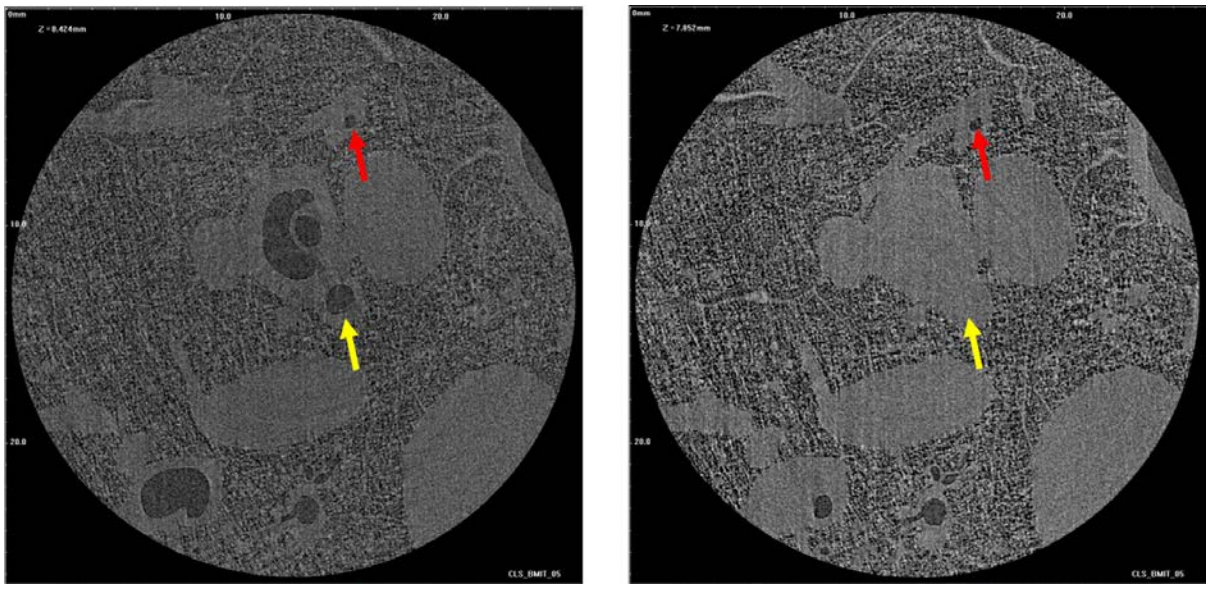

Fig. A.2. *Ex vivo* imaging of the small airway in a piglet. Left: un-treated lung, small airways (diameter = 100 µm) are visible, as indicated by the red arrow. A larger distal airway (600 µm in diameter) is indicated by the yellow arrow. Right: after an obstruction (mucus) is introduced into the airway (yellow arrow), the airway disappears in the image. (Adapted from Wysokinski et al., 2016).

To make sure we image the swine lung at the same respiratory state in each projection (at the end of inspiration), we use a respiratory monitoring and gating system (m2m BioVet system) to sense the respiratory cycle of the animal and trigger the shutter of the beam at the desired point in the cycle. By using the BioVet to control the image gating at BMIT-ID line, we can successfully image swine lungs *in vivo*. As shown Fig. A.3., distal airways with larger than 200 μm in diameter can be easily detected by synchrotron-based PCI CT. And using reconstruction software, the respiratory tree in this swine lung can be mapped (Fig. A.4.).

Fig. A.3. ***In vivo*** **imaging of a 7-day old swine.** Re-sliced phase contrast CT pig lung image while using BioVet system to monitor and gate the imaging process. The white bar indicated 2 mm.

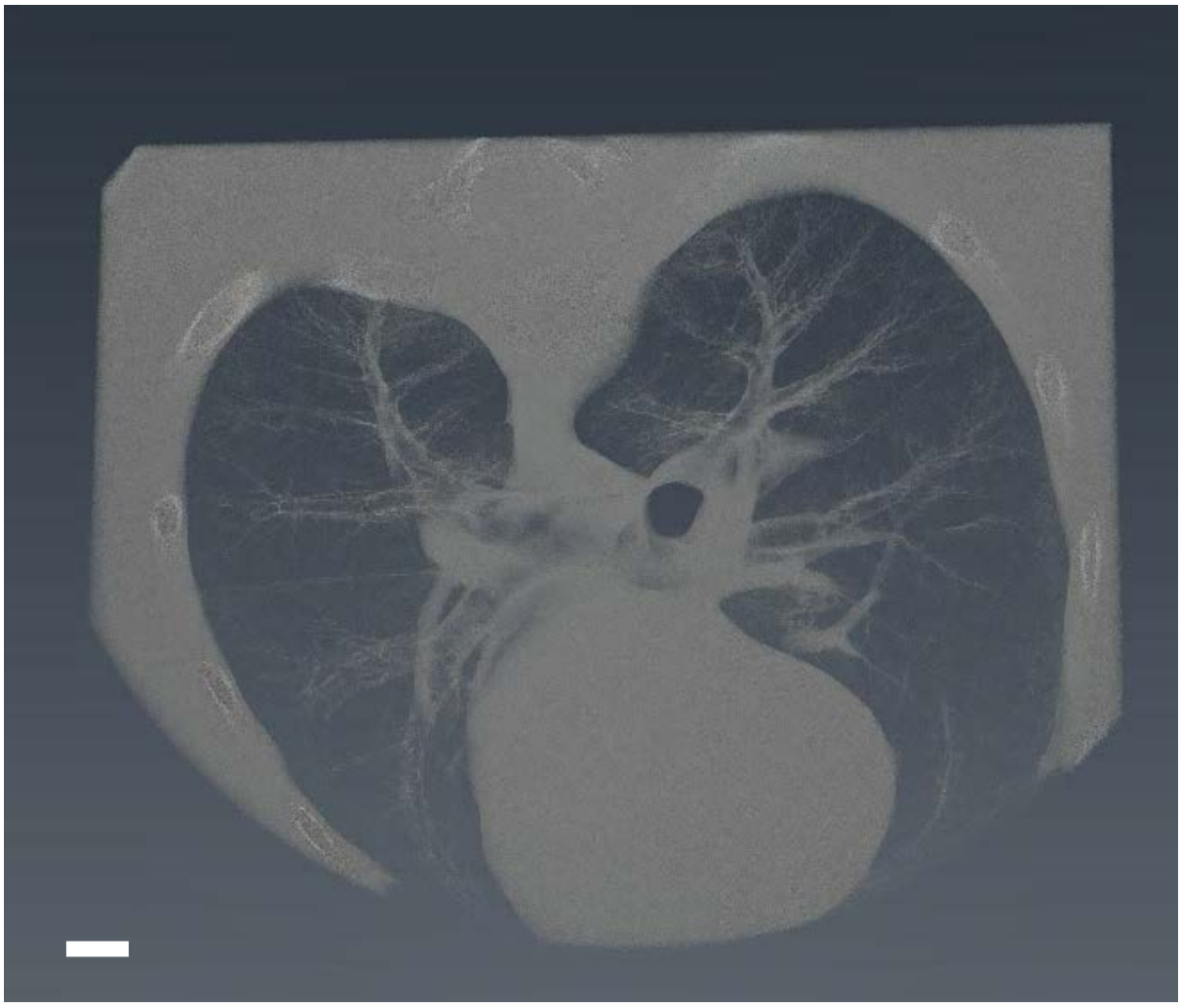

Fig. A.4. Avizo reconstruction of swine lung *in vivo*. The distal airways in the respiratory tree can be tracked in this swine lung. The white bar indicated 2 mm.

Our results suggest that PCI CT would allow us to image small airways *in vivo*, as well as determine the presence of fluid, thus allowing us to test our hypothesis. In the future, we will compare the small airway anatomy for both wild-type and CF swine. Our ultimate goal is to investigate the changes in airway anatomy and the development and content (i.e. air vs liquid) of lesions in early disease *in vivo* in CF swine. We will try to follow the progression of the disease over time as the CF animals develop infection and inflammatory (within weeks after birth) and to correlate these findings with lung function using force oscillation technique, pathology studies, and electrophysiology techniques available in our lab to study the progression of CF lung disease.

This synchrotron-based PCI CT for the small airway promises to be a major breakthrough in the CF research field. We hope to be able to determine the early changes suffered by CF airways and produce a more in-depth description of the early CF airway disease. The knowledge acquired though this project will help identify novel treatment for CF airway disease patients.

Chapter 6

General Discussion

This dissertation outlined the development of a novel imaging technique for studying the production of airways surface liquid *in vivo* in wild-type and $CFTR^{-/-}$ swine. We tested the effect of inhaled bacteria and hypertonic saline nebulization on liquid secretion in the upper airway of swine *in vivo*. We described the abnormal function of airway submucosal gland liquid secretion and its possible role in CF airway disease. We also described the function of the gland in health and disease.

6.1 Major findings

1) The development of the synchrotron-based phase contrast imaging allows the study of ASL secretion in the upper airway of a living swine for the first time.

2) The discovery of bacteria-triggered, CFTR-dependent ASL secretion as part of the normal innate immune response to inhaled bacteria. CFTR is required for normal fluid secretion, which washes mucins and antimicrobial compounds from the submucosal glands into the airway lumen.

3) The bacteria-triggered ASL secretion fails in $CFTR^{-/-}$ swine, which would facilitate chronic infection and inflammation.

4) A basal level of CFTR-dependent ASL secretion is present in the trachea of live swine which perhaps contributes to ensure the minimal amount of ASL required for the background protection through mucociliary clearance. For example, protection against non-pathogenic

particles which, in contrast to pathogenic bacteria, do not trigger ASL secretion.

5) The basal ASL secretion by submucosal glands fails in $CFTR^{-/-}$ swine, predisposing the airways to infection.

6) Hypertonic saline nebulization, a standard treatment to rehydrate CF patients' airway, does not only depend on osmotically driven fluid production but also relies on the neuron-mediated ASL secretion from airway epithelium.

7) The Na^+ and Cl^- transport in serous acini, collecting duct, and ciliated duct regions of airway submucosal gland contribute to ASL production and secretion, and these functions are missing in $CFTR^{-/-}$ swine glands.

8) The synchrotron-based phase contrast CT we developed would be a useful tool to study the pathogenesis of CF lung disease specifically in the distal airway.

6.2 Contribution to the field of CF research

My work is the first to describe the two CFTR-dependent ASL secretion mechanisms that contribute to the normal innate immune system: a bacteria-triggered, and a basal spontaneous ASL secretion in the upper airway *in vivo*. This work provides a better understanding of the airways innate immune response to inhaled pathogens, and why CF airway have a deficient innate immune defence system.

6.2.1 Innate immune response to inhaled bacteria

My experiments showed that *P. aeruginosa*-triggered ASL is mediated by the activation of TLR5 on the airway surface epithelium, which in turn stimulates ASL secretion from airway

submucosal glands. Moreover, two other bacteria commonly found in CF patients, *S. aureus* and *H. influenzae*, neither of which express flagellin, stimulated CFTR-dependent ASL secretion, possibly via stimulation of TLR4 receptors by the endotoxin, lipopolysaccharide. On the other hand, non-pathogenic bacteria, *E. coli* DH5-α and *B. subtilis* did not trigger significant amount of ASL secretion in the airway. The results indicate that pathogen-triggered ASL secretion via PRRs, especially TLRs, is an important and previously unknown component of the airway innate immune defense system to against bacteria (Basu and Fenton, 2004; Mayer and Dalpke, 2007).

Furthermore, my results showed that non-pathogenic bacteria seem not to trigger ASL-related innate immune response, which may be an important aspect of the respiratory microbiome formation. The lung has been previously thought to be sterile. However, since the development of non-culture dependent techniques to detect bacteria, evidence suggests that the respiratory system contains, similarly to the gut, a microbiome in healthy humans (Charlson et al., 2015; Bassis et al., 2015). Moreover, the lung microbiome seems to have a critical role in the development of a healthy immune system, and evidence suggests that dysbiosis of lung microbiome is involved in the development of chronic pulmonary disease, including CF (Shukla et al., 2017). A primary requisite for commensal or symbiotic bacteria to survive in the airway, and to form the microbiome, is that the innate immune system would not destroy it. Our discovery that some bacteria (i.e. non-pathogenic) do not trigger the innate immune response provides evidence that the lung would normally select against pathogenic bacteria and in favor of commensal or symbiotic microbes, thus providing a pathway for the development of a respiratory microbiome (Dickson and Huffnagle, 2015).

Our experiments using $CFTR^{-/-}$ swine showed that the ASL secretion response to inhaled bacteria is missing. This is the first study to show direct relation between ASL secretion and inhaled bacteria *in vivo*, and the absence of ASL secretion in CF airway. The lack of ASL with antimicrobial factors would result in the failure of bacteria eradication in CF patients. Thus, the bacteria would tend to survive longer in airway which might favor infection and biofilm formation (especially from *P. aeruginosa*). This would lead to chronic infection and inflammation, which may eventually result in respiratory failure in CF patients. This missing innate immune defense response to inhaled pathogenic bacteria might to be the first step of developing of CF lung disease. Moreover, there may be consequences for the microbiome, since the selection pressure imposed by the innate immune system on pathogen secretion would be absent. Whether the microbiome is abnormal in CF and whether there is a pathological consequence due to an 'abnormal' microbiome is unknown.

6.2.2 Role of the basal spontaneous ASL secretion on airway defense

It has been proposed for a long time that there may be a basal level of ASL production in the airways (Wine, 2007). However, due to the lack of a technique to study ASL secretion *in vivo*, this hypothesis was never tested. This study provides the first demonstration and investigation of the proposed basal spontaneous ASL secretion. This could only be performed *in vivo*, since only in this condition, are all the regulatory mechanisms intact (i.e. nervous, humoral, paracrine and circulatory systems). Thus, we used our synchrotron imaging method to study the possible basal ASL secretion in live swine. We observed that there is a CFTR-dependent basal spontaneous ASL secretion from airway submucosal gland in the upper airway

of live wild type swine. The basal spontaneous ASL secretion seems to provide a basal amount of liquid in the surface of the airway, which is important for mucociliary clearance. Also, the constant release of liquid from airway submucosal glands results in the steady washout of antimicrobial factors from the glands and into the lumen of the airways (Dajani et al., 2005; Widdicombe and Wine, 2015). The presence of antimicrobial factors would also be an important part of airway defense mechanism. Since this basal spontaneous ASL secretion is CFTR-dependent, this process is significantly limited in CF airway. This basal glandular ASL secretion may be recovered by hypertonic saline nebulization treatment. Thus, in addition to increasing ASL hydration, hypertonic saline treatment increases antimicrobial factors and mucins in the airway. Thus, it would predispose the airway to fight infections. Other procedures that cause vagal stimulation of the airway, such as heavy exercise, may offer similar advantages.

6.2.3 Impacts on the treatment of CF airway disease

As many experiments suggest, abnormal ASL in CF airways is the pathogenic event that triggers a cycle of infection and inflammation that can eventually lead to respiratory failure (Joris et al., 1993; Smith et al., 1996; Choi et al., 2009; Pezzulo et al., 2012; Widdicombe and Wine, 2015). My research further provides the evidence of failure of ASL secretion in response to inhaled bacteria in the CF airway, which reduces bacteria killing and impaired mucociliary clearance. The repeated cycles of infection and inflammation would finally result in airway remodeling, obstruction, and lung failure in the CF patients.

Thus, treatments that focus on improving bacteria clearing would benefit CF patients, and may avoid the progression of the lung disease to more severe stages.

6.3 Limitations of this study

Despite the novel findings of my research, there are also some limitations. 1) Using the synchrotron-based PCI method that we developed, the height of the ASL layer could only be measured using the agarose beads at the top and bottom of the trachea (Chapter 2 and 3). As a result, our method did not necessarily provide an overall detail about the height of the ASL layer covering the entire trachea, but rather a measurement just at the sites where the beads are located. 2) We used the agarose bead as a 'measuring rod' to measure the height of the ASL layer (Chapter 2 and 3). The beads on the airway resulted in slight deformation of trachea surface, which might stimulate the rapidly adapting pulmonary stretch receptors in the upper airway and trigger ASL scretion (Widdicombe, 2001). However, since we focus on the changes in the height of the ASL layer over time triggered by bacteria-laden and bacteria-free beads, both of wich would have the same mechanical effect on the receptors, the mechanical effect on the trachea should not affect our conclusions. 3) In our SIET experiments, in order to improve our signal-to-noise ratio of our measurements, we reduced Na^+ and Cl^- concentrations in the Krebs solution while we measured the Na^+ and Cl^- transports at different segements of airway submucosal gland (Chapter 5). The reduction of Na^+ or Cl^- ions in the bath might affect the electrochemical gradients driving ion transport, and thus the ion transport rate and direction. The absolute value of transport rate is, therefore, an artifact of the experimental conditions. However, the patterns of response to stimulation with forskolin and carbachol are informative. To interprete our results, we also use well established secretion assays to inform our conclusions.

6.4 Future directions and perspectives

There are several future experiments that can be done to enhance the understanding bacteria-airway submucosal gland interaction, to improve HTS treatment for CF patients, and to draw the full picture of airway submucosal gland function.

1) We have shown that inhaled bacteria stimulated ASL secretion from airway submucosal gland, but there is a link missing in the process. The question that remains is, what paracrine signal(s) is/are involved in the bacteria-triggered response? Evidence suggests that proinflammatory cytokines may be involved. ELISA and MultiPlex techniques can be used to test whether one or more paracrine signals are released from airway surface epithelia to stimulate the airway submucosal gland cells. Also, histology can be used to investigate whether other immune cells contribute to this fast-acting airway innate immune defense against inhaled bacteria.

2) We described that HTS stimulates airway sensory neurons and triggers epithelia ion transport, which produces ASL secretion. As a result, this is a possible target to modify the current HTS treatment approach to extend the effect of HTS, which would further help CF patients to improve their respiratory symptoms. Pharmacological agents that may modulate neuronal function, such as capsaicin, can be used to recruit airway sensory neurons during hypertonic saline treatment to manipulate the intensity and duration of the treatment on ASL secretion.

3) Measuring intraluminal pH changes at different segments of airway submucosal gland would be an interesting experiment. Since CFTR anion channel transports both Cl^- and HCO_3^- ions, and the ASL pH seems to play important role in determining the ASL properties and

efficacy of the airway innate immune defence. As a result, each segment of airway submucosal gland might have different contributions to the pH change in ASL, and it would be interesting to know their function to better understand of submucosal gland function on CF pathophysiology.

Finally, the future for CF patients looks promising. Advances on the understanding of the lung disease pathogenesis, as well as the recent developments of CFTR correctors of trafficking to the membrane deficiency, as well as a potentiators, that increases the opening probability of CFTR, hold tremendous potential to improve the prognosis of CF patients. Recently, using high throughput screening of large compounds libraries, CF researchers have developed correctors and potentiators (e.g. lumacaftor and ivacaftor) that help CF patients with G551D mutation, and to a lesser extent some other mutations, to significantly improve the activation of CFTR and improve their health (Accurso et al., 2010). It is expected that new drugs may be discovered to help patients with other mutation. Furthermore, better understanding to CF pathogenesis will allow for the development of therapies to abrogate or slow the onset of CF lung disease.

References

Accurso FJ, *et al.* (2010) Effect of VX-770 in persons with cystic fibrosis and the G551D-CFTR mutation. *N Engl J Med* 363(21):1991-2003.

Adam RJ, *et al.* (2013) Air trapping and airflow obstruction in newborn cystic fibrosis piglets. *Am J Respir Crit Care Med* 188(12):1434-1441.

Allen TG & Burnstock G (1990) A voltage-clamp study of the electrophysiological characteristics of the intramural neurones of the rat trachea. *J Physiol* 423:593-614.

Andersen DH (1938) cystic fibrosis of the pancreas and its relation to celiac disease. A clinical and pathologic study. *Am J Dis Child* 56(2):344-399.

Audie JP, *et al.* (1993) Expression of human mucin genes in respiratory, digestive, and reproductive tracts ascertained by in situ hybridization. *J Histochem Cytochem* 41(10):1479-1485.

Ballard ST & Inglis SK (2004) Liquid secretion properties of airway submucosal glands. *J Physiol* 556(Pt 1):1-10.

Ballard ST, Evans JW, Drag HS, & Schuler M (2016) Pathophysiologic Evaluation of the Transgenic Cftr "Gut-Corrected" Porcine Model of Cystic Fibrosis. *Am J Physiol Lung Cell Mol Physiol*:ajplung 00242 02016.

Baltimore RS, Christie CD, & Smith GJ (1989) Immunohistopathologic localization of Pseudomonas aeruginosa in lungs from patients with cystic fibrosis. Implications for the pathogenesis of progressive lung deterioration. *Am Rev Respir Dis* 140:1650-1661.

Baniak N., Luan, X., Grunow, A., Machen, T. E. & Ianowski, J. P. (2012) The cytokines interleukin-1β and tumor necrosis factor-α stimulate CFTR-mediated fluid secretion by swine airway submucosal glands. *Am J Physiol Lung Cell Mol Physiol.* 303, L327-L333.

Baraniuk JN, Ali M, Yuta A, Fang SY, & Naranch K (1999) Hypertonic saline nasal provocation stimulates nociceptive nerves, substance P release, and glandular mucous exocytosis in normal humans. *Am J Respir Crit Care Med* 160(2):655-662.

Barnes PJ. (1998) NANC nerves and neuropeptides. *Asthma: Basic Mechanism and Clinical Management*, eds Barnes PJ, Roger IW, Thomson NC (Academic Press, London), pp 423–458.

Barnes PJ (2001) Neurogenic inflammation in the airways. *Respir Physiol* 125(1-2):145-154.

Barry PH & Diamond JM (1984) Effects of unstirred layers on membrane phenomena. *Phys Reviews* 64: 763-872.

Bartlett JA, *et al.* (2016) Newborn cystic fibrosis pigs have a blunted early response to an inflammatory stimulus. *Am J Respir Crit Care Med* 194(7):845-854.

Bassis CM, *et al.* (2015) Analysis of the upper respiratory tract microbiotas as the source of the lung and gastric microbiotas in healthy individuals. *MBio* 6(2):e00037.

Basu S & Fenton MJ (2004) Toll-like receptors: function and roles in lung disease. *Am J Physiol Lung Cell Mol Physiol* 286(5):L887-892.

Ben Mohamed F, *et al.* (2012) A crucial role of Flagellin in the induction of airway mucus production by Pseudomonas aeruginosa. *PLoS One* 7(7):e39888.

Bennett WD, *et al.* (2015) Duration of action of hypertonic saline on mucociliary clearance in the normal lung. *J Appl Physiol (1985)* 118(12):1483-1490.

Boucher RC (1994) Human airway ion transport. Part one. *Am J Respir Crit Care Med*

150(1):271-281.
Boucher RC (2007) Airway surface dehydration in cystic fibrosis: pathogenesis and therapy. *Annu Rev Med* 58:157-170.
Bowes D & Corrin B (1977) Ultrastructural immunocytochemical localisation of lysozyme in human bronchial glands. *Thorax* 32(2):163-170.
Bowes D, Clark AE, & Corrin B (1981) Ultrastructural localisation of lactoferrin and glycoprotein in human bronchial glands. *Thorax* 36(2):108-115.
Brau ME, Branitzki P, Olschewski A, Vogel W, & Hempelmann G (2000) Block of neuronal tetrodotoxin-resistant Na^+ currents by stereoisomers of piperidine local anesthetics. *Anesth Analg* 91(6):1499-1505.
Cash HA, Woods DE, McCullough B, Johanson WG, Jr., Bass JA (1979) A rat model of chronic respiratory infection with Pseudomonas aeruginosa. *Am Rev Respir Dis* 119(3):453-459.
Castellani C & Assael BM (2017) Cystic fibrosis: a clinical view. *Cell Mol Life Sci* 74(1):129-140.
Cazzarolli C, Tartali C, & Pradal U (2016) The Advantages of Adding Hyaluronic Acid or Mannitol to Hypertonic Saline Inhalation Treatment in Cystic Fibrosis. *J Aerosol Med Pulm Drug Deliv*.
Charlson ES, *et al.* (2011) Topographical continuity of bacterial populations in the healthy human respiratory tract. *Am J Respir Crit Care Med* 184(8):957-963.
Chen JH, *et al.* (2010) Loss of anion transport without increased sodium absorption characterizes newborn porcine cystic fibrosis airway epithelia. *Cell* 143(6):911-923.
Chmiel JF, Konstan MW, Berger M (2002) Murine models of CF airway infection and inflammation. *Methods Mol Med* 70:495-515.
Cho HJ, Joo NS, Wine JJ (2011) Defective fluid secretion from submucosal glands of nasal turbinates from $CFTR^{-/-}$ and $CFTR^{\Delta F508/\Delta F508}$ Pigs. *PLoS One* 6(8):e24424.
Choi JY, *et al.* (2009) Substance P stimulates human airway submucosal gland secretion mainly via a CFTR-dependent process. *J Clin Invest* 119(5):1189-1200.
Chou YL, Scarupa MD, Mori N, & Canning BJ (2008) Differential effects of airway afferent nerve subtypes on cough and respiration in anesthetized guinea pigs. *Am J Physiol Regul Integr Comp Physiol* 295(5):R1572-1584.
Conway S, *et al.* (2014) European Cystic Fibrosis Society Standards of Care: Framework for the Cystic Fibrosis Centre. *J Cyst Fibros* 13 Suppl 1:S3-22.
Cutting GR (2015) Cystic fibrosis genetics: from molecular understanding to clinical application. *Nat Rev Genet* 16(1):45-56.
Dajani R, *et al.* (2005) Lysozyme secretion by submucosal glands protects the airway from bacterial infection. *Am J Respir Cell Mol Biol* 32(6):548-552.
Dartt DA (2009) Neural regulation of lacrimal gland secretory processes: relevance in dry eye diseases. *Prog Retin Eye Res* 28(3):155-177.
Davis PB (2006) Cystic fibrosis since 1938. *Am J Respir Crit Care Med* 173(5):475-482.
Delporte C (2014) Aquaporins in salivary glands and pancreas. *Biochim Biophys Acta* 1840(5):1524-1532.
Dickson RP & Huffnagle GB (2015) The Lung Microbiome: New Principles for Respiratory Bacteriology in Health and Disease. *PLoS Pathog* 11(7):e1004923.
Donaldson SH, *et al.* (2006) Mucus clearance and lung function in cystic fibrosis with

hypertonic saline. *N Engl J Med* 354(3):241-250.
Donnelley M, *et al.* (2014) Non-invasive airway health assessment: synchrotron imaging reveals effects of rehydrating treatments on mucociliary transit in-vivo. *Sci Rep* 4:3689.
Doughty JM & Langton PD (2001) Measurement of chloride flux associated with the myogenic response in rat cerebral arteries. *J Physiol* 534:753-761.
Egan ME (2016) Genetics of Cystic Fibrosis: Clinical Implications. *Clin Chest Med* 37(1):9-16.
Elkins MR, *et al.* (2006) A controlled trial of long-term inhaled hypertonic saline in patients with cystic fibrosis. *N Engl J Med* 354(3):229-240.
Ellemunter H, Eder J, Fuchs S, Gappa M, & Steinkamp G (2016) Long-term improvement of lung clearance index in patients with mild cystic fibrosis lung disease: Does hypertonic saline play a role? *J Cyst Fibros* 15(1):123-126.
Engelhardt JF, *et al.* (1992) Submucosal glands are the predominant site of CFTR expression in the human bronchus. *Nat Genet* 2(3):240-248.
Finkbeiner WE, *et al.* (2011) Cystic fibrosis and the relationship between mucin and chloride secretion by cultures of human airway gland mucous cells. *Am J Physiol Lung Cell Mol Physiol* 301(4):L402-414.
Flume PA, *et al.* (2009) Cystic fibrosis pulmonary guidelines: airway clearance therapies. *Respir Care* 54(4):522-537.
Flume PA & Van Devanter DR (2012) State of progress in treating cystic fibrosis respiratory disease. *BMC medicine* 10:88.
Fox AJ, Barnes PJ, & Dray A (1995) Stimulation of guinea-pig tracheal afferent fibres by non-isosmotic and low-chloride stimuli and the effect of frusemide. *J Physiol* 482 (Pt 1):179-187.
Goetz DM & Singh S (2016) Respiratory System Disease. *Pediatr Clin North Am* 63(4):637-659.
Guggino WB (1999) Cystic fibrosis and the salt controversy. *Cell* 96(5):607-610.
Haack A, Aragao GG, & Novaes MR (2013) Pathophysiology of cystic fibrosis and drugs used in associated digestive tract diseases. *World J Gastroenterol* 19(46):8552-8561.
Hall GL, *et al.* (2011) Air trapping on chest CT is associated with worse ventilation distribution in infants with cystic fibrosis diagnosed following newborn screening. *PLoS One* 6:e23932.
Hamed R. & Fiegel J. (2013) Synthetic tracheal mucus with native rheological and surface tension properties. *J Biomed Mater Res A* 102:1788-1798.
Hamutcu R, *et al.* (2002) Clinical findings and lung pathology in children with cystic fibrosis. *Am J Respir Crit Care Med* 165:1172-1175.
Haq IJ, Gray MA, Garnett JP, Ward C, & Brodlie M (2016) Airway surface liquid homeostasis in cystic fibrosis: pathophysiology and therapeutic targets. *Thorax* 71(3):284-287.
Hoegger MJ, *et al.* (2014) Impaired mucus detachment disrupts mucociliary transport in a piglet model of cystic fibrosis. *Science* 345(6198):818-822.
Hoffmann N, et al. (2005) Novel mouse model of chronic Pseudomonas aeruginosa lung infection mimicking cystic fibrosis. *Infect Immun* 73(4):2504-2514.
Humphrey SP & Williamson RT (2001) A review of saliva: normal composition, flow, and function. *J Prosthet Dent* 85(2):162-169.

Hybiske K, Ichikawa JK, Huang V, Lory SJ, Machen TE (2004) Cystic fibrosis airway epithelial cell polarity and bacterial flagellin determine host response to *Pseudomonas aeruginosa*. *Cell Microbiol* 6(1):49-63.

Ianowski JP, Choi JY, Wine JJ, & Hanrahan JW (2007) Mucus secretion by single tracheal submucosal glands from normal and cystic fibrosis transmembrane conductance regulator knockout mice. *J Physiol* 580(Pt 1):301-314.

Ianowski JP, Choi JY, Wine JJ, & Hanrahan JW (2008) Substance P stimulates CFTR-dependent fluid secretion by mouse tracheal submucosal glands. *Pflugers Arch* 457(2):529-537.

Illek B, *et al.* (2008) Flagellin-stimulated Cl- secretion and innate immune responses in airway epithelia: role for p38. *Am J Physiol Lung Cell Mol Physiol* 295(4):L531-542.

Inglis SK & Wilson SM (2005) Cystic fibrosis and airway submucosal glands. *Pediatr Pulmonol* 40:279-284.

Itani OA, *et al.* (2011) Human cystic fibrosis airway epithelia have reduced Cl^- conductance but not increased Na^+ conductance. *Proc Natl Acad Sci U S A* 108(25):10260-10265.

Jayaraman S, Joo NS, Reitz B, Wine JJ, & Verkman AS (2001) Submucosal gland secretions in airways from cystic fibrosis patients have normal [Na(+)] and pH but elevated viscosity. *Proc Natl Acad Sci U S A* 98(14):8119-8123.

Jiang Q & Engelhardt JF (1998) Cellular heterogeneity of CFTR expression and function in the lung: implications for gene therapy of cystic fibrosis. *Eur J Hum Genet* 6(1):12-31.

Joo NS, Wu JV, Krouse ME, Saenz Y, & Wine JJ (2001) Optical method for quantifying rates of mucus secretion from single submucosal glands. *Am J Physiol Lung Cell Mol Physiol* 281(2):L458-468.

Joo NS, Saenz Y, Krouse ME, Wine JJ (2002) Mucus secretion from single submucosal glands of pig. Stimulation by carbachol and vasoactive intestinal peptide. *J Biol Chem* 277(31):28167-28175.

Joo NS, *et al.* (2002) Absent secretion to vasoactive intestinal peptide in cystic fibrosis airway glands. *J Biol Chem* 277(52):50710-50715.

Joo NS, Lee DJ, Winges KM, Rustagi A, & Wine JJ (2004) Regulation of antiprotease and antimicrobial protein secretion by airway submucosal gland serous cells. *J Biol Chem* 279(37):38854-38860.

Joo NS, Irokawa T, Robbins RC, & Wine JJ (2006) Hyposecretion, not hyperabsorption, is the basic defect of cystic fibrosis airway glands. *J Biol Chem* 281(11):7392-7398.

Joo NS, Cho HJ, Khansaheb M, & Wine JJ (2010) Hyposecretion of fluid from tracheal submucosal glands of CFTR-deficient pigs. *J Clin Invest* 120(9):3161-3166.

Joo NS, Krouse ME, Choi JY, Cho HJ, & Wine JJ (2016) Inhibition of airway surface fluid absorption by cholinergic stimulation. *Sci Rep* 6:20735.

Joris L, Dab I, & Quinton PM (1993) Elemental composition of human airway surface fluid in healthy and diseased airways. *Am Rev Respir Dis* 148(6 Pt 1):1633-1637.

Kawai T & Akira S (2010) The role of pattern-recognition receptors in innate immunity: update on Toll-like receptors. *Nature immunology* 11(5):373-384.

Kerem B, *et al.* (1989) Identification of the cystic fibrosis gene: genetic analysis. *Science* 245(4922):1073-1080.

Khansaheb M, *et al.* (2011) Properties of substance P-stimulated mucus secretion from porcine

tracheal submucosal glands. *Am J Physiol Lung Cell Mol Physiol* 300(3):L370-379.
Kishioka C, Okamoto K, Kim JS, & Rubin BK (2003) Hyperosmolar solutions stimulate mucus secretion in the ferret trachea. *Chest* 124(1):306-313.
Knowles MR & Boucher RC (2002) Mucus clearance as a primary innate defense mechanism for mammalian airways. *J Clin Invest* 109(5):571-577.
Kreda SM, Gynn MC, Fenstermacher DA, Boucher RC, & Gabriel SE (2001) Expression and localization of epithelial aquaporins in the adult human lung. *Am J Respir Cell Mol Biol* 24(3):224-234.
Kreda SM, *et al.* (2005) Characterization of wild-type and deltaF508 cystic fibrosis transmembrane regulator in human respiratory epithelia. *Mol Biol Cell* 16(5):2154-2167.
Kuhtreiber WM & Jaffe LF (1990) Detection of extracellular calcium gradients with a calcium-specific vibrating electrode. *J Cell Biol* 110: 1565-1573.
Kunkel JG, *et al.* (2006) Use of Non-Invasive Ion-Selective Microelectrode Techniques for the Study of Plant Development. *Plant Electrophysiology: Theory and Methods*, ed Volkow AG (Springer, Heidelberg), pp 109-137.
Lambrecht BN & Hammad H (2012) The airway epithelium in asthma. *Nat Med* 18(5):684-692.
Lavelle GM, White MM, Browne N, McElvaney NG, & Reeves EP (2016) Animal Models of Cystic Fibrosis Pathology: Phenotypic Parallels and Divergences. *Biomed Res Int* 2016:5258727.
Lee RJ & Foskett JK (2010) cAMP-activated Ca^{2+} signaling is required for CFTR-mediated serous cell fluid secretion in porcine and human airways. *J Clin Invest* 120(9):3137-3148.
Lee WL, *et al.* (2011) Muco-ciliary transport: Effect of mucus viscosity, cilia beat frequency and cilia density. *Comput Fluids* 49(1): 214-221.
Lewis R.A., *et al.* (2005) Dynamic imaging of the lungs using x-ray phase contrast. *Phys Med Biol* 50:5031-40.
Li JD, *et al.* (1998) Activation of NF-αB via a Src-dependent Ras-MAPK-pp90rsk pathway is required for *Pseudomonas aeruginosa*-induced mucin overproduction in epithelial cells. *Proc Natl Acad Sci U S A* 95: 5718–5723.
Luan X, Chapman D, Ianowski JP (2013) Novel method to observe the mucus layer in the living swine using synchrotron-based phase contrast imaging. *Pediatric Pulmonology* S36:239.
Luan X, *et al.* (2014) Pseudomonas aeruginosa triggers CFTR-mediated airway surface liquid secretion in swine trachea. *Proc Natl Acad Sci U S A* 111(35):12930-12935.
Luan X, *et al.* (2017) Cystic fibrosis swine fail to secrete airway surface liquid in response to inhalation of pathogens. *Nat Commun* 8(1):786.
Machen TE (2006) Innate immune response in CF airway epithelia: hyperinflammatory? *Am J Physiol Cell Physiol* 291(2):C218-230.
Maggi CA, Giachetti A, Dey RD, & Said SI (1995) Neuropeptides as regulators of airway function: vasoactive intestinal peptide and the tachykinins. *Physiol Rev* 75(2):277-322.
Martens C.J., *et al.* (2011) Mucous solids and liquid secretion by airways: studies with normal pig, cystic fibrosis human, and non-cystic fibrosis human bronchi. *Am J Physiol Lung*

Cell Mol Physiol 301:L236-L246.
Matkovic Z & Miravitlles M (2013) Chronic bronchial infection in COPD. Is there an infective phenotype? *Respir Med* 107(1):10-22.
Mayer AK & Dalpke AH (2007) Regulation of local immunity by airway epithelial cells. *Arch Immunol Ther Exp (Warsz)* 55(6):353-362.
Melis N, *et al.* (2014) Revisiting CFTR inhibition: a comparative study of CFTRinh -172 and GlyH-101 inhibitors. *Br J Pharmacol* 171(15):3716-3727.
Messerli MA, Collis LP, & Smith PJ (2009) Ion trapping with fast-response ion-selective microelectrodes enhances detection of extracellular ion channel gradients. *Biophys J* 96:1597-1605.
Meyerholz DK, Stoltz DA, Pezzulo AA, Welsh MJ (2010) Pathology of gastrointestinal organs in a porcine model of cystic fibrosis. *Am J Pathol* 176(3):1377-1389.
Meyrick B, Sturgess JM & Reid L (1969) A reconstruction of the duct system and secretory tubules of the human bronchial submucosal gland. *Thorax* 24:729–736.
Meyrick B & Reid L (1970) Ultrastructure of cells in the human bronchial submucosal glands. *J Anat* 107 (2): 281-299
Mohamed FB, *et al.* (2012) A crucial role of Flagellin in the induction of airway mucus production by *Pseudomonas aeruginosa*. *PLoS One* 7:e39888.
Morgan KS, *et al.* (2013) Measuring airway surface liquid depth in *ex vivo* mouse airways by x-ray imaging for the assessment of cystic fibrosis airway therapies. *PLoS One* 8(1):e55822.
O'Sullivan BP & Freedman SD (2009) Cystic fibrosis. *Lancet* 373(9678):1891-1904.
Oakland M, Sinn PL, & McCray PB, Jr. (2012) Advances in cell and gene-based therapies for cystic fibrosis lung disease. *Mol Ther* 20(6):1108-1115.
Ostedgaard LS, *et al.* (2011) The DeltaF508 mutation causes CFTR misprocessing and cystic fibrosis-like disease in pigs. *Sci Transl Med* 3(74):74ra24.
Parsons DW, *et al.* (2008) High-resolution visualization of airspace structures in intact mice via synchrotron phase-contrast X-ray imaging (PCXI). *J Anat* 213(2):217-227.
Pedersen KE, Meeker SN, Riccio MM, & Undem BJ (1998) Selective stimulation of jugular ganglion afferent neurons in guinea pig airways by hypertonic saline. *J Appl Physiol (1985)* 84(2):499-506.
Pezzulo AA, *et al.* (2012) Reduced airway surface pH impairs bacterial killing in the porcine cystic fibrosis lung. *Nature* 487(7405):109-113.
Pier GB, Grout M, & Zaidi TS (1997) Cystic fibrosis transmembrane conductance regulator is an epithelial cell receptor for clearance of Pseudomonas aeruginosa from the lung. *Proc Natl Acad Sci U S A* 94(22):12088-12093.
Pilewski JM, Frizzell RA (1999) Role of CFTR in airway disease. *Physiol Rev* 79(1 Suppl):S215-255.
Pineros MA, Shaff JE, & Kochian LV (1998) Development, Characterization, and Application of a Cadmium-Selective Microelectrode for the Measurement of Cadmium Fluxes in Roots of Thlaspi Species and Wheat. *Plant Physiol* 116(4):1393-1401.
Quinton PM (1979) Composition and control of secretions from tracheal bronchial submucosal glands. *Nature* 279(5713):551-552.
Quinton PM (1990) Cystic fibrosis: a disease in electrolyte transport. *FASEB J* 4(10):2709-

2717.
Quinton PM (2007) Too much salt, too little soda: cystic fibrosis. *Sheng Li Xue Bao* 59(4):397-415.
Quinton PM (2007) Cystic fibrosis: lessons from the sweat gland. *Physiology (Bethesda)* 22:212-225.
Ramsey BW, *et al.* (2012) Future directions in early cystic fibrosis lung disease research: an NHLBI workshop report. *Am J Respir Crit Care Med* 185(8):887-892.
Rapacchietta, A, Neumann A. & Omenyi S. (1977) Force and free-energy analyses of small particles at fluid interfaces. *J Colloid Interface Sc.* 59:541-554.
Reeves EP, *et al.* (2015) Inhaled hypertonic saline for cystic fibrosis: Reviewing the potential evidence for modulation of neutrophil signalling and function. *World J Crit Care Med* 4(3):179-191.
Reid, L. (1960) Measurement of the bronchial mucous gland layer: a diagnostic yardstick in chronic bronchitis. *Thorax* 15:132–141.
Reiniger N, *et al.* (2007) Resistance to *Pseudomonas aeruginosa* chronic lung infection requires cystic fibrosis transmembrane conductance regulator-modulated interleukin-1 (IL-1) release and signaling through the IL-1 receptor. *Infect Immun* 75(4):1598-1608.
Rheault MR & O'Donnell MJ (2001) Analysis of epithelial K(+) transport in Malpighian tubules of *Drosophila melanogaster*: evidence for spatial and temporal heterogeneity. *J Exp Biol* 204(Pt 13):2289-2299.
Riordan JR, *et al.* (1989) Identification of the cystic fibrosis gene: cloning and characterization of complementary DNA. *Science* 245(4922):1066-1073.
Robinson M, *et al.* (1996) Effect of hypertonic saline, amiloride, and cough on mucociliary clearance in patients with cystic fibrosis. *Am J Respir Crit Care Med* 153(5):1503-1509.
Robinson M, *et al.* (1997) Effect of increasing doses of hypertonic saline on mucociliary clearance in patients with cystic fibrosis. *Thorax* 52(10):900-903.
Rogers CS, *et al.* (2008) The porcine lung as a potential model for cystic fibrosis. *Am J Physiol Lung Cell Mol Physiol* 295(2):L240-263.
Rommens JM, *et al.* (1989) Identification of the cystic fibrosis gene: chromosome walking and jumping. *Science* 245(4922):1059-1065.
Roy MG, *et al.* (2014) Muc5b is required for airway defence. *Nature* 505(7483):412-416.
Rubenstein E, *et al.* (1986) Transvenous coronary angiography in humans using synchrotron radiation. *Proc Natl Acad Sci U S A.* 83:9724-9728.
Saga K (2002) Structure and function of human sweat glands studied with histochemistry and cytochemistry. *Prog Histochem Cytochem* 37(4):323-386.
Scholz A, Kuboyama N, Hempelmann G, & Vogel W (1998) Complex blockade of TTX-resistant Na^+ currents by lidocaine and bupivacaine reduce firing frequency in DRG neurons. *J Neurophysiol* 79(4):1746-1754.
Schurch S, Gehr P, Im Hof V, Geiser M, & Green F (1990) Surfactant displaces particles toward the epithelium in airways and alveoli. *Respir Physiol* 80(1):17-32.
Sheppard DN & Welsh MJ (1999) Structure and function of the CFTR chloride channel. *Physiol Rev* 79(1 Suppl):S23-45.
Shinkai, H., *et al.* (2006) Biased distribution of single nucleotide polymorphisms (SNPs) in porcine Toll-like receptor 1 (TLR1), TLR2, TLR4, TLR5, and TLR6 genes.

Immunogenetics 58:324-30.
Sims DE, Horne MM (1997) Heterogeneity of the composition and thickness of tracheal mucus in rats. *Am J Physiol* 273:L1036-1041.
Siu KK, *et al.* (2008) Phase contrast X-ray imaging for the non-invasive detection of airway surfaces and lumen characteristics in mouse models of airway disease. *Eur J Radiol* 68(3 Suppl):S22-26.
Shipley AM, & Feijo' JA (1999) The use of the vibrating probe technique to study steady extracellular currents during pollen germination and tube growth. *Fertilization in Higher Plants*, eds Cresti M, Cai G, Moscatelli A (Springer, Heidelberg), pp 235-252.
Shukla SD, Budden KF, Neal R, & Hansbro PM (2017) Microbiome effects on immunity, health and disease in the lung. *Clin Transl Immunology* 6(3):e133.
Sly PD, *et al.* (2009) Lung disease at diagnosis in infants with cystic fibrosis detected by newborn screening. *Am J Respir Crit Care Med* 180:146-152.
Smith JJ, Travis SM, Greenberg EP, & Welsh MJ (1996) Cystic fibrosis airway epithelia fail to kill bacteria because of abnormal airway surface fluid. *Cell* 85(2):229-236.
Smith PJ, Hammar K, Porterfield DM, Sanger RH, & Trimarchi JR (1999) Self-referencing, non-invasive, ion selective electrode for single cell detection of trans-plasma membrane calcium flux. *Microsc Res Tech* 46:398-417.
Smith PJ & Trimarchi J (2001) Noninvasive measurement of hydrogen and potassium ion flux from single cells and epithelial structures. *Am J Physiol Cell Physiol* 280:C1-11.
Somieski P & Nagel W (2001) Measurement of pH gradients using an ion-sensitive vibrating probe technique (IP). *Pflugers Arch* 442(1):142-149.
Song Y & Verkman AS (2001) Aquaporin-5 dependent fluid secretion in airway submucosal glands. *J Biol Chem* 276(44):41288-41292.
Stoltz DA, *et al.* (2010) Cystic fibrosis pigs develop lung disease and exhibit defective bacterial eradication at birth. *Sci Transl Med* 2(29):29ra31.
Stoltz DA, *et al.* (2013) Intestinal CFTR expression alleviates meconium ileus in cystic fibrosis pigs. *J Clin Invest* 123(6):2685-2693.
Stoltz DA, Meyerholz DK, & Welsh MJ (2015) Origins of cystic fibrosis lung disease. *N Engl J Med* 372(4):351-362.
Sun X, *et al.* (2010) Disease phenotype of a ferret CFTR-knockout model of cystic fibrosis. *J Clin Invest* 120(9):3149-3160.
Tang XX, *et al.* (2016) Acidic pH increases airway surface liquid viscosity in cystic fibrosis. *J Clin Invest* 126(3):879-891.
Tarran R, Button B, & Boucher RC (2006) Regulation of normal and cystic fibrosis airway surface liquid volume by phasic shear stress. *Annu Rev Physiol* 68:543-561.
Tay B., Jung K, & Srinivasan M. (2006) *In Vivo* Mechanical Behavior of Intra-abdominal Organs. *IEEE Trans Bio Med Eng* 53:2129-2138.
Tildy BE & Rogers DF (2015) Therapeutic options for hydrating airway mucus in cystic fibrosis. *Pharmacology* 95(3-4):117-132.
Tos M (1966) Development of the tracheal glands in man. Number, density, structure, shape, and distribution of mucous glands elucidated by quantitative studies of whole mounts. *Acta Pathol Microbiol Scand* 68:Suppl 185:183+.
Tuggle KL, *et al.* (2014) Characterization of defects in ion transport and tissue development in

cystic fibrosis transmembrane conductance regulator (CFTR)-knockout rats. *PLoS One* 9(3):e91253.\

Ueki I, German VF, & Nadel JA (1980) Micropipette measurement of airway submucosal gland secretion. Autonomic effects. *Am Rev Respir Dis* 121(2):351-357.

Umeno E, McDonald DM, & Nadel JA (1990) Hypertonic saline increases vascular permeability in the rat trachea by producing neurogenic inflammation. *J Clin Invest* 85(6):1905-1908.

Van Vlierberghe S, Graulus GJ, Samal S & Dubruel P (2014) Porous hydrogel biomedical foam scaffolds for tissue repair. *Biomedical foams for tissue engineering applications*, ed Netti PA (Woodhead publishing, Sawston), pp 335-390.

Verkman AS, Song Y, & Thiagarajah JR (2003) Role of airway surface liquid and submucosal glands in cystic fibrosis lung disease. *Am J Physiol Cell Physiol* 284(1):C2-15.

Wark P & McDonald VM (2009) Nebulised hypertonic saline for cystic fibrosis. *Cochrane Database Syst Rev* (2):CD001506.

Widdicombe J (2001) Airway receptors. *Respir Physiol* 125(1-2):3-15.

Widdicombe JH (2002) Regulation of the depth and composition of airway surface liquid. *J Anat* 201(4):313-318.

Widdicombe JH & Wine JJ (2015) Airway Gland Structure and Function. *Physiol Rev* 95(4):1241-1319.

Williams HD & Davies JC (2012) Basic science for the chest physician: Pseudomonas aeruginosa and the cystic fibrosis airway. *Thorax* 67:465-467.

Wine JJ (2001) Cystic fibrosis: the 'bicarbonate before chloride' hypothesis. *Curr Biol* 11(12):R463-466.

Wine JJ & Joo NS (2004) Submucosal glands and airway defense. *Proc Am Thorac Soc* 1(1):47-53.

Wine JJ (2007) Parasympathetic control of airway submucosal glands: central reflexes and the airway intrinsic nervous system. *Auton Neurosci* 133(1):35-54.

Wine JJ, *et al.* (2011) Measurement of fluid secretion from intact airway submucosal glands. *Methods Mol Biol* 742:93-112.

Worthington EN, Tarran R. (2011) Methods for ASL measurements and mucus transport rates in cell cultures. *Methods Mol Biol.* 742:77-92.

Wu JV, Krouse ME, & Wine JJ (2007) Acinar origin of CFTR-dependent airway submucosal gland fluid secretion. *Am J Physiol Lung Cell Mol Physiol* 292(1):L304-311.

Wysokinski, TW, *et al.* (2007) Beamlines of the biomedical imaging and therapy facility at the Canadian Light Source-Part 1. *Nuc. Instr Meth Phys Res A* 582: 73-76.

Yuan Y. & Lee T. (2013) Contact Angle and Wetting Properties. *Surf Sci Tech* 51:3-34.

Zitta K, *et al.* (2010) Interleukin-1β regulates cell proliferation and activity of extracellular matrix remodelling enzymes in cultured primary pig heart cells. *Biochem Biophys Res Commun* 399(4):542-547.